A Systems Chemistry Approach to Understanding Cucurbit[7]uril-Guest Dynamics

by

Kevin Andrew Vos
Bachelor of Science, University of Victoria, 2015

A Dissertation Submitted in Partial Fulfillment
of the Requirements for the Degree of

DOCTOR OF PHILOSOPHY

in the Department of Chemistry

Supervisory Committee

A Systems Chemistry Approach to Understanding Cucurbit[7]uril-Guest Dynamics

by

Kevin Andrew Vos
Bachelor of Science, University of Victoria, 2015

Supervisory Committee

Dr. Cornelia Bohne (Department of Chemistry)
Supervisor

Dr. David Berg (Department of Chemistry)
Departmental Member

Dr. Fraser Hof (Department of Chemistry)
Departmental Member

Dr. Perry Howard (Department of Biochemistry and Microbiology)
Outside Member

Abstract

Systems chemistry is an emerging field of chemistry that studies complex mixtures of molecules that give rise to emergent properties that are not always predictable when studying the components of the mixtures in isolation. A systems chemistry approach has been adopted in fields such as self-assembly and self-sorting, where the dynamic recognition of complementary binding motifs to organize molecules is the central focus. Supramolecular systems are assembled through reversible, non-covalent interactions. The reversibility of supramolecular systems makes them dynamic. Understanding the dynamic nature of complex systems will allow for a bottom-up approach to the rational design of complex mixtures, such as kinetically trapped self-sorting systems.

The first objective of this work was to understand the effects the identity and concentration of biologically relevant metal cations have on a the mechanism of binding and rate of kinetics of a cucurbit[7]uril (CB[7])-guest complex. Metal cations are frequently added to cucurbit[n]uril (CB[n]) systems. While metal cations are known to decrease the overall equilibrium constant of a CB[n]-guest complex, there has not been much consideration about how different metal cations can affect the CB[n]-guest binding mechanism beyond introducing competitive equilibria. Kinetic studies of the interactions between CB[7] and 1-(2-naphthyl)-ethylammonium (NpH^+) in the presence of Ca^{2+} and Na^+ were investigated. It was found that the binding mechanism between NpH^+ and CB[7] was the formation of an exclusion complex and an inclusion complex. An exclusion complex is the formation of a complex where the cationic ammonium group of the guest associates to the carbonyl lined portals of CB[7], while the aromatic group remains exposed to the surrounding; while an inclusion complex is formed when the aromatic group of the guest enters the hydrophobic cavity of CB[7]. By increasing the metal cation concentrations, the exclusion complex was seen to disappear from the overall kinetics. When Ca^{2+} cations were used instead of Na^+ cations, a Ca^{2+} cation capped inclusion complex was formed. The Ca^{2+} cation capped inclusion complex was found to have a lower dissociation rate constant than the uncapped complex between NpH^+ and CB[7].

The second objective of this work was to understand how the structure of guest molecules effected the kinetic time scale of reaction with CB[7]. The kinetics between CB[7] and three different aromatic dications were measured to understand the structural features that

influence the change in kinetic time scales: methyl viologen (MV^{2+}), benzidine (Bn^{2+}) and 2,7'-dimethyl-diazapyrenium ($MDAP^{2+}$). It was found that moving the cationic charges further apart slowed down the kinetics from the sub millisecond time scale (MV^{2+}) to the millisecond time scale (Bn^{2+}); further, it was found that adding rigidity and width to the molecule ($MDAP^{2+}$) slowed down the kinetics onto the minute time scale.

The final objective of this work was to use the understanding of complexity gained in the metal cation project and the guest design for kinetic time scales project to rationally design a kinetically-trapped self-sorting system. The equilibrium constants and time scale of kinetics between a ditopic guest molecule and three host molecules (CB[6], CB[7] and β-CD) were determined to investigate the feasibility of the kinetically-trapped self-sorting system. Due to the complexity introduced by metal cations discovered earlier, β-cyclodextrin (β-CD) was used to modulate the concentration of guest that could be bound by CB[n]s. As a concentration modulator the requirements of β-CD were that the kinetics must be faster than the millisecond time scale and the equilibrium constant with the guest must be much lower than the equilibrium constants between the guest and CB[n]s. CB[6] was proposed as a thermodynamic sink due to its slow kinetics for complex formation with benzyl ammonium. The requirements for the guest complexation with CB[6] were that the kinetics had to be on the minute to hour time scale and the equilibrium constant with the guest had to be the highest of the three host molecules. CB[7] was chosen as the kinetic trap of the self-sorting system. The requirements for the CB[7] complex were that the kinetics had to be on the millisecond to second time scale and the equilibrium constant needed to be lower than the equilibrium constant of the guest@CB[6] complex, but higher than the guest@β-CD complex. The kinetic and thermodynamic requirements between the guest molecule and CB[7], and between the guest molecule and β-CD were met. The kinetics between CB[6] and the guest molecule were on the hour time scale, meaning the kinetic requirement was met, however, the equilibrium constant was found to be lower than the equilibrium constant between the guest molecule and CB[7]. The results in this work showed that the rational design of kinetically-trapping self-sorting systems is possible, but some modifications to the structure of the guest molecule is required to make this self-sorting system work.

Table of Contents

List of Tables

List of Figures

List of Charts

List of Schemes

List of Abbreviations

A	Absorbance
α_x	Pre-exponential factor
A	Adenosine
@	Inclusion complex
BH_3-THF	Borane tetrahydrofuran
Bn^{2+}	Benzidine
BNA	N-Benzyl-2-naphthylamine
BNA^+	N-Benzyl-2-naphthylammonium
C	Cytosine
c	Concentration
Cob^+	Bis(cyclopentadienyl)cobalt (II)
CB[n]	Cucurbit[n]uril
CB[5]	Cucubrit[5]uril
CB[6]	Cucurbit[6]uril
CB[7]	Cucurbit[7]uril
CB[8]	Cucurbit[8]uril
CD	Cyclodextrin
cm	Centimeters
°C	Degrees celcius
DCLs	Dynamic Combinatorial Libraries
DNA	Deoxyribonucleic Acid
DFT	Density Functional Theory
ε	Molar extinction coefficient
eq	Equation
eq	Equilibrium
G	Guest
G	Guanosine
H	Host
h	Hour
HCl	Hydrochloric Acid

k_{obs}	Observed rate constant
k_{+}	Association rate constant
k_{-}	Dissociation rate constant
l	Pathlength of light
MV^{2+}	Methyl viologen
$MV^{\bullet+}$	Electrochemically reduced methyl viologen
M	Molar
mM	Millimolar
μM	Micromolar
μL	Microliter
mL	Milliliter
mg	Milligram
MOFs	Metal Organic Frameworks
$MDAP^{2+}$	2,7'-dimethyl-diazapyrenium
nm	nanometer
NMR	Nuclear Magnetic Resonance
NpH^{+}	1-(2-Naphthyl)-ethylammonium
NpOH	2-Naphthylethanol
T	Thymine
UV-Vis	Ultraviolet-Visible

Acknowledgments

I would like to express my gratitude to Dr. Cornelia Bohne, my supervisor, for her support, help and guidance through my graduate degree. Outside her academic leadership, Dr. Bohne has taught me invaluable life lessons and has helped shape my understanding of the world. I would like to extend that gratitude to Luis Netter for his technical and software support, as well as his conversation about world politics and soccer.

I would like to thank the present and previous members of the Bohne group: Suma, Mehraveh, Jessy, Helia, Ankur, Guan, Sree, Prakhar, Elisa, Alessandra, Amilcar and Stas; for their conversation and academic support through different phases of my graduate degree. I would like to deeply thank Dr. Neil Burford for allowing me, an inexperienced biochemistry student, an opportunity to experience working in a chemistry laboratory, which inspired my change from biochemistry to chemistry for graduate school. I would like to thank my committee for their patience and input on how to successfully complete my degree. I would like extend a special thank you to Dr. David Berg for taking the time to help me synthesize a compound used in chapter 3.

I need to express my deepest thank you to my parents and close family: mom, dad and aunt Joan for their unwavering support through all stages of my life that has led to this point. They have all done more for me than anyone could every ask or expect of a family member, and I do not believe they can understand how much I appreciate everything they have done.

I would also like to thank Dean Kerpan, manager of Capital Ballroom, for always being supportive of my education and working with my schedule to allow me to stay employed throughout my graduate degree.

I would like to express my gratitude to my friends whom are an extension of family to me. Dylan, Stewart, Taylor S., Liam, Hayden, Bernard and Alex T., I appreciate how you have all stuck by my side through the highs and the lows, and through the being distant when I was busy. You are all the family I chose, and there are no other people I would rather be around.

Dedication

To Mom, Dad, and all my friends and family who have helped me along this journey

Chapter 1: Introduction

1.1 Supramolecular Chemistry

Chemistry has evolved from the combination of atoms that form elaborate molecules, to supramolecular systems built from non-covalent interactions between molecules.[1-3] Supramolecular chemistry is commonly referred to as chemistry beyond the molecule.[4] The scale of supramolecular structures ranges from simple host-guest complexes to large molecular assemblies.[2, 4-5] The non-covalent interactions that are responsible for the assembly of supramolecular structures are reversible and cause supramolecular structures to be dynamic.[6] The reversible interactions in supramolecular assemblies are ionic, ion-dipole, hydrogen bonding, dipole-dipole and π-π interactions, and Van der Waals dispersion interactions.[3-4, 7-9] The hydrophobic effect can play a large role in the assembly of supramolecular structures, however the hydrophobic effect is not an interaction.[10-11] The hydrophobic effect defines the phenomenon that two non-polar entities will associate with one another in polar solvents, decreasing the interactions between the non-polar solutes and polar solvent molecules.[10-11] The non-polar molecules lose entropy as they associate with one another, but the system overall gains entropy from the release of coordinated solvent molecules. The association of the two non-polar molecules cause the displacement of polar solvent molecules associated with them which increases the entropy on the polar molecules. The polar solvent molecules lose enthalpy as the bonds between then break when the non-polar solute molecules associate with each other; however, the system gains enthalpy as the released polar solvent molecules are released and increase the number of hydrogen bonds per solvent molecule in bulk solution.[10-11]

Supramolecular systems have gained interest as synthetic surrogates of biological structures.[3, 8-9] The interest in complex supramolecular systems is that the majority of biological structures are supramolecular assemblies.[3-4, 12] The secondary structure of proteins is made from covalent bonds in the back bone of the protein, however the majority of tertiary and quaternary structures in proteins are a result of the same reversible, non-covalent interactions described above.[3, 13] The double helix of DNA is another example of

a biological, self-assembled, supramolecular structure that is associated through reversible, non-covalent interactions.[3, 6] Beyond individual, biologically relevant structures, the entire biological cell is comprised of compartmentalized, self-assembled, supramolecular structures.[3, 14]

There are two major categories of supramolecular molecular systems: host-guest complexes and self-assembled structures. Self-assembly is a broad topic that refers to the spontaneous association of supramolecular structures from individual components in solution. Self-assembly is often used to define the assembly of large metal-ligand structures such as MOFs.[2, 15-18] Host-guest complexes are a form of self-assembly, in that host-guest complexes spontaneously form, however, host-guest complexes describe the encapsulation of a smaller guest molecule within a larger supramolecular host (scheme 1.1).[3, 5, 9, 12, 19]

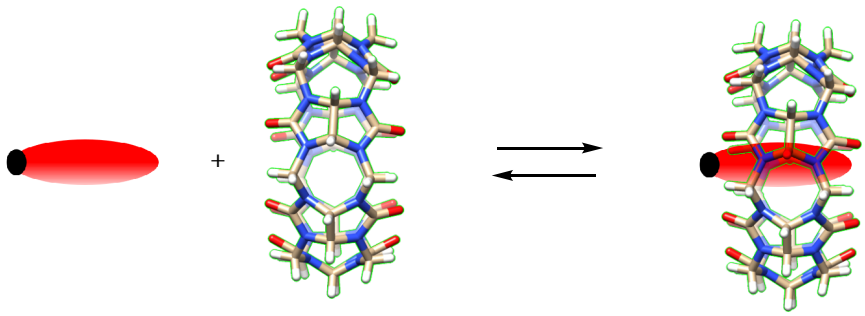

Scheme 1.1 Schematic representation of the formation of a host-guest complex.

Host-guest chemistry uses a host molecule like synthetic receptors for smaller guest molecules.[20-22] The first examples of host-guest chemistry came from the binding between crown ethers and alkali metal cations.[23] From the crown ethers, the recognition of metal cations was continued with bicyclic cryptands.[12, 23] The array of host molecules as synthetic receptors has expanded. The hosts used in supramolecular chemistry are calixarenes, cucurbit[n]urils, cyclodextrins, pillarenes and more.[9, 12, 19, 24] The different families of host-molecules have different selectivities for small guest molecules with respect to size and charge.[12] Cucurbit[n]urils show an increase in equilibrium constants with guest molecules that have a positive charge of ~10^3 M^{-1} over the conjugate neutral guest species,[24] whereas, cyclodextrins show a decrease in equilibrium constants with a given guest molecule when a charge is introduced to that guest molecule.[25] The interest in host-guest complexes is in the fields of drug delivery and synthetic receptors because the reversible interactions are similar to the interactions found in protein-substrate or protein-drug interactions.[12, 19, 23]

Host-guest complexes have applications in cross-linked hydrogels,[26] catalysis,[27] cell adhesion,[28] protein recognition,[29] self-assembly,[2, 15-16, 18, 30-33] self-sorting[31-39] and sensors.[40]

1.2 Supramolecular Dynamics

The reversibility of the intermolecular interactions in supramolecular systems is an important aspect to study in order to rationally design supramolecular systems.[17, 41-42] In theory, all chemical reactions are reversible, however supramolecular structures, such as host-guest complexes, are reversible on the human time scale.[12, 42] Understanding the dynamic nature of how supramolecular systems work goes beyond studying the thermodynamics and structural features of a system, and requires an understanding of the kinetics of the system.[17, 38, 42]

By studying the dynamics of a system, the thermodynamic and structural information can be extracted (scheme 1.2).[42-43] When a molecule is synthesized, or a host-guest complex assembles, structural information can be acquired from techniques like X-ray crystallography, mass spectrometry and NMR spectroscopy.[43] Thermodynamic information of a host-guest complex can be determined by NMR, fluorescence or UV-Vis spectroscopies.[43] It should be noted that NMR, UV-Vis and fluorescence spectroscopies can also be used to study the kinetics of a system. The acquired structural information of the system can give insight into the thermodynamic results, and vice-versa, the thermodynamic results can give information on the structural aspects of the system.[42-43] Neither the structural nor thermodynamic information of the system can give information about the dynamics of the system.[42-43] An evolving system may have transient species that are visible when studying the kinetics in real time, but not visible when only studying the thermodynamics.[21, 44] The equilibrium constant, a thermodynamic parameter, is the ratio of the association and dissociation rate constants.[41] Two systems can have the same equilibrium constant, but the time scale of their kinetics can be orders of magnitude apart, which has applications in pharmacology and drug delivery.[45-46]

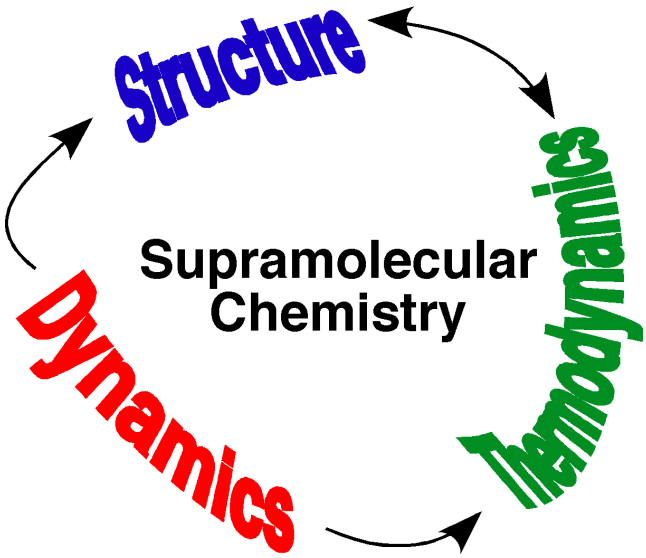

Scheme 1.2 Representation of the relationship between dynamics, structure and thermodynamics in supramolecular systems. Reprinted with permission from Bohne's work.[43] Copyright (2006) American Chemical Society.

The difficulty in studying supramolecular dynamics is measuring the kinetics in real time. The traditional method of measuring kinetics is using relative rates. Using relative rates relies on the comparison of the rate of product generation between a known standard reaction and the desired unknown reaction.[47] The relative rate method is contingent on the mechanism being similar, so the rates can be directly compared. In supramolecular systems, there is a lack of 'standard' reactions and the mechanistic diversity of binding is still being investigated.[21, 44, 47-51] Therefore, the study of the kinetics of supramolecular systems is dependent on small, sudden changes in concentration, pressure or temperature to the system that can be analyzed on different time scales: chemical relaxation techniques.[41] The size of the components of the supramolecular system are on the nanometer scale and the diffusion controlled limit of these species is in the nanosecond to microsecond time scale for concetrations used ($\leq$ 1 mM).[52-53] Because of the size scale of the components and the diffusion rates, the choice of analysis technique for kinetic studies needs to be on the nanosecond to second time scale. Relaxation techniques, where a small chemical perturbation is introduced to the system, are available to study these systems on different time scales.[41, 54]

1.2.1 Relaxation Kinetics

Relaxation kinetics are used to study systems that have been exposed to a chemical perturbation, as that system evolves to equilibrium.[41] Common chemical perturbations include concentration jump, electric-field jump, pressure jump and temperature jump methods.[41, 54] To study relaxation kinetics, the chemical perturbation must be faster than the time scale of the chemical reaction.[54] The experimental work conducted in this thesis was conducted using a concentration jump method, where two solutions are mixed in a 1:1 ratio.

The formation of a simple 1:1 host:guest complex is given by eq. 1.1, where H represents the host molecule, G represents the guest and G@H represents the host:guest complex.

$$H + G \underset{k^-}{\overset{k^+}{\rightleftharpoons}} G@H \qquad \text{(Eq. 1.1)}$$

The rate equation that defines the relaxation kinetics following a chemical perturbation of the system is given by eq. 1.2:

$$\frac{d[G@H]}{dt} = k^+[H][G] - k^-[G@H] \qquad \text{(Eq. 1.2)}$$

At equilibrium, eq. 1.2 is equal to zero because the forward rate of reaction is equal to the rate for the reverse reaction. Equation 1.3 shows the relationship between the rate constants and the thermodynamic equilibrium constant (K_{11}):

$$K_{11} = \frac{[G@H]}{[H][G]} = \frac{k^+}{k^-} \qquad \text{(Eq. 1.3)}$$

If the relaxation kinetics are conducted under pseudo-first order conditions, where the concentration for the host molecule is in large excess over the guest concentration ($[H] >>> [G]$), the perturbed equilibrium can be expressed as an exponential function. From the

exponential function, an observed rate constant (k_{obs}) can be obtained. The observed rate constant is related to the association and dissociation rate constants as shown in eq. 1.4.

$$k_{obs} = k^{+}[H] + k^{-} \quad \text{(Eq. 1.4)}$$

More complex systems require the kinetics to be fit to a sum of exponentials function.[41] The number of relaxation processes in any chemical system is equal to the number of individual rate equations for a system.[41] The constraints for the analysis of the kinetics for these systems with multiple relaxation processes are that all the relaxation processes must be on the time scale for the kinetic measurements and that the concentration changes of the species being monitored be above the detection limit of the analysis technique used.[41] For multiple step mechanisms, the relaxation times are dependent on the association and dissociation rate constants of the multiple processes, meaning the equilibria of the various dynamic processes are coupled. The association process time scale of a reaction for a bimolecular reaction can be slowed down by manipulating the concentration of species available to form the host-guest complex.[41] The dissociation rate constant of a simple host-guest system is a unimolecular process that is independent of the concentration of host and guest.

1.2.2 Stopped Flow

The concentration jump method used in this thesis to study the relaxation kinetics of host-guest complexes is stopped flow. Scheme 1.3 shows the schematic set up of a stopped-flow device. In a stopped-flow device, the two solutions, one in each syringe, are mixed under pressure into a mixing chamber in under 1 ms. For a host-guest system, one syringe is loaded with the host molecule and the other syringe is loaded with the guest molecule. Because the solutions are mixed in a 1:1 ratio, the host and guest solutions, in the syringes, are two-fold the experimental concentrations. The mixed solution leaves the mixing chamber and enters the analysis chamber in 1-2 ms, which is the time resolution of a stopped-flow experiment. When the sample enters the analysis chamber, it is continuously irradiated and the change in absorption or fluorescence is detected over a desired time scale.

As stated in the name, the key feature of a stopped-flow device is the stop syringe that keeps the 1:1 mixed solution in the analysis chamber until the reaction is complete. The stop syringe is what differentiates a stopped-flow device from continuous flow methods.

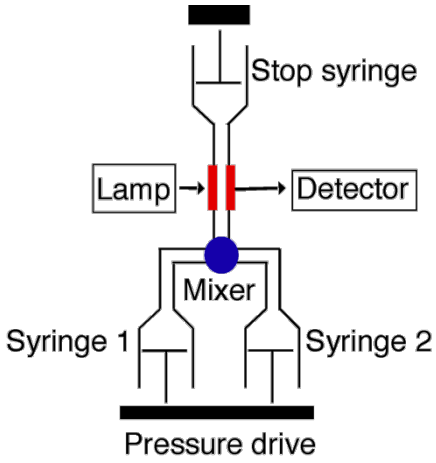

Scheme 1.3 Schematic diagram of a stopped-flow device. Reprinted with permission by John Wiley & Sons, Inc from Bohne's work.[55]

Stopped-flow experiments can be conducted analyzing the change in absorption or fluorescence. Fluorescence measurements are more sensitive than absorption measurements. Due to the sensitivity of fluorescence measurements, stopped-flow fluorescence experiments can easily be conducted under pseudo-first order conditions. However, absorption experiments cannot be done under pseudo-first order conditions with respect to the host molecule as it is done in fluorescence experiments. The absorption of a guest molecule is dependent on the concentration and the path length of light through the sample (eq. 1.5). In equation 1.5, A is the absorbance, l is the path length of light, c is the concentration of guest molecule and ε is the molar absorptivity coefficient. Experiments can be conducted in pseudo-first order conditions with respect to the guest by decreasing the path length of light and increasing the concentration of guest molecules. The path length of a stopped-flow device can be changed between 1.0 cm, which is a common path length in absorption experiments, and 0.2 cm which allows for elevated concentrations of guest.

$$A = l\varepsilon c \qquad \text{(Eq. 1.5)}$$

1.2.3 Stopped-flow kinetic traces

Stopped-flow kinetic traces show a change in absorption or fluorescence with respect to time. The core components of stopped-flow kinetic traces that must be seen are the growth or decay of signal, and the kinetics must reach equilibrium on the analyzed time scale, which is shown by the trace flattening out. Figure 1.1 shows some hypothetical kinetic traces acquired from a fluorescence stopped-flow experiment.

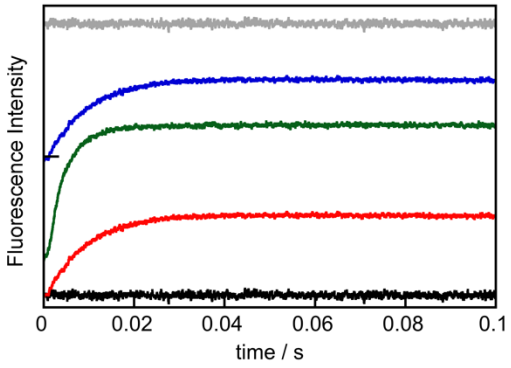

Figure 1.1 Hypothetical examples of kinetic traces seen on a stopped-flow device for a host-guest system. The black line represents a baseline trace where the guest molecule is mixed with solvent. The red trace represents the mixing of a host solution and guest solution where all the kinetics are captured in the time window measured. The green trace represents the mixing of host and guest solutions with a component of the kinetics having a relaxation rate constant close to the mixing time of the instrument. The blue trace represents the mixing of host and guest solutions with an offset. The grey kinetic trace represents the mixing of the host and guest solutions where all the kinetics are faster than the mixing time of the instrument.

The red trace in figure 1.1 shows what is considered “a simple” kinetic trace. The red trace is considered a simple trace because the kinetics begin from the baseline, and the kinetics reach equilibrium on the desired time scale. The green trace shows a small change in fluorescence intensity from the baseline before the growth of the kinetic trace becomes visible. This small change in fluorescence intensity is called an offset. To determine if this is a true offset or an artifact of the mixing time of the device, the fit to a sum of exponentials function (eq. 1.6) needs to be examined. If the fit line extrapolates to the baseline, the offset is an artifact of the mixing time of the device. An artifact of the mixing time means that there is a relaxation process that has an observed rate constant that is close to the mixing

time of the device (k_{obs} = 500-1000 s^{-1}). The green trace, therefore, is an example of a kinetic trace that fits to the sum of multiple exponentials function, with one relaxation time that is close to the mixing time of the device. The blue kinetic trace shows a trace that has a real offset, followed by kinetics on a millisecond time scale. When the blue trace is fit to a sum of exponentials function, the fit line does not extrapolate to the baseline. This means that there is a relaxation process that is faster than the time resolution of the device, followed by a slower process that is on the millisecond time scale. Finally, the grey trace only shows a change in amplitude with no kinetics. This means that all the kinetics are faster than the time resolution on the stopped-flow device.

$$\Delta I = \alpha_0 + \alpha_1 e^{-k_{obs1}t} + \alpha_2 e^{-k_{obs2}t} + \alpha_3 e^{-k_{obs3}t} \quad \text{(Eq. 1.6)}$$

Equation 1.6 shows the fit to the sum of exponentials function equation. In equation 1.6, ΔI represents the total change in absorption or fluorescence intensity. The α_x (x = 0-3) terms refer to the pre-exponential factors for each relaxation process, α_0 is the amplitude for any relaxation process that is faster than the time resolution of the instrument used. The observed rate constant (k_{obs}) for each relaxation process is multiplied by the total time and raised to an exponential.

1.3 Systems Chemistry

Systems chemistry is an emerging field that studies complex mixtures of molecules that give rise to new emergent properties that are not intuitively predictable when studying the components in isolation.[5, 56-59] Systems chemistry is being developed in parallel with systems biology to understand the complex chemistry of the origin of life.[56, 60] Beyond assisting systems biology, various fields are adopting a systems chemistry approach to understand the inherent complexity of chemical systems, that have been traditionally viewed as 'simple'.[5, 14, 56-59] A systems chemistry approach has become integral in the discovery of new drugs,[61] self-assembly,[2, 56] self-sorting,[31, 37-38, 62] prebiotic chemistry,[60, 63] self-replicators,[64] small molecule synthesis[57] and dynamic combinatorial libraries.[65-66]

Biological systems operate in a compartmentalized, kinetic state.[14, 63] Due to the reversible nature of the interactions in supramolecular systems, supramolecular systems are ideal candidates to study the assembly of complex systems on their way to equilibrium, in kinetic traps or systems considered far from equilibrium.[5]

A systems chemistry approach to synthetic mixtures, such as dynamic combinatorial libraries (DCLs), looks to analyze the thermodynamic outcomes of different supramolecular structures when the stoichiometry is altered.[66] The control of product distribution is reported by controlling the stoichiometries of the reactants, however there lacks a bottom up approach for the rational design of these systems.[56-57, 66] Scheme 1.4 shows an examples of evolving mixtures of molecules that end in thermodynamically controlled supramolecular synthetic assemblies.[67]

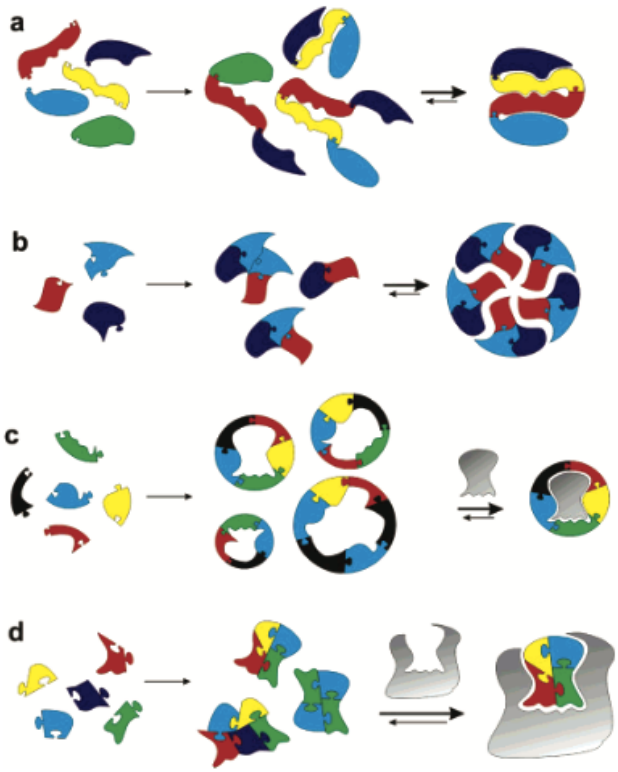

Scheme 1.4 Schematic representation of different ways dynamic combinatorial libraries made of multiple components can evolve with and without external inputs, such as substrates or macrocyclic hosts. Reprinted with permission from Otto's work.[67] Copyright (2006) American Chemical Society.

Supramolecular host-guest chemistry has become a useful tool in systems chemistry.[5] Host molecules can be seen as synthetic receptors to design more simple versions of biological

systems.[2, 5, 38, 56] Due to the dynamic nature of host-guest complexes, they have been proposed as an avenue to study kinetically trapped systems and systems that are far from equilibrium.[5] Within systems chemistry, a principal use of host-guest chemistry is in self-sorting systems.[2-3, 15, 30-31, 37-38] The host-guest self-sorting systems analyze complex mixtures of multiple host molecules and multiple guest molecules for their kinetic and thermodynamic products.[1, 37-38] The host-guest systems are analyzed with no real rational design on how to study systems in kinetic traps or far from equilibrium states; therefore, there is a need for the rational design of systems that can be studied in kinetic traps.

1.4 Self-sorting and self-assembly systems

Self-sorting and self-assembly systems are a division of systems chemistry that describes the organization of complex mixtures through self-recognition or favourable interactions. The terms self-sorting and self-assembly tend to be used interchangeably in the literature, however there are slight differences. Self-sorting is defined as the recognition of self- or non-self in complex mixtures through complementary binding motifs.[32-33, 36, 39, 62] Self-sorting systems are largely considered a part of systems chemistry as self-sorting systems rely on complementary recognition motifs that result in an ordered system evolving from a complex, disordered system.[5, 56, 58] Self-assembly has a more elastic definition.[16] Self-assembly is typically defined as the auto assembly of 'disorganized' components of a system into 'organized' assemblies.[2, 16, 31] When self-assembly and self-sorting are used to define the same system, the term self-sorting has been defined as the mutual recognition of complementary species in an artificial self-assembly.[36] This definition suggests that the formation of a dynamic supramolecular self-assembled structure requires a degree of self-sorting.[36] DNA is a biological example of a self-assembled structure that is created by the self-sorting recognition of A-T and G-C base pairs.[36] Self-assembled metal-organic frameworks (MOFs) are created through a degree of self-sorting, and the MOFs can then be used as a self-sorting component for the recognition of guest molecules in complex mixtures.[31-33] These examples show that self-sorting is a major pathway that results in self-assembled supramolecular structures.[2, 15-16, 33, 36]

In order to develop an understanding of the rational design of the self-assembly of supramolecular structures, a fundamental understanding of how to rationally design self-sorting systems is required. Self-sorting is divided into two main categories: narcissistic and social self-sorting.[36, 38-39] Narcissistic self-sorting refers to the recognition of self in complex mixtures.[36, 38] Social self-sorting refers to the recognition of non-self within complex mixtures.[36, 38] For the work presented in this thesis, the focus will be on social self-sorting.

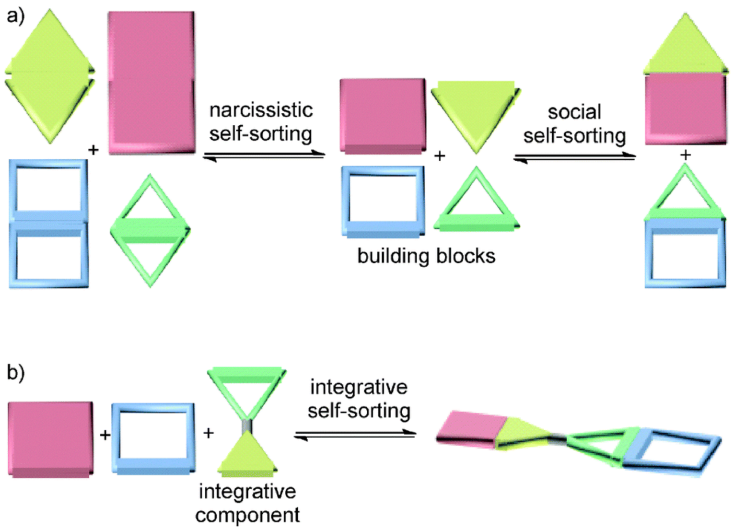

Scheme 1.5 Schematic representation of different self-sorting pathways. Reprinted with permission from the Royal Society of Chemistry, 2015. Scheme reprinted from Zhenfeng's work.[34]

Supramolecular host molecules (calixarenes, cucurbit[n]urils, cyclodextrins, pillarenes) are macrocycles that can act as synthetic receptors.[3, 5, 68] Due to the dynamic nature of host-guest interaction, supramolecular hosts are candidates for the development of self-sorting systems.[38] Self-sorting systems are can be used to design systems that have kinetic traps or exist in far-from equilibrium states.[5, 56] Kinetically trapping an evolving system is dependent on equation 1.3. An evolving system will eventually end up at its thermodynamic equilibrium; however, the introduction of a kinetic trap with a lower equilibrium constant, but faster kinetics, would allow for self-sorting systems to be used to study kinetically trapped systems within systems chemistry.

1.5 Cucurbit[n]uril-guest chemistry

Cucurbit[n]urils (CB[n]) are a family of macrocycles made from the reaction of glycouril units with paraformaldehyde through an acid-catalyzed dehydration.[69] The synthesis of CB[n]s was first reported in 1905,[70] however the crystal structure and physical characterization of the first CB[n], CB[6], was worked out by Mock and coworkers in the 1980s.[24, 69] Early characterization of CB[6] showed that it has a similar size to the naturally occurring α-cyclodextrin (CD), however the structure of CB[6] is more rigid, and is symmetrical, where CD's are not.[24, 69] Further, both CB[6] and α-CD have a hydrophobic cavity capable of binding a hydrophobic guest molecule, however, the carbonyl lined portals of CB[6] are capable of stabilizing cationic charges on guest molecules.[24] The stabilizing of a positive charge is a result of ion-dipole interactions between the cationic charge of the guest and the carbonyl line portals of the CB[n]s (chart 1.1). The result of the stabilized cationic charge is an increase in the pK_a of the guest molecules when bound to a CB[n].[44, 71-73] In 2000, Kim and coworkers showed the synthesis and isolation of different homologues of CB[n]s (n = 5, 7, 8), with different sizes and selectivities (chart 1.2).[69, 74]

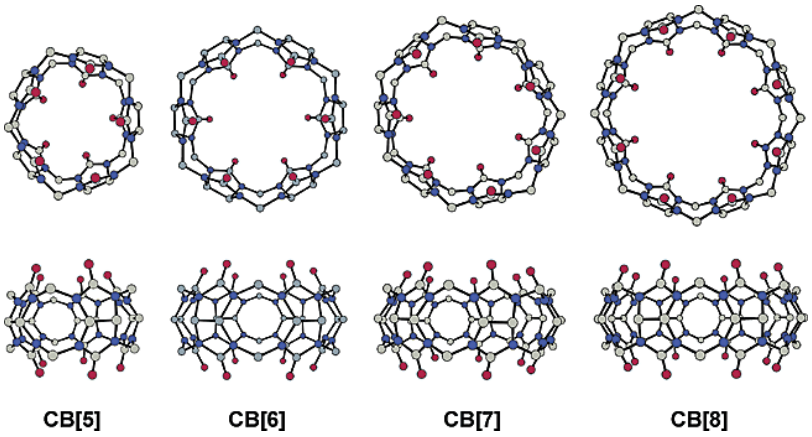

Chart 1.1 Representation of the sizes of the different CB[n] homologues. The chart was reconfigured with permission from Kim's work.[69] Copyright (2003) American Chemical Society.

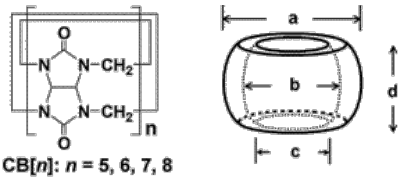

		CB[5]	CB[6]	CB[7]	CB[8]
outer diameter (Å)	a	13.1	14.4	16.0	17.5
cavity (Å)	b	4.4	5.8	7.3	8.8
	c	2.4	3.9	5.4	6.9
height (Å)	d	9.1	9.1	9.1	9.1
cavity volume (Å^3)	-	82	164	279	479

Chart 1.2 Tabulation of the sizes of the different CB[n] homologues. The chart reconfigured with permission from Kim's work.[69] Copyright (2003) American Chemical Society.

The different homologues of CB[n]s have different selectivities based on the size of their cavities.[69] A large driving force for the binding of guest molecules to CB[n] is the release of hydrogen bond deficient water within the cavities of CB[n]s.[75] CB[5] is unique in the family of CB[n]s because of its small cavity. CB[5] is small enough that it is calculated to have no water molecules in its cavity.[75] CB[5] can form exclusion complexes, where the cationic charge of the guest associates with the carbonyl line portals but the aliphatic or aromatic group remains exposed to solvent,[76] CB[5] can also bind small di-atomic molecules such as O_2 and N_2.[69] CB[6] is selective for binding alkyl-ammonium cations, and can bind small aromatic ammonium cations such as benzylammonium.[21, 69, 76] CB[7] has received increased attention compared with the other homologues in the CB[n] family due to its increased solubility, ability to bind larger aromatic guests and form complexes with higher equilibrium constants than the biotin-streptavidin complex.[44, 49, 77-78] Finally, CB[8] is unique in the series of CB[n]s as it is large enough to accommodate two aromatic guest molecules in a 1:1:1 guest:guest:host hetero-terniary complex.[20, 26] One of the guest molecules in CB[8] is an electron deficient molecule, such as methyl viologen, and the second guest will be an electron rich guest molecule such as a hydroxy-naphthalene derivative. The two guests form charge transfer complexes in the cavity of CB[8].[20, 26] Beyond the selectivity for different binding motifs, the CB[n] homologues have a wide

range of kinetic time scales for the formation CB[n]-guest complexes. CB[n]s have been proposed as supramolecular containers for catalysis,[79] drug delivery,[72, 80] hydrogels,[20, 26] self-sorting[37-38] and other fields. Because of the increased stability of the interactions between CB[n]s and guest molecules, the complexes tend to have slower kinetics than the kinetics of CD-guest complexes.[81] The kinetics of CB[n] systems can be on the millisecond to minute time scale, whereas similar CD-guest systems will be faster than the millisecond time scale.[21, 38, 44, 49, 79, 81]

1.6 CB[n] affinity for metal cations

The carbonyl lined portals of CB[n]s bind to cationic charges.[49, 82-86] CB[n]s bind to metal cations with higher equilibrium constants than other families of host molecules.[79, 86] Within the family of CB[n]s, different homologues have different selectivities and different equilibrium constants for metal cations.[50, 84, 87-88] For example, the reported equilibrium constants between sodium cations (Na^+) and CB[6][48] are as high as an order of magnitude higher than the equilibrium constants between Na^+ cations and CB[7].[49] However, the community of scientists who work with CB[n]s are not in complete agreement on whether one or two metal cations bind to the portals of CB[n]s.[48-51, 82-83, 85-90]

Density Functional theory (DFT) calculations support that two metal cations will bind to CB[n]s with one at each portal.[50, 88] Scheme 1.5 represents the schematic representation of the sequential binding of two metal cations to a CB[n]. The maximum value for the second equilibrium constant between a metal cation and a CB[n] is one quarter the equilibrium constant of the first equilibrium constant.[91] The reason for this decrease for the metal second binding constant is derived from equation 1.3 discussed earlier: one portal of the CB[n] is already bound to a metal cation, the association rate constant of the second metal cation is a maximum of one half of the first association rate constant. Once the second cation is bound, there are two opportunities for a metal cation to dissociate from the complex, therefore the dissociation rate constant of the two-metal cation complex is double what the dissociation rate constant is for the single metal cation complex. Recall, the equilibrium constant is the ratio of the association and dissociation rate constant, therefore, if the association rate constant is half and the dissociation rate constant is doubled, the

maximum value of the equilibrium constant is one quarter the first metal cation binding to a CB[n] equilibrium constant.[91]

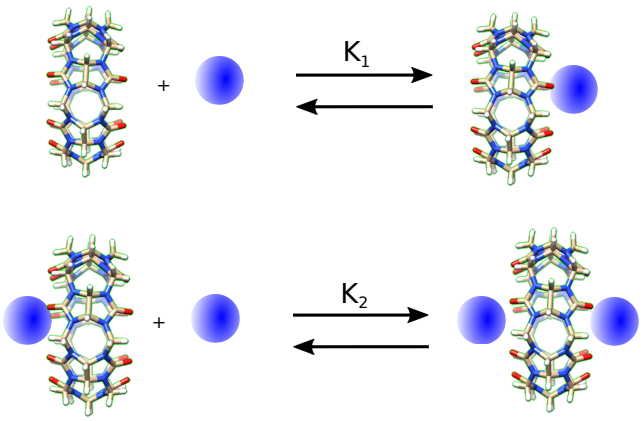

Scheme 1.6 Sequential binding of metal cations to CB[7].

The presence of metal cations have been known to decrease the overall equilibrium constant between a guest molecule and CB[n]s.[38, 92-95] The metal cations present competitive equilibria for the binding of CB[n]s, reducing the amount of free CB[n] in solution to bind the guest molecule which decreases the overall equilibrium constant (eq. 1.7).[49] The relationship between the overall binding constant and the concentration of cations should be linear when only one metal cation binds the CB[n]s. In the reality that two metal cations bind to CB[n]s, the relationship between the overall equilibrium constant and the concentration of metal cations appears linear at elevated concentrations of metal cations.[49] It is at low concentrations of metal cations that there is a deviation from linearity in the relationship: the overall equilibrium constant is lower than what is predicted from a linear trend.[49]

$$\beta_{11} = \frac{K_{11}}{1+K_1[M^{y+}]+K_1K_2[M^{y+}]^2} \qquad \text{(Eq. 1.7)}$$

Most mechanistic work reported in the literature of CB[n]-guest systems acknowledge that two metal cations bind to a single CB[n].[38, 48-49, 82, 94] In the publications that report only a single cation binding to CB[n], the experiments tend to be conducted in the concentrations of metal cations where the relationship appears linear regardless of the considerations of one or two metal cations binding CB[n], and the mechanism of CB[n]-guest binding is not

central to the work.[92-94] There is a recent publication that suggests that the binding of one or two metal cations is dependent on the identity of the metal cation and the homologue of CB[n].[86] The equilibrium constants were determined using isothermal calorimetry, however, on examination of the fit of the data it becomes clear that there are large deviations from the fit when the one cation model is suggested.[86] Further, some of the authors of this paper have published previous mechanistic studies that state that two metal cations bind to a single CB[n].[48] The equilibrium constants published for the 1:1 metal-CB[n] complexes also appear to be quite high in this paper. For example, the equilibrium constant between CB[7] and Ca^{2+} is published at 1.7×10^4 M^{-1}.[86] The problem with an equilibrium constant this high between a metal cation and CB[7] is there will be no significant binding between the guest and CB[7] if the concentration of Ca^{2+} cation is 100 mM, if a guest molecule has an equilibrium constant of 10^6-10^7 M^{-1} and the guest concentration is ~ 1-5 μM. The work presented in this thesis will show that there is guest binding at elevated concentrations of Ca^{2+}, and uses the assumption that two metal cations bind to CB[n]s.

1.7 Objectives

The objective of this thesis is to understand the complexity of CB[7]-guest systems, and apply that complexity to design a CB[n] based self-sorting system. In chapter 2, the influence of biologically relevant metal cations (Ca^{2+} and Na^{+}) on the dynamics of a previously studied CB[7]-guest system is examined. The dynamics are assessed for the effect the concentration and identity of the metal cations has on CB[7]-guest binding mechanisms.[49] In chapter 3, the influence of changes in guest structure on the time scale of the dynamics of CB[7]:guest complexes is examined using three aromatic dications as guests. This project will have an impact on the development of drug delivery systems, as the design shifts towards slow dynamics between a drug and a drug carrier system in order to decrease undesirable competitive interactions with off-target species.[46] In chapter 4, the understanding of complexity of CB[n]-guest chemistry and understanding of how guest structure affects the dynamic time scales will be used to rationally design a kinetically trapped self-sorting system.

Chapter 2: Introducing complexity in CB[7]-guest binding mechanisms with biologically relevant metal cations.

Kevin A. Vos, Christie Lombardi, Sree Gayathri Talluri and Cornelia Bohne

SGT and CB conceived the idea of testing other biological cations on the NpH^+@CB[7] system after the 2011 published work[49] and identified Ca^{2+} cations as the metal cation to study due to an apparent decreased dissociation rate constant. CL did the preliminary stopped-flow experiments between NpH^+ and CB[7] in the presence of different Ca^{2+} cations. KV analyzed the data, conducted the steady-state fluorescence experiments and stopped-flow kinetic experiments. KV proposed revisiting the mechanism between NpH^+ and CB[7] in the presence of Na^+ cations.

2.1 Introduction

2.1.1 Background

Supramolecular chemistry, as a discipline, has traditionally existed in a space of examining intermolecular interactions in isolation.[56, 66] Development of new analytical techniques has allowed for the analysis of more complex mixtures of molecules. This has given rise to the field of systems chemistry.[56, 60, 66] Systems chemistry is the study of multi-variable, complex systems.[60, 66, 96] Studying complex mixtures can give rise to new emergent properties that are not intuitively predictable when examining the individual components in isolation.[66] An overarching goal of systems chemistry is to assist biology in understanding the beginning of life, and create model systems that can be analogous to biological systems.[60]

The importance of studying complex mixtures has brought systems chemistry to the forefront of various fields. Dynamic combinatorial libraries (DCLs), from a synthetic perspective, have received much of the attention within systems chemistry.[56, 65-66] Research on DCLs relies on the mixture of components, usually a metal center with varying concentrations of ligand, to study how concentration ratios can control the distribution of products. Drug discovery has begun to adapt to the necessity of studying complex mixtures due to the tendency of drugs to bind undesirable targets.[63] Because of this promiscuity of drugs, chemical biology is recognizing the need to test drugs against many targets at once to understand the cross-reactivity between drugs and off-target structures. Further,

prebiotic chemistry, in the quest to solve questions surrounding the origin of life, studies how complex mixtures come together, intersecting with systems chemistry.[63] However, most of the studies in these fields rely on the mixing of reactants and analyzing the products that are produced, keeping the field of systems chemistry in a state of trial and error. There is the need for more work at the ground level in systems chemistry to move this field from a trial and error phase, to a phase of rational design. Understanding the mechanistic evolution of complex systems would give chemists the ability to control, design and divert complex mixtures to desired outcomes.

Supramolecular chemistry is well situated to be integrated into systems chemistry because of the reversible, non-covalent nature of supramolecular interactions; further, most biological structures are supramolecular assemblies.[96] Cucurbit[n]urils (CB[n], n=5-8,10, chart 2.1) are a family "pumpkin-shaped" macrocycles.[44, 49, 79, 93] Of the CB[n] family, CB[7] has received increased attention due to its higher solubility and its ability to form inclusion complexes with equilibrium constants as high as 10^{17} M^{-1}.[77] CB[n]s have applications in catalysis,[97-99] sensing,[100-101] materials,[20, 26] and self-sorting.[38, 102]

In CB[n]-guest systems the presence of auxiliary species other than a CB[n] and a guest molecule, such as metal cations, can have profound effects on the thermodynamic outcome, or the mechanistic evolution of a system.[49, 51, 82-83, 85, 92-94, 103] Despite the importance of these auxiliary species, their presence is frequently neglected when reporting equilibrium constants of CB[n]-guest complexes. Buffered solutions, and solutions containing Na^+ cations with concentrations between 0.1 and 0.2 M, are frequently used for systems where equilibrium constants between CB[n]s and guests are determined, without regarding the affect the metal cations or buffers have on the binding efficiency of the host-guest complex.[92, 104]

In 2004, the effect that the concentrations of Na^+ and Ca^{2+} cations had on the equilibrium constant between methyl viologen and CB[7] was examined.[92] To determine the effect metal cations had on the stability of the CB[7]-guest complex, the binding constant between methyl viologen and CB[7] in the absence of metal cations needed to be determined. However, the equilibrium constant in the absence of metal cations was determined in the presence of 0.030 M tris-buffer. The authors acknowledged that the equilibrium constant between methyl viologen and CB[7] they reported in 0.030 M tris-

buffer is close to what had been reported by others in 0.050 M tris-buffer and in 0.2 M NaCl with no tris-buffer. The paper acknowledges that the protonated tris-buffer may compete for the binding of CB[7] with methyl viologen. Therefore, though the results showed that Ca^{2+} cations had a greater effect on the equilibrium constant than Na^+ cations did, the effect of the metal cations had on the overall equilibrium constant was not as drastic as it would have been if the equilibrium constant had been reported in the presence of no metal cations. To compare to what the actual affect Na^+ cations should have on the equilibrium in a CB[7] guest systems, the effect that Na^+ cations have on the overall equilibrium constant for a 1:1 CB[7]-guest complex is given by eq. 2.1:[49]

$$\beta_{11} = \frac{K_{11}}{1+K_1[Na^+]+K_1K_2[Na^+]^2} \qquad \text{(Eq. 2.1)}$$

Using the reported equilibrium constants between CB[7] and Na^+ cations (K_1 = 130 M^{-1}, K_2 = 21 M^{-1})[49] one can calculate the effect on the overall equilibrium constant (β_{11}) versus the equilibrium constant in the presence of no buffers of metal cations (K_{11}). From eq. 2.1, the effect of 10 mM Na^+ cations should decrease the equilibrium constant by approximately 61%, however, the salt effects in the methyl viologen paper show a much smaller decrease of only 25% in the overall equilibrium constant when the starting point was reported in 0.030 M tris-buffer.[92] This analysis shows that the tris-buffer was playing a competitive role binding to CB[7] which decreased the reported equilibrium constant between CB[7] and methyl viologen without cations.

Thiazole orange (TO) binding to CB[7] gives an example of the difference in thermodynamic outcomes of a system in the presence of Ca^{2+} cations versus Na^+ cations.[84] At low concentrations of Ca^{2+} cations and Na^+ cations there is a 1:1 inclusion complex formed between TO and CB[7]. At elevated concentrations of Ca^{2+} cations and Na^+ cations, however, there are different thermodynamic results for the complexes being formed in the system. In the presence of elevated Na^+ cation concentrations, the solution becomes turbid from what is proposed to be the formation of elongated assemblies of 1:1 complexes with TO and CB[7] with an Na^+ cation bound with TO at the portals of CB[7]. The TO molecules were bound by two CB[7]s, but because of the elongated assemblies the ratio of TO to CB[7] was 1:1, with the Na^+ cation being bound to the CB[7] that is bound to the side of

the TO molecule opposite to the TO cationic charge. But in the presence of elevated Ca^{2+} cation concentrations, there is the formation of a 2:2 TO:CB[7] complex with Ca^{2+} capping the ends of CB[7]s resulting in an increased fluorescence intensity of TO.[84]

There are several studies reporting the binding of metal cations to CB[7]. The equilibrium constants between metal cations and CB[n]s are determined by examining how the equilibrium constant between a guest molecule and CB[7] is affected by the concentration of the metal cation. A question when studying the binding interactions between metal cations and CB[7] is whether one or two metal cations bind to the portals of CB[7]. To address this issue, the inverse of the equilibrium constant is plotted against the concentration of metal cation. If the relationship between the inverse of the binding constant and the concentration of metal cation is not linear, there are two cations binding the CB[7].[49, 93] Crystal structures of CB[n]s and metal cations are reported with multiple cations bound to CB[n].[49-50, 83, 85, 94] Though some reports claim only one metal cation binds to CB[n]s. [82, 85, 103, 105] This chapter will examine how Na^+ cations and Ca^{2+} cations affect the dynamics of a CB[7]-guest system. The binding constant of Ca^{2+} cations to CB[7] was reported at 700 M^{-1}, with only one Ca^{2+} cation binding to CB[7].[82] However, molecular dynamics calculations predict that two Ca^{2+} cations bind to CB[n].[50] Further, experimental results suggest CB[7] binds two Na^+ cations bound.[49, 93] The effect Na^+ cations on the binding dynamics of 1-(2-naphthyl)ethylammonium (NpH^+) and CB[7] serves as an example of how changing concentrations of metal cations can affect dynamics of a host-guest system.[49]

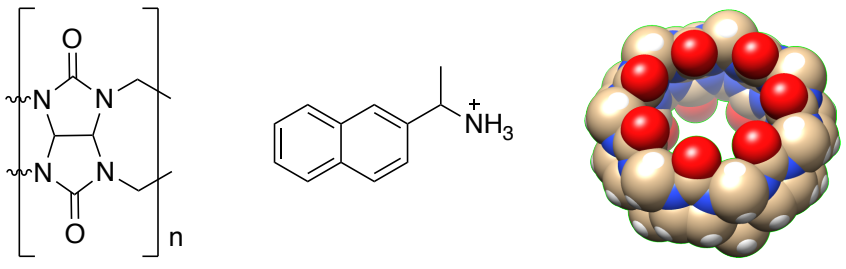

CB[n] NpH^+ CB[7]

Chart 2.1 The generic structure of CB[n], the structure of NpH^+ and the space filling model of CB[7].

In 2011, the dynamics between 1-(2-naphthyl)ethylammonium cation (NpH^+, chart 2.1) and CB[7] in the presence of Na^+ cations were reported.[49] At concentrations of Na^+ cations ranging from 0.075-0.200 M and CB[7] concentrations from 2.5-12.5 μM, all the dynamics on the millisecond time scale showed that the perturbed chemical system returned to equilibrium through a single process involving CB[7] and NpH^+ (scheme 2.1). The kinetic data fit to a single exponential function corresponding to a single observed rate constant for the system returning to equilibrium. The published mechanism (scheme 2.1) was consistent with Na^+ cations binding sequentially to CB[7], and NpH^+ binding to free CB[7] to form an inclusion complex.[49] The presence of Na^+ cations was shown to slow down the kinetics, lowering the observed rate by modulating the concentration of free CB[7]. The reported association rate constant was $(6.3 \pm 0.3) \times 10^8$ $M^{-1}s^{-1}$ and the apparent rate constant for the association process decreased at higher Na^+ cation concentrations. The dissociation rate constant was not affected by the presence of Na^+ cations, remaining at 55 $\pm$ 7 s^{-1} across all Na^+ cation concentrations studied.

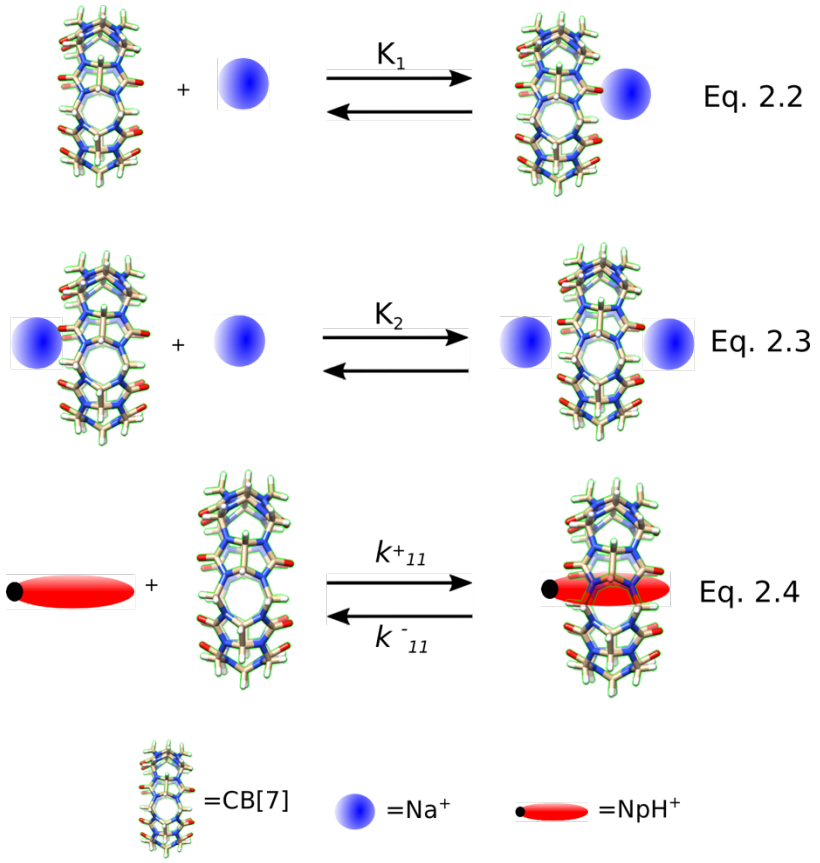

Scheme 2.1 Proposed mechanism for the binding of NpH^+ to CB[7] in the presence of Na^+.

2.1.2 Objective

The objective of the work described in this chapter was to determine the mechanistic differences of a seemingly simple CB[7]-guest complex with different metal cations present in solution: Ca^{2+} and Na^+. Using the previously reported NpH^+ binding to CB[7] system,[49] preliminary results showed that the dissociation rate constant in the presence of Ca^{2+} cations was lower than the previously reported dissociation rate constant in the presence of Na^+ cations. The expected change in the dynamics, when changing the metal cation from Na^+ to Ca^{2+}, was that the mechanism would remain the same as shown in scheme 2.1, but Ca^{2+} cations would bind stronger to CB[7] causing the overall kinetics to be slower due to less free CB[7] being present to bind NpH^+. However, the prediction from the mechanism in scheme 2.1 was that the dissociation rate constant would remain the same irrespective of the nature of the metal cation. The preliminary results in the presence of Ca^{2+} cations showing a decrease in the dissociation rate constant changed the scope of this

project to determine if changing the metal cation in solution from Na^+ to Ca^{2+} added complexity to the binding mechanism of NpH^+ to CB[7]. Metal cations have traditionally been used to modulate the concentration of CB[n]s, but if these metal cations can affect the binding mechanism of CB[n]-guest systems, it may be time to consider seemingly simple CB[n]-guest systems within the realms of systems chemistry. Further, in this chapter the determination of the binding constants of Ca^{2+} cations to CB[7] will be resolved.

2.2 Experimental

2.2.1 Materials

NpH^+ (≥ 99.0%), methyl viologen dichloride hydrate (98%), sodium chloride (NaCl), glycouril (97%), paraformaldehyde and bis(cyclopentadienyl)cobalt (II) (Cob^+) were purchased from Sigma-Aldrich and were used without any further purification. CB[7] was obtained from a synthesis conducted by a previous graduate student in the group, Dr. Suma Thomas, and CB[7] was synthesized again using the same procedure.[47] Calcium chloride dihydrate ($CaCl_2$•$2H_2O$) was purchased from Biobasic Canada Inc. Hydrochloric acid (HCl, ACS grade, 36.5-38%), and sulfuric acid (ACS grade, 95-98%), were purchased from VWR Analytical and were used as obtained. Spectral grade methanol, for use in the ultraviolet region of the spectrum, was purchased from Fisher Chemical and was used as received. Aqueous solutions were prepared using de-ionized water from a Barnstead NANOpure deionizing system (≥ 17.3 MΩ cm).

2.2.2 Sample preparation

Stock solutions of NpH^+, CB[7], $CaCl_2$•$2H_2O$, NaCl and HCl were made every 3-4 weeks. The stock solutions were then used to prepare samples for the experiments listed below. Stock solutions of 2 mM NpH^+ were made in spectral grade methanol. Stock solutions of both Ca^{2+} and Na^+ were made to 1.0 M by dissolving their solids in de-ionized H_2O. The HCl stock solutions were made to 1.0 M from a 4.0 N HCl solution. CB[7] stock solutions were made assuming the solids were completely dry. CB[n]s are hygroscopic, and therefore

the actual concentration of CB[7] in the stock solutions was determined using a literature reported method.[95] CB[7] stock solutions were made by dissolving 6-7 mg in 5 mL of de-ionized H_2O. Assuming a 100% purity (completely dry) the concentration of the CB[7] stock solution was between 1.0-1.3 mM. A stock solution of methyl viologen was made with extreme caution because methyl viologen is highly poisonous. To make a stock solution of methyl viologen, capped volumetric flasks were pre-weighed and solid methyl viologen was added in the confines of a fumehood. A methyl viologen stock solution was made to 1.79 mM in de-ionized water. Cob^+ stock solutions were made to 1 mM in spectral grade methanol. When the Cob^+ stock solutions were diluted into experimental solutions, the actual concentrations were determined using the molar extinction coefficient of 34200 $M^{-1}cm^{-1}$ at 261 nm.[95]

Stopped flow: In stopped-flow experiments, the following solutions were prepared: 25 mL solutions of 2.0 μM NpH^+ were made at 1.0 mM HCl and with metal cation (Ca^{2+} or Na^+) concentrations of 10, 25, 50, 75 or 100 mM. The solution with 2 μM NpH^+ was diluted in half in the stopped-flow experiments. CB[7] solutions were made to 10 mL containing 1 mM HCl and the appropriate concentration of metal cations to match the metal cation concentrations in the NpH^+ solutions. The CB[7] solutions, like the NpH^+ solution, were made to double the experimental concentration due to the dilution in the stopped-flow experiment: 10, 20, 30, 50 and 80 μM before dilution. Aqueous control solutions of 25 mL contained 1 mM HCl and the corresponding metal cation concentration used in a specific experiment.

Fluorescence: In steady-state fluorescence experiments, a 5 mL solution of 1 μM NpH^+, 1 mM HCl and the concentration of Ca^{2+} cations needed for each particular experiment was made. A 5 mL CB[7] solution was made by adding 3-4 mL of a 1 mM CB[7] stock and the appropriate amount of HCl and Ca^{2+} cations to ensure that the concentration of HCl and Ca^{2+} cations in the CB[7] solution matched the concentrations of these species in the NpH^+ solution. To a fluorescence cell, 2.5 mL of the NpH^+ solution was added and small sequential additions ($\leq$ 25 μL) of the CB[7] solution were made. After each addition, an emission scan was taken from 300 to 450 nm using an excitation wavelength of 280 nm. With each addition of CB[7] the fluorescence intensity increased until saturation was met, and the fluorescence intensity stopped increasing.

CB[7] titrations: A Cob^+ solution of 15 μM was made from the 1 mM stock solution of Cob^+. To an absorbance cell, 2.5 mL of the 15 μM Cob^+ solution was added. The actual concentration of Cob^+ was determined using the reported molar extinction coefficient.[95] To the 2.5 mL of the Cob^+ solution, sequential 8 μL additions of the ~1.0 mM CB[7] stock solution were made. Absorption spectra were taken after each addition of CB[7], and the additions continued until the absorption at 261 nm stopped decreasing (figure 2.1). A titration curve was made from the absorbance values at 261 nm against the concentration of CB[7] to determine the purity of the CB[7] stock solutions.

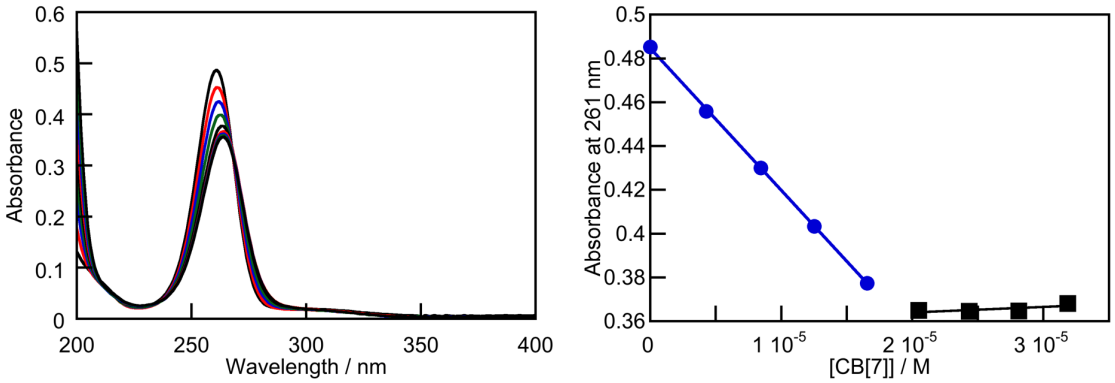

Figure 2.1. Left: Absorption spectra for the titration of a 15 µM Cob^+ solution with a 1 mM CB[7] stock solution assuming a 100% purity for CB[7]. **Right:** Titration curve made from the absorption at 261 nm versus the CB[7] concentration.

A control spectrum of water was recorded and the absorption at 261 nm was subtracted from each of the Cob^+ absorption spectra. The absorbance values at 261 nm were corrected for dilution before determining the equivalence point. The equivalence point was determined from the titration plot in figure 2.1. The purity percentage was calculated using eq. 2.5 by comparing the number of moles of CB[7] added assuming 100% purity versus the number of moles of Cob^+. The concentration of Cob^+ multiplied by the initial volume (V_i) divided by the concentration of CB[7], assuming 100% pure, multiplied by the end volume (V_e), which is the volume of CB[7] stock solution added at the equivalence point.

$$\%purity = \frac{[Cob^+]\times V_i}{[CB[7]]\times V_e} \qquad \text{(Eq. 2.5)}$$

Methyl viologen binding isotherms to CB[7]: Methyl viologen solutions at a concentration of 20 µM were prepared in solutions containing 2, 5 and 10 mM Ca^{2+} cations. A 5 mL CB[7] solution was made by adding 3 mL of a 1 mM CB[7] stock solution and the required amount of a 1.0 M Ca^{2+} cation stock solution, so the concentration of Ca^{2+} cations in the CB[7] solution matched the concentration of Ca^{2+} cations in the methyl viologen solutions. Sequential additions of 9 µL of the CB[7] solution were made until the absorption at 247 nm stopped decreasing (figure 2.2).

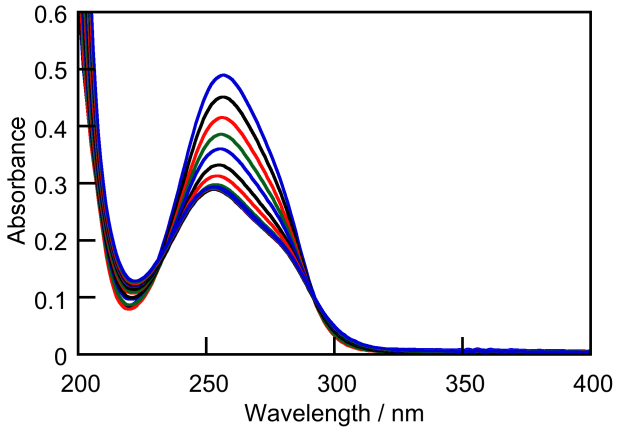

Figure 2.2 Absorption spectra for the titration of a 20 µM methyl viologen solution containing 5 mM Ca^{2+} with a 1 mM CB[7] solution containing 5 mM Ca^{2+}.

2.2.3 Equipment

Fluorimeter: Steady-state fluorescence experiments were conducted on a PTI QM-40 spectrofluorimeter. The emission spectra were collected between 300 and 450 nm. The samples were excited at 280 nm with excitation and emission bandwidth of 2 nm. The step size for the collection of the spectra was 0.5 nm and the integration time was set to 0.25 s. The samples were equilibrated to 20 °C for 5 min after the addition of CB[7].

UV/Vis Spectroscopy: The absorption spectra were collected on a Varian Cary 100-Bio UV-Vis spectrophotometer or a Varian Cary 1E UV-Vis spectrophotometer. UV-Vis spectra were collected from 200 to 400 nm. The spectra were collected against an air background. Experimental spectra were corrected by taking a trace of solvent and subtracting the solvent spectrum from the experimental spectra

Stopped flow: Kinetic experiments were performed on an Applied Photophysics SX-20 stopped-flow device. A Hg-Xe vapor lamp was used as the excitation source. The solutions were mixed under pressure at a 1:1 ratio. The samples were excited at 280 nm with the slits set to 1 mm on the monochromator used to select the excitation wavelength. The 1.0 mm slit width corresponds to a bandwidth of 4.65 nm for the excitation beam. The fluorescence was collected through a 320 nm cut-off filter, where all light below the wavelength of 320 nm was excluded. The samples were held at 20 °C for 10 min before kinetic traces were collected. Kinetic traces were corrected by collecting kinetic traces of all components

except the fluorophore, and subtracting the control experiment trace from the trace corresponding to the sample.

2.2.4 Binding isotherm model for the formation of the 1:1 NpH^+@CB[7] complex

The emission spectra of NpH^+ solutions mixed with CB[7] solutions were integrated from 315 to 350 nm. The integrated values were divided by the integrated value measured for a NpH^+ solution with no CB[7] to convert the integrated emission intensity into a relative integrated intensity value (I). The plot being fit was the dependence of the relative integrated intensity values against the concentration of CB[7]. The data was fit to a 1:1 model using numerical analysis on the Scientist 3 software from Micromath:

$$[G@CB[7]]_{eq} = \beta_{11} \times [CB[7]]_{eq} \times [G]_{eq} \quad \text{(Eq. 2.6)}$$

$$[CB[7]]_{eq} = [CB[7]]_T - [G@CB[7]]_{eq} \quad \text{(Eq. 2.7)}$$

$$[G]_{eq} = [G]_T - \left[G@CB[7]\right]_{eq} \quad \text{(Eq. 2.8)}$$

$$I = R \times ([G]_{eq} + C_{11} \times \left[G@CB[7]\right]_{eq}) \quad \text{(Eq. 2.9)}$$

$$R = \frac{I_0}{[G]_T} \quad \text{(Eq. 2.10)}$$

Where the concentration restraints for the dependent variables are:

$$0 < [G]_{eq} < [G]_T \quad \text{(Eq. 2.11)}$$

$$0 < \left[CB[7]\right]_{eq} < \left[CB[7]\right]_T \quad \text{(Eq. 2.12)}$$

$$0 < [G@CB[7]]_{eq} < [G]_T \quad \text{(Eq. 2.13)}$$

The total concentrations of CB[7] and guest molecules present in solution are represented by $[CB[7]]_T$ and $[G]_T$. The equilibrium concentrations of CB[7], guest and the 1:1 CB[7]-guest complex are denoted as $[CB[7]]_{eq}$, $[G]_{eq}$ and $[G@CB[7]]_{eq}$, respectively. The concentration of CB[7] at equilibrium, $[CB[7]]_{eq}$, includes all species of CB[7] not bound to NpH^+: free CB[7], CB[7] bound to a single Ca^{2+} cation and CB[7] bound to two Ca^{2+} cations. The overall equilibrium constant for the formation of the CB[7]-guest complex at

a given concentration of Ca^{2+} cations was denoted as β_{11}. The integrated intensity of NpH^+ in the absence of CB[7] was denoted as I_0. R corresponded to the ratio of fluorescence intensity of NpH^+ in the absence of CB[7] (I_0) to the total guest concentration ($[G]_T$). C_{11} was the ratio of the emission quantum yields of the NpH^+@CB[7] and NpH^+ free in solution.

2.2.5 Binding isotherms model for the 1:1 complex between methyl viologen and CB[7]

The model remains the same as the one described in section **2.2.4** with 2 modifications because these experiments are done using absorption measurements. R is now equal to the molar extinction coefficient which is the ratio of the initial absorption of the guest molecule in the absence of CB[7] (A_0) and the total guest concentration ($[G]_T$). C_{11} is the ratio of molar extinction coefficients of the 1:1 complex between methyl viologen and CB[7], and methyl viologen free in solution.

2.2.6 Simulations of methyl viologen binding to CB[7] in the presence of different Ca^{2+} cation concentrations

Using the Scientist 3 software from Micromath, the effect of Ca^{2+} cations on the equilibrium constant between methyl viologen and CB[7] was calculated. The equilibrium constant between methyl viologen and CB[7] was $(4.7 \pm 0.3) \times 10^7$ M^{-1}, which was determined by calculating equilibrium constants in the presence of Na^+ cations from the overall equilibrium constants in the literature using eq. 2.1[92, 106-108] and binding isotherms done in the presence of Na^+ cation concentrations conducted by myself. The metal cation concentrations used for the simulations were between 0 and 100 mM Ca^{2+}cations. The ratio of the overall binding constant (β_{11}) and the equilibrium constant in the presence of no metal cations (K_{11}), represented in eq. 2.14 by X, was used to determine the effect Ca^{2+} cations had on the 1:1 host:guest equilibrium constant. The first equilibrium constant between Ca^{2+} cations and CB[7] was denoted as K_3 and the second binding constant of Ca^{2+} cations to CB[7] is denoted as $0.25*K_3$, which corresponds to the highest possible value

for this equilibrium constant based on statistical considerations.[91] The value of K_3 was varied between 300 and 700 M^{-1}.

$$X = \frac{1}{1+K_3[\mathrm{Ca}^{2+}]+0.25K_3^2[\mathrm{Ca}^{2+}]^2} \quad \text{(Eq. 2.14)}$$

2.2.7 Analysis of stopped-flow data

In stopped-flow experiments, 18 traces were collected, the first 2 were removed and the remaining 16 were averaged. The traces were fit to a sum of exponentials function (Eq. 2.15).

$$\Delta I = \alpha_0 + \alpha_1 e^{-k_{obs1}t} + \alpha_2 e^{-k_{obs2}t} + \alpha_3 e^{-k_{obs3}t} \quad \text{(Eq. 2.15)}$$

The change in fluorescence intensity is denoted as ΔI. The change in fluorescence intensity is equal to the sum of the exponentials multiplied by the amplitude for each term (α_x, where x = 0, 1, 2 or 3). Each exponential term corresponds to a single observed rate constant (k_{obs}). There was one amplitude which was not multiplied by an exponential term, α_0, which corresponds to any change in amplitude where the observed rate constant was faster than the time resolution of the instrument used.

2.2.8 Synthesis of CB[7]

CB[7] was synthesized and purified using the same method publish in Dr. Suma Thomas' thesis,[47] which was adopted from previously reported literature procedures.[74, 109] The synthesis of CB[7] produced all homologues of the CB[n] family. The solid from the synthesis was washed with deionized water and vacuum filtered. The filtrate contained CB[5] and CB[7] as these homologues are more soluble than CB[6] and CB[8], which were left in the solid phase. The filtrate was mixed with methanol to precipitate the CB[5] and CB[7]. This filtration and precipitations process was repeated twice more on the crude solid to obtain 3 fractions from the CB[n] synthesis. Each of the 3 fractions were analyzed by electrospray mass spectrometry. For the ESI-MS, fractions of the CB[n] synthesis were dissolved in 20% formic acid to 100 μM of a given CB[n] assuming 100% purity. Standards

with CB[n] mixtures were created using CB[n] samples of known purity to compare the relative intensities of different CB[n]s in the fractions obtained from the synthesis. A standard of 60 μM CB[5], CB[6] and CB[7] was created, as well as a standard of 60 μM CB[6] and CB[8]. The standards were chosen based on the relative solubilities of the CB[n]s and which homologues were expected to be together in each fraction.

2.3 Results

2.3.1 Kinetics in the presence of Na^+ cations

After the work between NpH^+ and CB[7] published in 2011,[49] the original idea for this project was to use the NpH^+ binding to CB[7] system as a convenient way to determine the equilibrium constants of other biologically relevant metal cations to CB[7], such as Ca^{2+}, K^+ and Mg^{2+}. The hypothesis was that the NpH^+@CB[7] system could be used to determine the relationship between the observed rate constant and the concentration of CB[7] at different metal cation concentrations. The equilibrium constants for cations other than Na^+ would be obtained from eq. 2.16 by substituting in the other biologically relevant cations for Na^+. Preliminary results in the presence of low Ca^{2+} cation concentrations suggested the presence of more than one relaxation process in the system, of which one was faster than expected from the mechanism proposed in scheme 2.1 and was close to the time resolution of the stopped-flow device, k_{obs} = 500-1000 s^{-1}. The appearance of this faster component in the kinetics at lower concentrations of Ca^{2+} cations, led to the investigation of the system at lower concentrations of Na^+ cations to determine if the NpH^+@CB[7] system was more complex than the mechanism originally proposed (scheme 2.1).

The previously published mechanism for the binding between NpH^+ and CB[7] (scheme 2.1)[49] was consistent for studies within the following concentrations: [NpH^+] = 0.5 μM, [Na^+] = 0.075-0.200 M and [CB[7]] = 2.5-12.5 μM. The kinetics at 0.5 μM NpH^+, 100 mM Na^+ cations and concentrations of CB[7] between 2.5 and 10 μM were revisited to confirm that the kinetic traces fit to a single exponential function as required for the proposed mechanism in scheme 2.1 (figure 2.3). The kinetic traces in figure 2.3 show that there is no initial offset in the kinetics, and the kinetic traces do fit to a single exponential function for

all the CB[7] concentrations studied. An offset would appear in a kinetic trace as a 'jump' in fluorescence intensity within the time resolution of the stopped-flow device (1-2 ms). An offset signifies that the kinetics are faster than the time resolution of the stopped-flow system and if the reaction was completed within the dead time of the stopped flow, then only a change in intensity would be observed as a flat line. An exponential function represents a pathway by which a perturbed system returns to equilibrium. If the kinetics fit to a single exponential function, there was only one pathway by which the perturbed system returned to equilibrium. This confirms that the mechanism published in 2011 (scheme 2.1) was consistent within the concentration ranges of reactants that were used.[49]

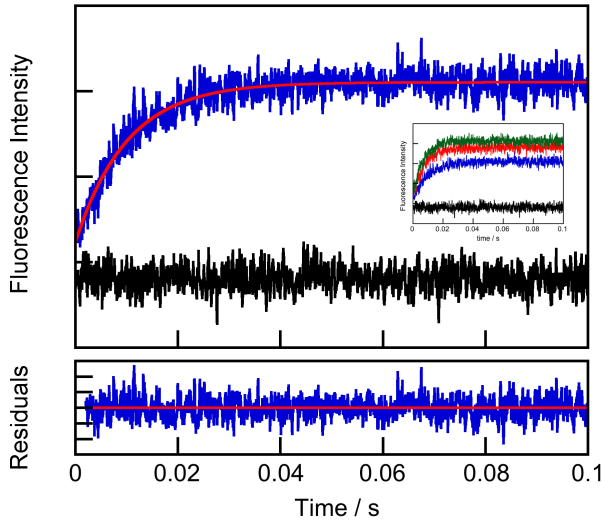

Figure 2.3 Top: Kinetic trace for the mixing of 5 μM CB[7] with 0.5 μM NpH^+ where both solutions contain 100 mM Na^+ (blue trace) and the fit to a single exponential function (red). **Bottom:** Residuals between the data and the fit (blue). The inset shows the kinetics of 0.5 μM NpH^+ mixing with different CB[7] concentrations in the presence of 100 mM Na^+ cations (CB[7] = 0, black; 5 μM, blue; 7.5 μM, red and 10 μM, green).

Assuming the mechanism in scheme 2.1, the relationship between the observed rate constant and the concentration of Na^+ cations is given in eq. 2.16:[49]

$$k_{obs} = \frac{k_{11}^{+}[\mathrm{CB[7]}]_T}{1+K_1[\mathrm{Na^+}]+K_1K_2[\mathrm{Na^+}]^2} + k_{11}^{-} \qquad \text{(Eq. 2.16)}$$

Where the association rate constant is 6.3×10^8 $M^{-1}s^{-1}$ and the dissociation rate constant is 55 s^{-1}.[49] The binding constants of Na^+ cations to CB[7] are represented as K_1 and K_2, where K_1 is 130 M^{-1} and K_2 is 21 M^{-1}.[49] Using eq. 2.16, the dynamics for the formation of the NpH^+@CB[7] complex at 50 mM Na^+ cations should be equal to the time resolution of the stopped-flow instrument and the dynamics at 10 mM Na^+ cations should be much faster than the dead time of the stopped-flow instrument used. In the latter case, the kinetic traces should appear as an offset, and the kinetic traces would be flat lines, because the kinetics would have reached equilibrium within 1 ms. The flat lines would indicate fluorescence intensity changes caused by the formation of the NpH^+@CB[7] complex, but the kinetics are faster than 1-2 ms. However, as seen in figure 2.4, the dynamics in the presence of 10 mM and 50 mM Na^+ cations were on the ms time scale. Figure 2.4 shows that at 10 mM Na^+ cations with 1 μM NpH^+ and 15 μM CB[7] the kinetics do not appear as just an offset, instead there was kinetics seen close to the mixing time of the stopped-flow instrument. Kinetics on the ms time scale suggests a reaction occurs that is not accounted for in mechanism shown in scheme 2.1. The reaction not present in scheme 2.1 is competing with the formation of the NpH^+@CB[7] inclusion complex, slowing down the overall kinetics onto the ms time scale. When the concentration of NpH^+ was increased from 0.5 to 1.0 μM (figure 2.4) the dynamics at 50 mM and 100 mM Na^+ with 15 μM CB[7] fit to a sum of two exponentials function. When looking at the dynamics in figure 2.4, the kinetics of 1 μM NpH^+ and 15 μM CB[7] appears to show a small off-set in the kinetic trace at 50 and 100 mM Na^+ cations. However, when the kinetic traces at 50 and 100 mM Na^+ cations were fit to a sum of two exponentials function, the kinetic trace was found to extrapolate down to the baseline (appendix, figure B2). Because the trace extrapolated to the baseline, it meant that the off-set is an artifact from the initial mixing time. Instead, the dynamics of the faster kinetic process were close to the time resolution of the stopped-flow device (1-2 ms) and more than one relaxation process occurred because the kinetics could not be fit to a single exponential function. In the case of the experiment at 10 mM Na^+ cations, the kinetics fit line does not extrapolate to the baseline (figure B2), showing that at this lower Na^+ cation concentration the kinetics were faster than the dead time of the experiment.

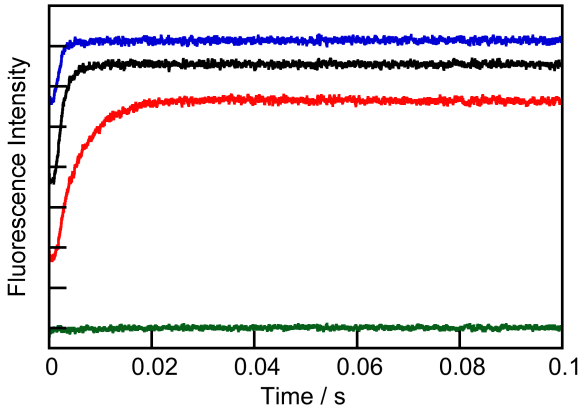

Figure 2.4 Kinetic traces for the mixing of 1.0 μM NpH^+ with 15 μM CB[7] at different Na^+ cation concentrations (100 mM, red; 50 mM, black and 10 mM, blue). The green trace corresponds to the control experiment in the absence of CB[7] ([Na^+] = 100 mM).

Figure 2.5 shows the residuals of the fits to a single exponential function and the residuals of the fits to a sum of two exponentials function of the kinetic traces for the solution containing 50 or 100 mM Na^+ cations. The residuals of a good fit show a random distribution across a fit line, shown in red in figure 2.5, whereas a systematic deviation from the fit line indicates the need to fit to the sum of additional exponentials function. For the fit of the kinetics to a single exponential function, the residuals are not random. This deviation shows that there was another reaction occurring with the increased concentration of NpH^+. The residuals for the fit of the data to a sum of two exponentials, however, showed no systematic deviation for the residuals, meaning it was a good fit. The appearance of a second exponential term showed that the originally published mechanism was not consistent across all concentrations of CB[7], NpH^+ and Na^+ cations.

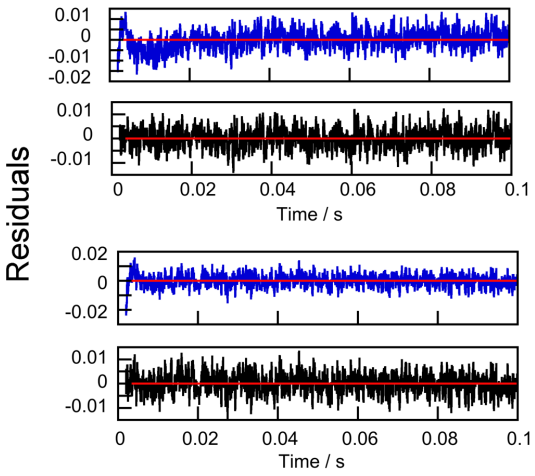

Figure 2.5 Residuals of the fits of the kinetic data (figure 2.4) to a single exponential (blue) and the sum of two exponentials function (black) for the mixing of 1.0 μM NpH^+ with 15 μM CB[7]. Top: $[Na^+]$ = 50 mM; bottom: $[Na^+]$ = 100 mM.

When fitting the kinetics of the NpH^+@CB[7] system to a sum of two exponentials function, the observed rate constant for the fast component varied between 700 and 2500 s^{-1} with large errors and no correlation between the observed rate constant and the concentration of CB[7]. These values of the observed rate constant were all higher, or as high, as the time constant for the resolution of the stopped-flow device used. Therefore, the observed rate constant for the faster exponential function was fixed to 1000 s^{-1}. The appearance of a faster kinetic process at lower concentrations of Na^+ cations was consistent with the proposed mechanism between 2-aminoanthracenium (AH^+) and CB[7].[44] Based on this literature precedence, the exponential function with the higher observed rate constant was proposed as an exclusion complex.[21, 44] An exclusion complex occurs when the cationic ammonium group of the guest molecule coordinates to the carbonyl portals of CB[7], while the aromatic group remains exposed to the surrounding solution. The exclusion complex has also been proposed in the binding mechanism between CB[6] and 4-methylbenzylammonium.[21] Further, exclusion complexes have been proposed based on a size exclusion premise; the idea of size exclusion is proposed when the guest molecule is too large to enter the CB[n] cavity, therefore the exclusion complex is the thermodynamic result of the CB[n]-guest system.[76, 110-112] Scheme 2.2 shows the proposed, expanded mechanism for NpH^+ binding to CB[7] in the presence of Na^+ cations. The first two steps remained as the sequential binding of Na^+ cations to CB[7]. The final step of the

mechanism was the previously reported formation of the inclusion complex with free CB[7]. The added step in the binding mechanism, is the formation of an exclusion complex.

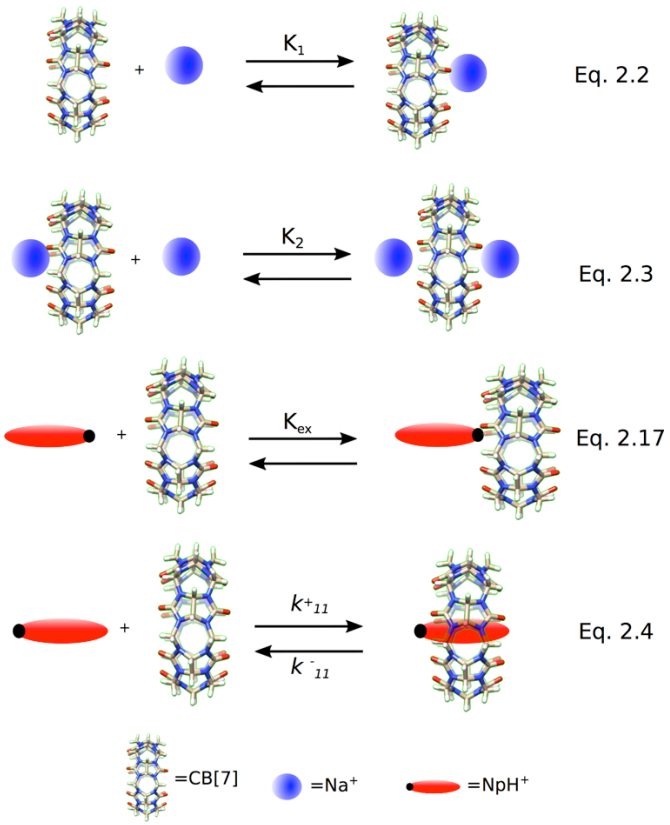

Scheme 2.2 Expanded mechanism for the binding between NpH^+ and CB[7] in the presence of Na^+ cations.

2.3.2 Kinetics and binding isotherm in the presence of Ca^{2+} cations

The equilibrium constants between Ca^{2+} cations and CB[7] were determined by performing binding isotherm studies between methyl viologen and CB[7] at different Ca^{2+} cation concentrations. The ratios between the overall equilibrium constant in the presence of Ca^{2+} cations (β_{11}) and the equilibrium constant in the presence of no metal cations (K_{11}) were simulated using eq. 2.18. The experimental overall binding constants were compared to the simulated ratios between β_{11} and K_{11} to determine the binding constants of Ca^{2+} cations and CB[7] (figure 2.6).

$$\beta_{11} = \frac{K_{11}}{1+K_3[Ca^{2+}]+0.25K_3^2[Ca^{2+}]^2} \qquad \text{(Eq. 2.18)}$$

Where K_3 is the first equilibrium constant between a Ca^{2+} cation and CB[7]. The second equilibrium constant between a Ca^{2+} cation and CB[7], denoted later in the mechanism as K_4, was represented as $0.25*K_3$ which corresponds to the highest possible value for the second equilibrium constant between Ca^{2+} cations and CB[7] based on statistical considerations.[91] The second equilibrium constant between Na^+ cations and CB[7] is close to 25% of the first equilibrium constant between CB[7] and Na^+ cations.[49] The simulated ratios between β_{11} and K_{11} were denoted as X in figure 2.6, and values of K_3 were varied from 300 to 700 M^{-1}.

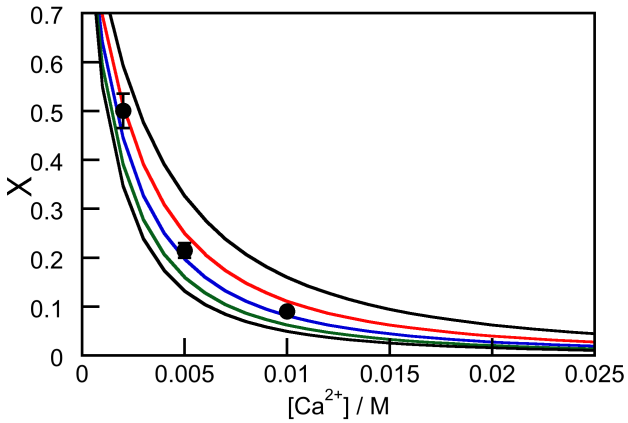

Figure 2.6 Simulations of the dependence of the ratio between β_{11} and K_{11} (X) and the Ca^{2+} concentration calculated from equation 2.18 (K_3 = 300 M^{-1}, top black; 400 M^{-1}, red; 500 M^{-1}, blue; 600 M^{-1}, green and 700 M^{-1}, bottom black. Experimental X values at 2, 5 and 10 mM Ca^{2+} are shown as black circles. The error bar for the data at 10 mM Ca^{2+} is smaller than the size of the circle.

The ratios, X, from figure 2.6, of the experimental binding isotherms fall between the simulated ratios of K_3 = 400 M^{-1} and K_3 = 500 M^{-1}. From the ratios of β_{11} to K_{11} values determined by the binding isotherms between methyl viologen and CB[7] in the presence of 2, 5 and 10 mM Ca^{2+} cations (figure B3) the binding constants of Ca^{2+} cations to CB[7] were determined to be $K_3 = 450 \pm 50$ M^{-1} and $K_4 = 110 \pm 10$ M^{-1}.

After determining the binding constants of Ca^{2+} cations to CB[7], the mechanism shown in scheme 2.2 was expected to be applicable in the presence of Ca^{2+} cations except the kinetics would be slower because Ca^{2+} cations bind stronger to CB[7] than Na^+ cations do. Figure 2.7 show the experiment in the presence of Ca^{2+} cations that is equivalent to figure

2.4 and 2.5 in the presence of Na^+ cations at 1 µM NpH^+,15 µM CB[7] and Ca^{2+} cation concentrations of 10, 50 and 100 mM.

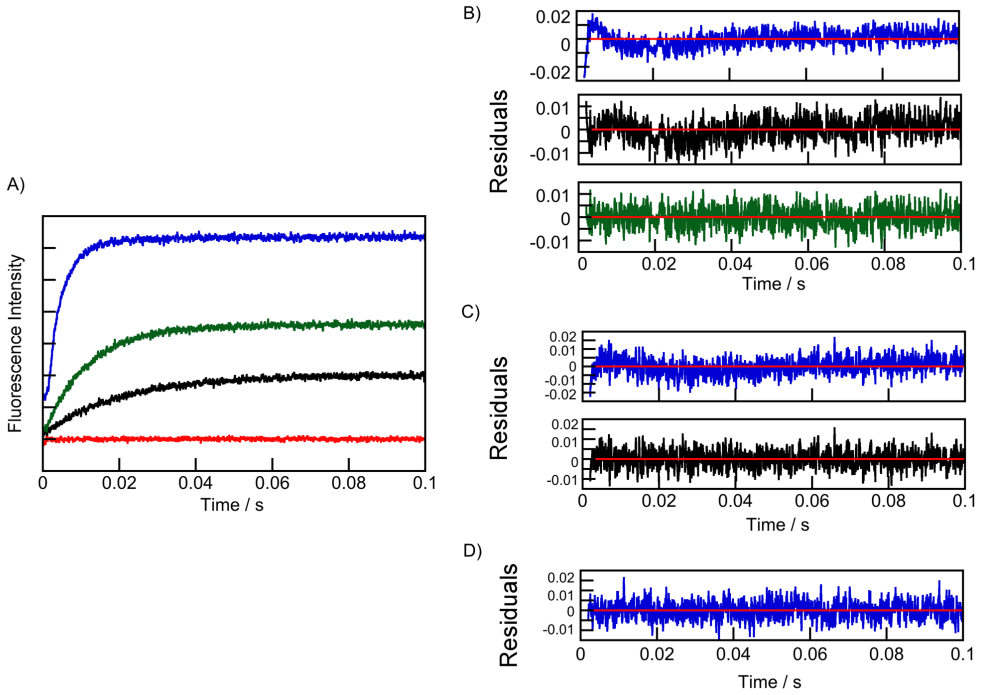

Figure 2.7 A: Kinetic traces for the mixing of 1.0 µM NpH^+ with 15 µM CB[7] at different Ca^{2+} concentrations (100 mM, black; 50 mM, green and 10 mM, blue). The red trace corresponds to the control experiment in the absence of CB[7] ([Ca^{2+} = 100 mM). **B-D**: residuals for the fits of the kinetic data in the presence of 10 mM Ca^{2+} (B), 50 mM Ca^{2+} (C) and 100 mM Ca^{2+} (D) cations. The residuals for the fit to a single exponential function are shown in blue, to the sum of two exponentials function are shown in black and to the sum of three exponentials function are shown in green.

The kinetics at 10 mM Ca^{2+} cations fits to a sum of three exponentials function. The kinetics at 10 mM Ca^{2+} cations appeared to show a small offset in figure 2.7, however when the kinetic trace was fit, the fit line extrapolated to the baseline (figure B4). Because the traces extrapolated to the baseline the dynamics contained a fast component that was the same as the fast component proposed as the exclusion complex for the reaction in the presence of Na^+ cations, with an observed rate constant fixed at 1000 s^{-1}. When the concentration of Ca^{2+} cations was increased to 50 mM the kinetics fit to a sum of two exponentials function. Finally, at 100 mM Ca^{2+} cations the kinetics fit to a single exponential function, which was the slowest of the exponentials from the kinetic traces at

10 and 50 mM Ca^{2+} cation. For reactions in the presence of 50 mM and 100 mM Ca^{2+} cations, no offset was observed at the start of the kinetics.

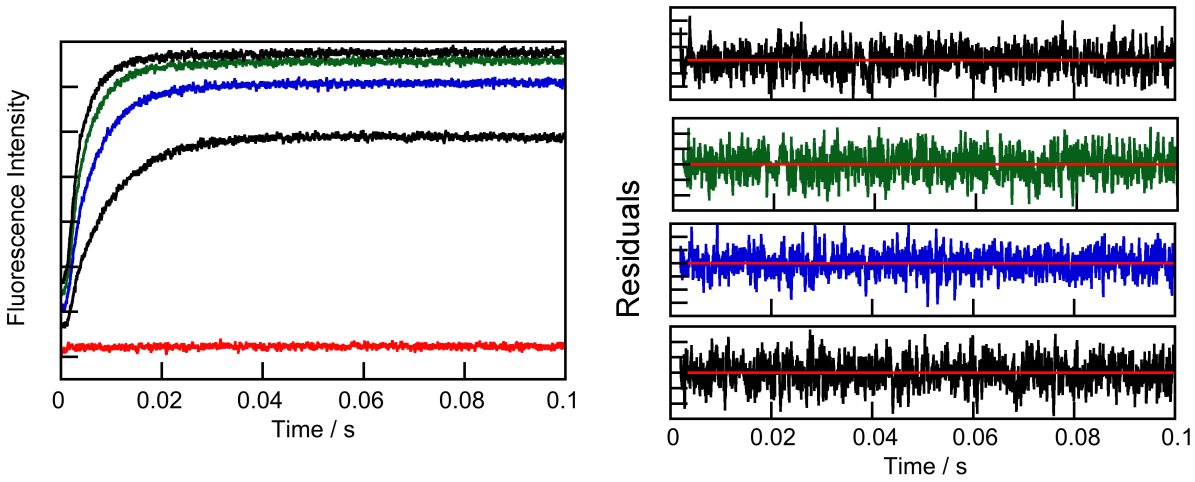

Figure 2.8 Left: Kinetic traces for the mixing of 1.0 µM NpH^+ with various CB[7] concentrations (5 µM, bottom black; 10 µM, blue; 15 µM, green and 20 µM, top black) in the presence of 10 mM Ca^{2+}. The red trace corresponds to the control experiment in the absence of CB[7] ([Ca^{2+} = 10 mM)**. Right:** Residuals of the fits of the kinetic data to a sum of three exponentials function for each of the kinetic traces.

Figure 2.8 shows an experiment at 10 mM Ca^{2+} cations with 1 µM NpH^+ and CB[7] concentrations between 5 and 20 µM. All the kinetic traces fit to a sum of three exponentials function and the kinetic traces extrapolate down to the baseline, showing that all the kinetic processes were captured in the time scale studied. From the fit to a sum of three exponentials function at 10 mM Ca^{2+} cations, one kinetic process was the proposed to be related to the formation of the exclusion complex. Of the other two kinetic processes, one must be the inclusion complex proposed in the presence of Na^+ cations, and a final kinetic process corresponds to a process that is not shown in scheme 2.2.

The third kinetic process, that is not shown in scheme 2.2, was determined by studying the kinetics at 100 mM Ca^{2+} cations. At 100 mM Ca^{2+} cations, all the kinetic traces fit to a single exponential function at all concentrations of CB[7] (figure 2.9). This presented an opportunity to create an observed rate constant versus concentration of CB[7] plot to determine the association and dissociation rate constants for this kinetic process.

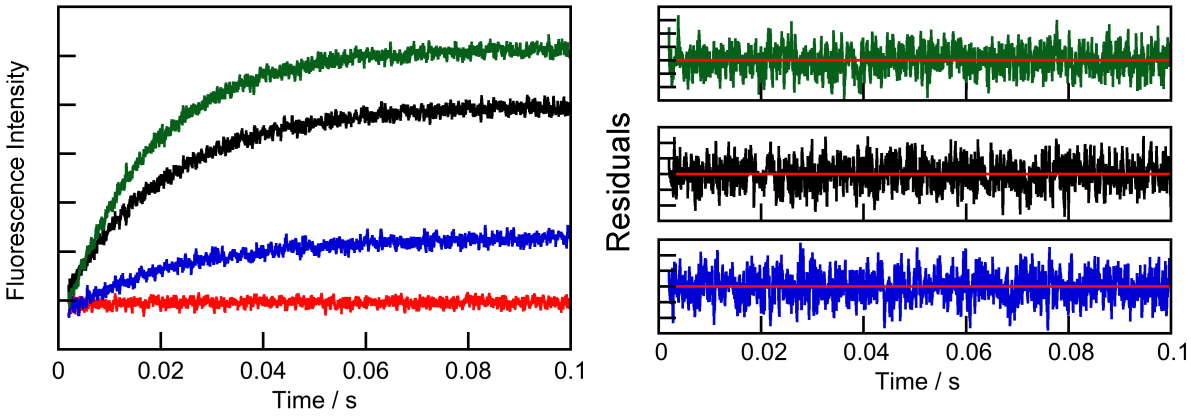

Figure 2.9 Left: Kinetic traces for the mixing of 1.0 μM NpH^+ with various CB[7] concentrations (5 μM, blue; 15 μM, black and 25 μM, green) in the presence of 100 mM Ca^{2+}. The red trace corresponds to the control experiment in the absence of CB[7] ([Ca^{2+} = 100 mM)**. Right:** Residuals of the fits of the kinetic data to a single exponential function for each of the kinetic traces.

The kinetic information in figure 2.9 can be used to create an observed rate constant versus concentration of CB[7] plot (figure 2.10). From figure 2.10 and using eq. 2.19, the dissociation rate constant for this kinetic process was 35 ± 1 s^{-1}. This kinetic process was found to have the lowest rate constant of the three kinetic processes. Eq. 2.19 is the equation corresponding to a pseudo-first order reaction, where the slope is the association rate constant and the y-intercept is the dissociation rate constant. This dissociation rate constant is 20 s^{-1} lower than the inclusion complex between NpH^+ and CB[7], which had a dissociation rate constant of 55 ± 7 s^{-1}.[49] This change in dissociation rate constant at 100 mM Ca^{2+} cations was independent of the concentration of NpH^+ (0.5 or 1.0 μM).

$$k_{obs} = k_+[CB[7]]_T + k_- \qquad \text{(Eq. 2.19)}$$

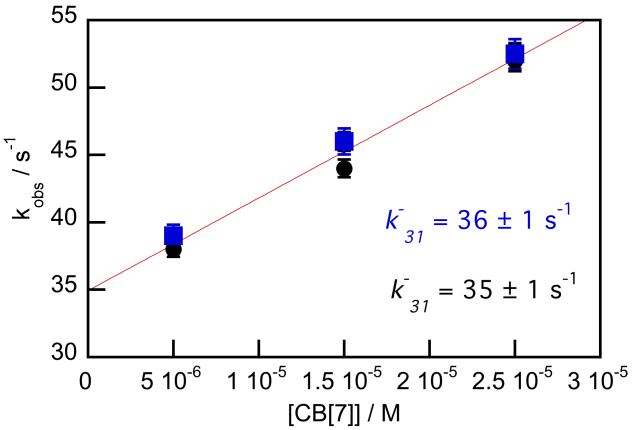

Figure 2.10 Dependence of the observed rate constant with the concentration of CB[7] in the presence of 100 mM Ca^{2+} cations generated from the fits of the kinetic traces to a single exponential function for NpH^+ concentrations of 0.5 μM (black circles) and 1.0 μM (blue squares) and CB[7].

Table 2.1. Association and dissociation rate constants recovered from the kinetic experiments (Eq. 2.19) for the mixing of NpH^+ with CB[7] in the presence of Ca^{2+} cation concentrations where the kinetic traces fit to a single exponential function.[a]

$[Ca^{2+}]$ / mM	$[NpH^+]$ / μM	k_{31}^{+} / 10^5 $M^{-1}s^{-1}$	k_{31}^{-} / s^{-1}
90	1.0	13 ± 3	27 ± 3
96	1.0	9 ± 2	34 ± 1
100	1.0	7 ± 1	36 ± 1
100	0.5	7 ± 1	35 ± 1
146	1.0	8 ± 3	30 ± 1

[a], the errors correspond to those recovered from the fits of the observed rate constant against the concentration of CB[7] shown in figure 2.10 and figures B5-7.

The values in table 2.1 were generated using eq. 2.19. At all the concentrations of Ca^{2+} cations analyzed in table 2.1, the kinetic traces fit to a single exponential function. The dissociation rate constant was calculated to be 33 ± 4 s^{-1}. The decreased dissociation rate constant is independent of Ca^{2+} cation concentration present.

From the kinetic experiments at 100 mM Ca^{2+}cations plotted in figure 2.10, an overall equilibrium constant (β) could be obtained from the ratio of association and dissociation rate constants (eq. 2.20). The β value takes into account the presence of Ca^{2+} cations.

$$\beta = \frac{k_{31}^{+}}{k_{31}^{-}} \qquad \text{(Eq. 2.20)}$$

Eq. 2.20 yielded an overall equilibrium constant of $(2.0 \pm 0.4) \times 10^4\ M^{-1}$. In a steady-state fluorescence experiment at 100 mM Ca^{2+} cations, the fluorescence intensity was integrated from 315 to 350 nm. From the relative integrated intensity versus CB[7] concentration binding isotherm, the overall equilibrium constant (β) recovered from the fit of the data was $(2.9 \pm 0.5) \times 10^4\ M^{-1}$ at 100 mM Ca^{2+} cations. The two values for β are within experimental error of each other.

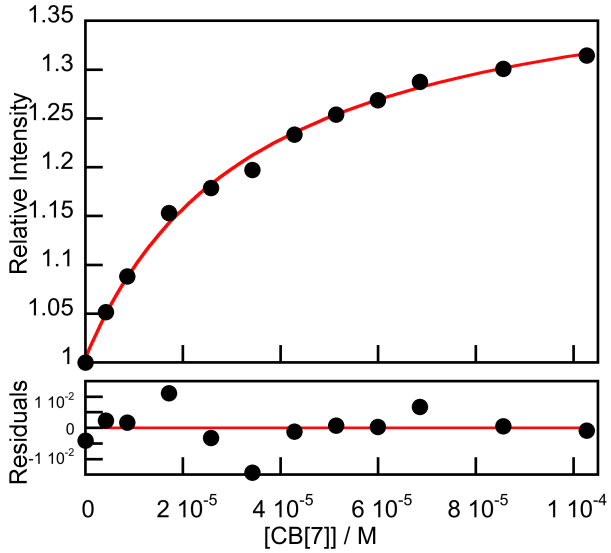

Figure 2.11 Fit of the steady-state fluorescence binding isotherm between NpH^+ (1.0 μM) and CB[7] in the presence of 100 mM Ca^{2+}.

2.4 Discussion:

In CB[n]-guest systems, the traditional view of metal cations, or components of buffered solutions, is that these species can affect the equilibrium constant of a CB[n]-guest complex, but, other than presenting competitive equilibria to the guest molecule, they are considered mechanistically inconsequential.[38, 92-93] However, the presence of metal cations appears to have mechanistic implications based on the identity and concentration of metal cationic species from the results presented above, showing that metal cations may not be inconsequential in the binding mechanism between CB[7] and a guest molecule. The results presented above show that an increase of metal cation concentration and the identity of the metal cation can affect the quantity and identity of each species in solution.

Because the concentration and identity of metal cations can have an effect on the binding mechanism of CB[7]-guest complex, it may be time to consider CB[n]-guest chemistry within the realm of systems chemistry. CB[n] systems have been proposed as carriers in drug delivery systems and functional materials, therefore understanding how CB[n]-guest systems are effected by components of complex media is important.[79-80] As discussed above, systems chemistry is defined as the study of a complex mixture of molecules that give rise to new properties that may not be intuitively predictable from studying the components in isolation.[56, 58, 61, 63, 65] The change in mechanism when the identity of the metal cation was changed from Na^+ cations to Ca^{2+} cations, may not have been predicted when studying the individual interactions between CB[7] and Ca^{2+} cations, or CB[7] and NpH^+ in isolation, coupled with the control of each species concentration by the identity and concentration of metal cations, CB[n]-guest systems should to be considered within the realm systems chemistry.

The first aspect to discuss is the control of the concentration of species in solution by the concentration of Na^+ cations. The appearance of, what is proposed as, an exclusion complex showed that the concentration of metal cations can control the observable species present in solution. In the presence of Na^+ cations the appearance of a second component with a higher observed rate constant for CB[7]-guest complexation, that was close to the dead time of the device, was consistent with what was proposed as an exclusion complex between AH^+ and CB[7].[44] Exclusion complexes have been proposed in other CB[n]-guest systems.[21, 44, 76, 112-113] The exclusion complex is proposed as a mechanistic step in the formation of an inclusion complex,[21, 44] or the major product if the guest molecule is too large to enter the cavity of the CB[n].[76, 112] The mechanistic step between an exclusion complex and inclusion complex has been presented as a direct insertion, where the cationic charge of the guest passes through the hydrophobic cavity of CB[n],[44] or a 'flip-flop' mechanism.[21] The 'flip-flop' mechanism suggests that once the exclusion complex is formed, then the guest molecule reorients itself to form the inclusion complex, but the cationic charge does not pass through the hydrophobic cavity of the CB[n]. It is possible that a charged molecule can pass through the hydrophobic cavity of CB[7] otherwise inclusion complexes with symmetric dicationic guest molecules such as methyl viologen would not exist.[106] The difference between the two mechanistic pathways is not

consequential except in the situation, discussed later, where there is the formation of an exclusion complex with metal cation capping the other portal of CB[7]. The formation of the inclusion complex would only occur through a flip-flop mechanism otherwise the two cationic charges would be in close proximity to one another.

Due to the formation of the exclusion complex, equation 2.16 needed to be expanded to account for the formation of the exclusion complex when the kinetics show a single relaxation process. Equation 2.21, derivation in the appendix, is the expanded equation for the observed rate constant with respect to the total concentration of CB[7]. The formation of the exclusion complex competes, in the same way the metal cations binding to CB[7] do, with the formation of the inclusion complex. The exclusion complex, therefore, slows down the formation of the inclusion complex. Using experimental conditions in the presence of Na^+ cations when the kinetics fit to a mono-exponential function, eq. 2.21 can be used to calculate the maximum value for K_{ex}. The value of K_{ex} was found to be $(2.9 \pm 0.3) \times 10^6$ M^{-1}. The equilibrium constant for the exclusion complex between AH^+ and CB[7] was reported to be two orders of magnitude smaller to the equilibrium constant between NpH^+ and CB[7] at $(2.6 \pm 0.6) \times 10^4$ M^{-1}.[44]

$$k_{obs} = \frac{k_+[CB[7]]_T}{1+K_1[Na^+]+K_1K_2[Na^+]^2+K_{ex}[CB[7]]_T} + k_- \qquad \text{(Eq. 2.21)}$$

The equilibrium constant is equal to the ratio of the association rate constant and the dissociation rate constant. The association rate constant for the formation of the exclusion complex is assumed to be close to the diffusion controlled limit ($\sim 10^9$ $M^{-1}s^{-1}$)[53] because the exclusion complex competes like a metal cation for the binding of a CB[7] portal which is a diffusion controlled process. From the equilibrium constant of the exclusion complex and the assumed association rate constant, the dissociation rate constant can be calculated to a value between 500 and 1000 s^{-1}. A dissociation rate constant between 500 and 1000 s^{-1} is consistent with the idea that the component of the kinetics with the highest observed rate constant being close 1000 s^{-1} is accurate and could be fixed for the data analysis.

The ability of Na^+ cations to control the formation of the exclusion complex on the overall kinetics shows that the exclusion complex competes like a metal cation for the binding of the CB[7] portals. The disappearance of the exclusion complex in the kinetics is governed

by the competition between concentrations and equilibrium constants: the concentration of NpH^+ multiplied by the binding constant of the exclusion complex is competing against the binding constant of Na^+ cations to CB[7] multiplied by the concentration of Na^+ cations (eq. 2.22). It cannot be ruled out that there is the potential for the formation of an exclusion complex with a metal cation coordinated to the other portal, which would be a metal cation capped exclusion complex. The equilibrium constant for the capped exclusion complex would be one half the equilibrium constant of the uncapped exclusion complex. There is only one CB[7] portal for NpH^+ to bind to, which decreases the association rate constant by half. The dissociation rate constant, however, remains unchanged, as the dissociation rate constant is unimolecular and not dependent on any other species present.

$$K_1[Na^+]_T > K_{ex}[NpH^+]_{eq} \quad \text{(Eq. 2.22)}$$

When the metal cation in solution was changed from Na^+ cations to Ca^{2+} cations the kinetics between NpH^+ and CB[7] showed a third relaxation process that had a lower dissociation rate constant than the NpH^+@CB[7] complex seen in the presence of Na^+ cations. When the Ca^{2+} cation concentration was increased to a concentration where the kinetics fit to a single exponential function, the dissociation rate constant was found to be 20 s^{-1} lower than the dissociation rate constant when the kinetics fit to a single exponential function in the presence of Na^+ cations. This new mechanistic step in the presence of Ca^{2+} cations was assigned to a Ca^{2+} cation capped inclusion complex.

There are published examples of small organic molecules forming inclusion complexes that are capped by inorganic metal cations,[85, 94, 114] and examples of metal cation mediated higher order CB[7]-guest complexes, where the thermodynamic result of the system is governed by the concentration and identity of the metal cation.[82, 84] Further, an example of how an increase in concentration of Na^+ cations changed the binding mechanism of N-phenyl-2-naphthylammonium (PNA) to CB[7]:[51] at low concentrations of Na^+ cations, there is a faster formation of CB[7] binding to the phenyl moiety, but the predominant product is a 1:1 CB[7]-PNA guest complex where CB[7] binds to the naphthyl moiety of PNA. However, when the Na^+ cation concentration was sufficiently high, a 2:1 CB[7]-PNA complex was formed, where the CB[7] bound to the phenyl moiety is capped by a

Na^+ cation and the second CB[7] bound to the naphthyl moiety remained uncapped. This result suggests that the naphthyl moiety is too large once included into CB[7] for a Na^+ cation to interact with the portal of CB[7] while the guest is bound. The naphthyl group being too large to be capped by a Na^+ cation is consistent with the result that no Na^+ cation capped inclusion complex was seen between NpH^+ and CB[7].

Equation 2.23 can be used as justification for Ca^{2+} cations capping a CB[7] complex with a naphthyl moiety when Na^+ cations cannot. The potential energy between a dipole and a charged species is directly proportional with the reciprocal of the square of the distance between the dipole and charge in solution. Therefore, the potential energy between Ca^{2+} cations and CB[7] is double the potential energy between Na^+ cation and CB[7] at the same distance. It should be noted that the hydrated ionic radii, and non-hydrated ionic radii, are the same for the Ca^{2+} cation and the Na^+ cation.[115]

$$E = -k\frac{q_1\mu_2}{r^2} \qquad \text{(Eq. 2.23)}$$

The ability of Ca^{2+} cations to cap the NpH^+@CB[7] complex decreases the dissociation rate constant by slowing down the influx of water into the cavity of CB[7] as the guest leaves. A thermodynamic driving force of CB[n]-guest is the release of 'high-energy' water from the cavity of CB[7].[75] Water within the cavity of CB[n]s is hydrogen bond deficient, when the guest molecule binds, the water is displaced to the bulk solution and gains hydrogen bonds, which is a large thermodynamic driving force to CB[n]-guest binding.[75] When the guest molecule dissociates from CB[n], the cavity will refill with water. In an uncapped complex the water will fill the cavity from the opposite end of the cavity that the guest is dissociating from, however, if that portal has a Ca^{2+} cation blocking the influx of water there becomes a 'vacuum-like' suction force in the cavity of CB[7] when the guest molecule dissociates from the cavity of the CB[7]. The water refilling the cavity of CB[7], therefore, needs to enter the CB[7] cavity through the same portal as the NpH^+ guest molecule is dissociating from, or move past the Ca^{2+} cation that is blocking the opposite portal. An alternative explanation for the decreased dissociation rate constant is that the guest has only one direction to dissociate from the complex. The uncapped NpH^+@CB[7] complex has a dissociation rate constant of 55 ± 7 s^{-1}, and the dissociation rate constant of the Ca^{2+} capped inclusion complex was 33 ± 4 s^{-1}. The dissociation rate constant of the

capped complex is slightly more than half of the highest value, including error, for the uncapped inclusion complex (62 s^{-1}). The unidirectional dissociation of NpH^+ from CB[7], because one portal is blocked by a Ca^{2+} cation, may account for the decrease in dissociation rate constant, assuming the dissociation of the ammonium group passing through the cavity of CB[7] is slower than the dissociation of the NpH^+ guest where the charge does not pass through the cavity of CB[7].

The principle of metal cation concentrations mediating the concentration of species present in solution is consistent when the metal cation changes. Based on the similarities in the binding mechanisms in the presence of Na^+ and Ca^{2+} cations, with the formation of the exclusion complex, inclusion complex and two metal cations binding to CB[7], a more inclusive mechanism for all metal cations can be proposed. Scheme 2.3 was constructed as an inclusive mechanism for the NpH^+@CB[7] binding mechanism in the presence of the metal cations to present all the possible avenues of binding in the presence of Na^+ or Ca^{2+} cations.

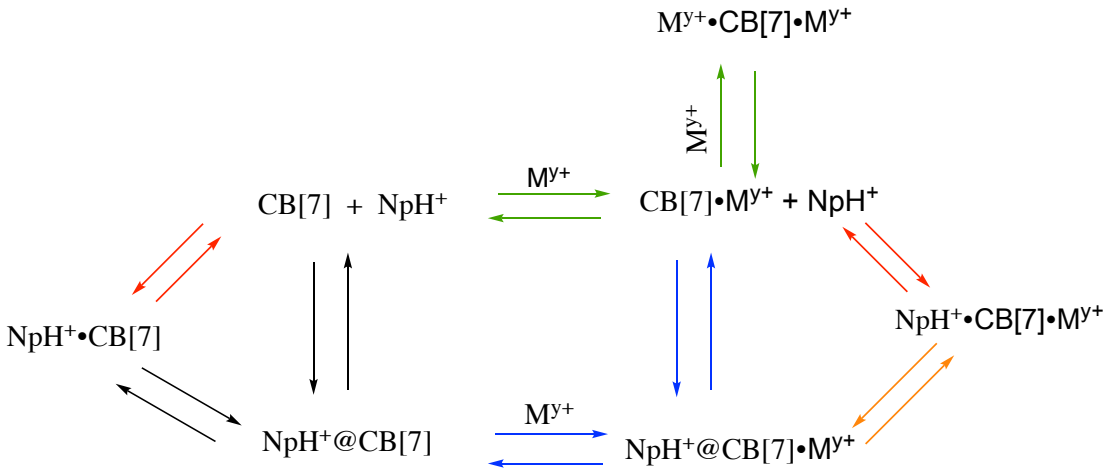

Scheme 2.3 Proposed overall mechanism for the binding of NpH^+ to CB[7] in the presence of cations.

The arrows of the same colour result in the formation of similar complexes that may or may not be able to be differentiated from one another when fitting the kinetic traces to a sum of exponentials function, for example, the formation of two different exclusion complexes may not have different fluorescent signatures. Therefore, the reactions shown are all potential contributors to the fit of the kinetics to the sum of exponentials function.

The green arrows show the sequential binding of the metal cations to CB[7]. The red arrows show the formation of the exclusion complex to a free CB[7] or a CB[7] with a metal cation bound the opposite portal. The black arrows represent the formation of the uncapped inclusion complex. The blue arrows represent the formation of the capped inclusion complex that only happens in the presence of Ca^{2+} cations. Finally, the orange arrows correspond to the formation of the capped inclusion complex through an exclusion complex via the previously discussed 'flip-flop' mechanism.

Aspects of scheme 2.3 can be simplified for a mechanism in the presence of Ca^{2+} cations. The formation of the exclusion complex is simplified to the formation of the exclusion complex to free CB[7] (NpH^+•CB[7]), rather than the cation capped CB[7] (NpH^+•CB[7]•M^{y+}). The single metal cation bound CB[7] is prevalent in relatively large amounts at all concentrations of metal cations in the presence of either Ca^{2+} cations or Na^+ cations (table B1). Therefore, the formation of the exclusion complex with a metal cation complexed to CB[7] (NpH^+•CB[7]•M^{y+}) should appear at all concentrations of metal cations, especially when the CB[7] concentration is elevated. However, from experiments in the presence of Ca^{2+} or Na^+ cations, the exclusion complex did not contribute to the overall kinetics at elevated concentrations of the metal cations. In the final mechanism, the exclusion complex (NpH^+•CB[7]) and uncapped inclusion complex (NpH^+@CB[7]) are expressed as independent reactions rather than the cyclic mechanism presented in scheme 2.3 because the 'flip-flop' mechanism between the exclusion complex (NpH^+•CB[7]) and the uncapped inclusion complex (NpH^+@CB[7]) is a redundant step for the formation of the inclusion complex (NpH^+@CB[7]), and when the metal cation concentration reaches a sufficiently high concentration the exclusion complex (NpH^+•CB[7]) does not play a role in the overall kinetics, therefore mechanistic pathway of the exclusion complex becoming the inclusion complex no longer plays a role in the overall kinetics. With respect to the orange arrows in scheme 2.3, the formation of the capped inclusion complex (NpH^+@CB[7]•M^{y+}) from the exclusion complex with a Ca^{2+} cation capping the other portal (NpH^+•CB[7]•M^{y+}) depends on the 'flip-flop' mechanism only, but the formation of the metal capped exclusion complex was ruled out above, therefore the reaction with the orange arrow does not contribute to the overall kinetics. Finally, there are two possible pathways for the formation of the Ca^{2+} cation capped inclusion complex

(NpH^+@CB[7]•M^{y+}). The bottom row of scheme 2.3 shows the capping of the NpH^+@CB[7] complex with a Ca^{2+} cation once the inclusion complex has been formed. At low concentrations of Ca^{2+} cations, the two reactions that form the Ca^{2+} capped complex are happening simultaneously, which is why there are multiple relaxation processes: the dissociation of the guest molecule from the capped inclusion complex and uncapped inclusion complex can be seen. However, at elevated concentrations of Ca^{2+} cations (>90 mM), there is no detectable formation of the uncapped inclusion complex (NpH^+@CB[7]). Because there is no detectable formation of the uncapped NpH^+@CB[7] complex, the pathway in scheme 2.3 where a Ca^{2+} cation caps the inclusion complex is not occurring. From table 2.1, the dissociation rate constant remains constant above 90 mM Ca^{2+} cations and there is only one relaxation process seen in the kinetics, so the mechanistic step will be simplified to NpH^+ binding the CB[7] with a Ca^{2+} cation coordinated to it.

From the discussion above, scheme 2.3 can be condensed to a simplified mechanism in scheme 2.4 in the presence of Ca^{2+} cations. The first two steps are the sequential binding of the Ca^{2+} cations to CB[7]. Equation 2.4 and 2.17 correspond to the formation of the inclusion complex and exclusion complex respectively. Finally, the formation of the capped inclusion complex is given by equation 2.25 for the reasons discussed above.

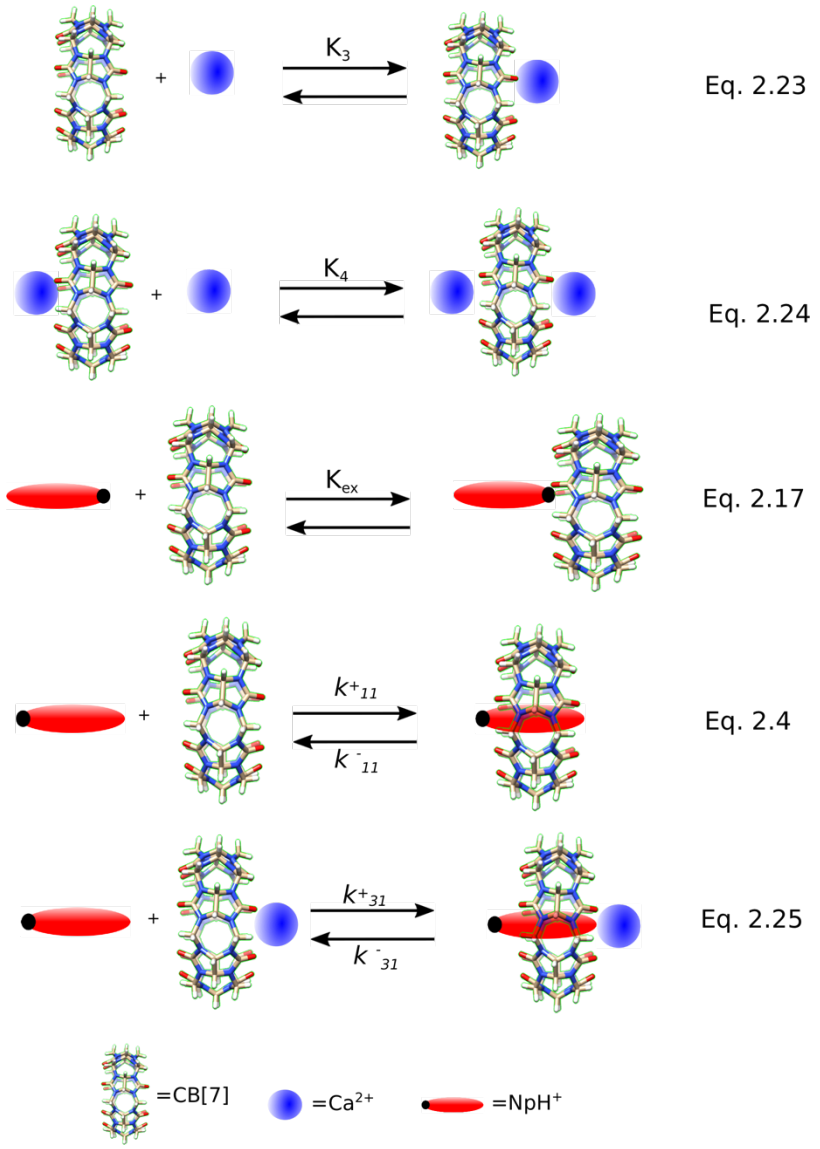

Scheme 2.4 Proposed mechanism for the binding between NpH^+ and CB[7] in the presence of Ca^{2+} cations.

While there are reports of metal cationic species affecting the thermodynamic parameters of a CB[n]-guest system,[38, 82, 84-85, 92, 94] and there are reports of how increasing the concentration of a metal cation can slow down the kinetics of CB[7]-guest complexation[49] or add complexity with increasing metal cation concentration,[51] this is the first study into how different metal cations and their concentrations can change the mechanism of host-guest binding and control the species present in solution. Understanding how all components of a system interact with one another is integral in the design of functional materials or drug delivery systems, where the environment becomes increasingly complex.

It is important to understand how the components of the medium will affect the dynamics within a designed system. Above the argument was made that due to the complexity introduced by the metal cations, or components of a buffered solution, used universally in CB[n]-guest chemistry that CB[n] chemistry should be considered within the realm of systems chemistry. But this chemistry also creates an opportunity to understand how to control complex systems using relatively simple host-guest systems, moving systems chemistry from the "trial and error" mentality used in DCLs, to the rational design of dynamic systems that can be controlled: a bottom up approach to systems chemistry.

Chapter 3: Investigating how guest structure affects kinetic time scales for the formation of complexes with CB[7]

Kevin A. Vos, Elisa Medeiros dos Santos, David Berg and Cornelia Bohne

KV and CB came up with the conceptual frame work for the project: guest molecules and experiment list. Dr. Berg and KV worked on the synthesis and isolation of $MDAP^{2+}$. KV perform all of the experiments between MV^{2+} and CB[7], and all the experiments between $MDAP^{2+}$ and CB[7]. EMS performed the preliminary experiments between Bn^{2+} and CB[7], the final experiments were conducted by KV. EMS also performed the molar absorptivity studies of Bn^{2+}.

3.1 Introduction

3.1.1 Background

In design of supramolecular drug delivery systems, self-sorting systems and functional materials the thermodynamic parameters, such as equilibrium constants, play the prominent role in their characterization.[46, 108, 113, 116-117] But, because of the reversibility of supramolecular interactions, understanding the dynamics between species is essential in the design and function of drug delivery systems, self-sorting systems and functional materials.[42, 46, 118-121] The equilibrium constant, as discussed in the previous chapter, is the ratio of the association rate constant and dissociation rate constant between two species. If the time scale of host-guest interactions in supramolecular systems is changed, the release profile of molecules from supramolecular systems or time scales over which self-sorting occurs, can be modified.[118] The analysis of the kinetics in a system becomes increasingly important as a system moves from being studied in isolation, to being studied in more complex media, such as biological samples, where competitive equilibria can interfere with a desired function, such as drug release.[120]

The design of new drug delivery systems is focused on achieving a controlled release over prolonged time scales.[45, 121-129] The purpose of designing controlled release drug delivery systems is to reduce the variability in blood drug levels by patients not following prescribed times between dosages, increase the bioavailability by not having drugs be orally administered, decreasing the number of doses required, and more targeted therapy because the drug delivery system can be administered in a specific tissue or at a specific site to

reduce off target reactivity.[125-126] Work in 3D-printing polymer systems, or the design of polymer systems, focus on the dissolution of the polymer over time for the controlled release of the drug.[45, 125-127] The hydrogels that are studied for drug delivery systems are often stimuli responsive, such as pH responsive, which is significant for the treatment different conditions, like cancer.[122, 124]

The analysis of most of these polymer based drug release systems attribute the drug release to Fickian diffusion, or other mathematical models, and show that the change in mass of drug in the gel with respect to time is directly proportional to the viscosity of the gel.[45, 118, 122, 124-125] For a supramolecular cross-linked hydrogel, the viscosity is related to the number of cross-links within the gel, which is a thermodynamic parameter, however, in the cross-linked hydrogels there can be erosion-based release of the drug which shows dependence on the kinetics of the intermolecular interactions.[118]

For self-sorting systems, the distribution of kinetic and thermodynamic products in social self-sorting is initially controlled by the association and dissociation rate constants between the host and guest molecules, and over time the thermodynamic equilibria dominate for the distribution of products.[38, 130] Therefore investigating how the structural features of guest molecules can affect the rate of reaction with CB[7] is important for the design of supramolecular systems with desired molecule release profiles, or kinetic traps for self-sorting systems.

A common guest molecule used with CB[7] and CB[8] is methyl viologen (MV^{2+}).[106] Since the first reported MV^{2+}@CB[n] complex,[131] these host-guest complexes have been used to examine how the concentration of salts effects the thermodynamic stability of a CB[7]-guest complex and to study the electrochemistry of MV^{2+} in a macrocyclic container.[92, 106, 131-133] CB[8] is large enough to accommodate two aromatic molecules. CB[8] can accommodate two electrochemically reduced $MV^{\bullet+}$ that dimerize in the cavity of CB[8].[134] Further, the two guest molecules in the cavity of CB[8] can be a combination of an electron deficient molecule and electron rich molecule. When MV^{2+} is added to a solution with CB[8] and an electron rich guest, such as a hydroxy-naphthalene derivative, a charge transfer complex inside the cavity of CB[8] is formed in what is called a 1:1:1 hetero-ternary complex.[131, 135] After the discovery of the 1:1:1 hetero-ternary complex in CB[8], the guest molecules were functionalized onto a polymer backbone. When the guest

molecules are functionalized onto a polymer backbone and CB[8] is added, the formation of the charge transfer complex in the cavity of CB[8] results in the formation of a supramolecular hydrogel.[20, 118, 136] These hydrogels have been proposed as a slow release drug delivery system.[118]

While the thermodynamic characteristics of MV^{2+}@CB[7] have been studied through electrochemistry,[132, 134] NMR[131] and absorbance spectroscopies,[106] the kinetics have not been reported on the ms time scale. Rheology experiments of a CB[8] cross-linked hydrogel reported the dissociation rate constant of MV^{2+} from CB[8] was 1200 s^{-1}, and an assumption can be made that the dissociation rate constant of the MV^{2+}@CB[7] complex would be similar.[118] A dissociation rate constant of 1200 s^{-1} suggests that the kinetics are faster than the ms time scale, which explains why the kinetics with CB[7] nor CB[8] have been reported using a stopped-flow device. The kinetics of a modified viologen, with aliphatic chains instead of methyl groups, showed some kinetics on the ms time scale by stopped flow. These kinetics showed the formation of a two CB[7] molecules to 1 guest molecule complex, where the CB[7] molecules were bound to the aliphatic chains.[137]

The fast kinetics between MV^{2+} and CB[7] presented an opportunity to study how the structure of guest molecules can change the time scale of the kinetics for CB[7]-guest complexes. (chart 3.1)

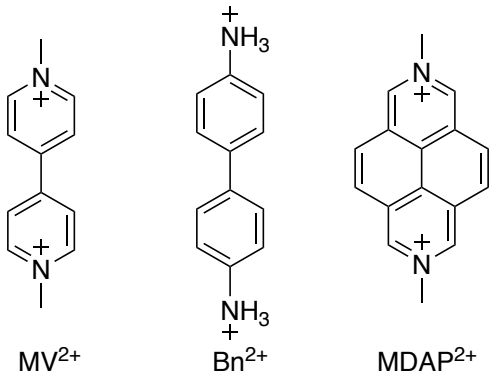

Chart 3.1 Chemical structures of MV^{2+}, Bn^{2+} and $MDAP^{2+}$.

Benzidine, Bn^{2+}, has a similar structure to MV^{2+} however the nitrogen atoms are primary ammoniums, whereas the nitrogen atoms are a part of the aromatic system in MV^{2+}. The binding of Bn^{2+} has not been extensively investigated with the CB[n] family, however, there is one report of an inclusion complex with CB[7] studied by electrochemistry and

one report of exclusion complexes with CB[6].[112, 138] The inclusion complex between benzidine and CB[7] was shown by electrochemistry, however the conditions are not reported and the equilibrium constant reported is indicative of benzidine not being protonated on either side.[138] Studies between Bn^{2+} and CB[6] by electrophoresis showed the formation of extended assemblies, made of exclusion complexes in a 1:1 ratio, in the crystalline state.[112]

The third guest chosen was 2,7'-dimethyl-diazapyrenium ($MDAP^{2+}$). $MDAP^{2+}$ is the pyrene derivative of MV^{2+}, which has the cationic nitrogens in the same position as MV^{2+}, but $MDAP^{2+}$ is wider and more rigid. While a full kinetic study of $MDAP^{2+}$ with CB[7] has never been reported, in determining the equilibrium constant with CB[7] it was noted that the peaks in the ^1H NMR spectra showed broadening as CB[7] was added to the solution. This result suggested that the kinetics occur on the NMR time scale, which is a longer time scale than the stopped-flow time scale.[104] Further, a dissociation rate constant between $MDAP^{2+}$ and CB[7] was published recently at 0.018 s^{-1} by using a competitive displacement assay on a stopped-flow device.[139] Because of the structure of $MDAP^{2+}$, it is capable of forming similar charge transfer complexes within the cavity of CB[8] as MV^{2+} does is in the presence of a second electron rich guest molecule.[40] $MDAP^{2+}$ has been used, with CB[8], as a catechol and dopamine sensor in solution through the formation of charge transfer complexes.[40]

3.1.2 Objectives

The objective of the work in this chapter is to determine the effect structural changes in guest molecules have on the time scale of the kinetics between guest molecules and CB[7]. Stopped-flow experiments between CB[7] and MV^{2+} were conducted to confirm whether, or not, the kinetics were faster than the ms time scale that can be measured on the stopped-flow device. The kinetic experiments were then conducted between CB[7] and both Bn^{2+} and $MDAP^{2+}$ to determine which structural changes would have a greater effect on the kinetics with CB[7]: the distance between charges or the width and rigidity. Further, binding isotherm studies were conducted to determine the difference in thermodynamic stability between the three CB[7]:guest complexes.

3.2 Experimental

3.2.1 Materials

Benzidine and naphthalene-1,4,5,8-tetracarboxylic dianhydride were purchased from TCI Chemicals and were used without any further purification. CB[7] was obtained from the same synthesis described in chapter 2. $MVCl_2$, NaCl, ammonium hydroxide, BH_3-THF, potassium carbonate, MnO_2, ammonium chloride (NH_4Cl), bis(cyclopentadienyl)cobalt (II) (Cob^+) and methyl iodide were purchased from Sigma-Aldrich and were used without any further purification. Hydrochloric acid (HCl, ACS grade, 36.5-38%) was purchased from VWR Analytical and was used as obtained. Spectral grade methanol, for use in the ultraviolet region of the spectrum, was purchased from Fisher Chemical and was used as received. Calcium chloride dihydrate ($CaCl_2•2H_2O$) was purchased from Biobasic Canada Inc. Aqueous solutions were prepared using de-ionized water from a Barnstead NANOpure deionizing system (≥ 17.3 MΩ cm).

3.2.2 Synthesis of $MDAP^{2+}$

$MDAP^{2+}$ was synthesized using a modified version of the method previously reported in the literature,[140-141] developed with the help of Dr. Dave Berg. A 1 L, two necked, flask was loaded with 12.5 g (46.6 mmol) of compound **A**. Then, compound **A** was dissolved in concentrated ammonium hydroxide (625 mL, 29.5% w/w). The reaction mixture was stirred for 6 h under N_2 atmosphere to produce compound **B**. The yellow powder, which is pure **B**, was filtered and washed with de-ionized water. Isolated compound **B** was dried under vacuum at 60 °C overnight.

The yellow powder of **B** was added to a three-necked flask with 125 mL of THF as a solvent. Under N_2 pressure, 1.0 M BH_3-THF was added dropwise at room temperature until the solid dissolved. The reaction mixture was refluxed for 60 h until the reaction mixture turned orange. The reaction mixture was cooled to 0 °C, then the reaction was quenched by adding ethanol and stirring the mixture for 30 min at room temperature. The resulting mixture had 6 M HCl added to it and was refluxed for 3 h. During the 3 h, the reaction

mixture was stirred vigorously to avoid foaming. The solvent was evaporated under reduced pressure, and the resulting solid was cooled to 0 °C. To the solid, a saturated solution of potassium carbonate was added until the pH was greater than 10. The solvent was then evaporated under reduced pressure again at 40 °C to produce compound **C**. To isolate compound **C**, a Soxhlet extraction in benzene was conducted for 1 week. The benzene was removed and compound **C** was recrystallized in fresh benzene to get pure compound **C**.

Compound **C** was then added to a 500 mL round bottom flask with a magnetic stir bar, reflux condenser, nitrogen inlet, gas vent and Dean Stark trap. To the flask, MnO_2 was added at a 25:1 ratio and the mixture was refluxed in benzene for 24 h. The mixture was then filtered and the warm benzene was kept as it contained the compound **D**. The remaining compound **D** was extracted from the remaining MnO_2 solid through a Soxhlet extraction in benzene for 3 d. The fractions of the Soxhlet extraction were combined and the solvent was removed under reduced pressure to isolate compound **D**. Compound **D** was added in a 1:2 molar ratio with methyl iodide in 25 mL of DMSO. The reaction mixture was heated to 60 °C under N_2 atmosphere. The resulting solid, $MDAP^{2+}$, was filtered off. The counter ion needed to be changed from I^-, because I^- quenches fluorescence. $MDAP^{2+}$ was dissolved in a 1:1 mixture of acetone and water, then a large excess of NH_4Cl was added and the reaction mixture was heated to 40 °C for 4 h. The solvent was evaporated away and the purification method used was the same as the previously reported synthesis.[140] The purity was confirmed by the ^1H NMR with signals at 9.93 (s), 8.75 (s) and 4.86 (s) when run in D_2O (figure C1).[140]

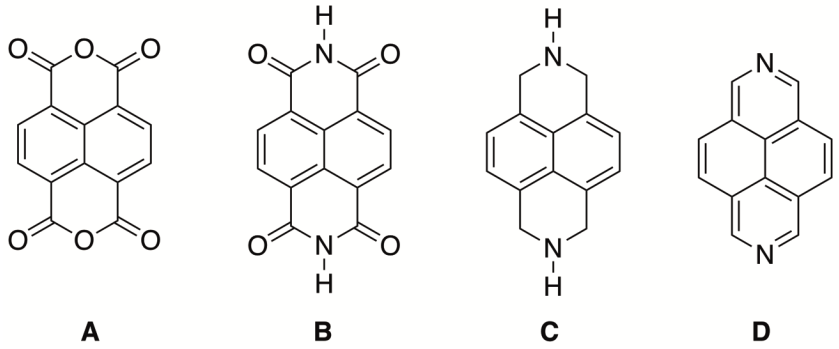

Chart 3.2 Chemical structures of intermediates produced in the synthesis of $MDAP^{2+}$.

3.2.3 Sample Preparation

Stock solutions of MV^{2+}, Bn^{2+}, $MDAP^{2+}$, CB[7], NaCl and HCl were made every 3-4 weeks. The stock solutions were then used to prepare samples for the experiments listed below. A stock solution of MV^{2+} was made with extreme caution because MV^{2+} is highly poisonous. To make a stock solution of MV^{2+}, capped volumetric flasks were pre-weighed and solid MV^{2+} was added in the confines of a fumehood. A MV^{2+} stock solution was made to 1.79 mM in de-ionized water. Stock solutions of 4 mM Bn^{2+} were made in spectral grade methanol. Bn^{2+} is toxic in solution, care should ben taken when solutions are made. Stock solutions of $MDAP^{2+}$ were made to approximately 100 μM by dissolving $MDAPCl_2$ in de-ionized H_2O, the solution was then diluted in an absorbance cell, and the concentration of the stock solution was determined using the molar extinction coefficient at 418 nm of 15000 $M^{-1}cm^{-1}$.[142] The toxicity of $MDAP^{2+}$ is unknown, so caution should be taken as the toxicity may be similar to MV^{2+}. Stock solutions of NaCl were made to 1.0 M by dissolving the solid in de-ionized H_2O. The HCl stock solutions were made to 1.0 M from the 4.0 N HCl solution. CB[7] stock solutions were made assuming the solids were completely dry. CB[n]s are hygroscopic, and therefore the actual concentration of CB[7] in the stock solutions was determined using a literature reported method as discussed in the previous chapter.[95] CB[7] stock solutions were made by dissolving 6-7 mg in 5 mL of de-ionized H_2O. Assuming a 100% purity (completely dry) the concentration of the CB[7] stock solution was between 1.0-1.3 mM. When the Cob^{+} stock solutions were diluted into experimental solutions, the actual concentrations were determined using the molar extinction coefficient of 34200 $M^{-1}cm^{-1}$ at 261 nm.[95]

Absorption binding isotherms: For absorption experiments guest solutions of 20-25 μM were made in the appropriate concentration of NaCl (10, 25, 50, 75 or 100 mM). Experiments with Bn^{2+} had enough 1.0 M HCl added for the pH to be below 2.15 to introduce a dicationic charge onto the molecule. CB[7] solutions were made to approximately 400 μM at the corresponding concentration of NaCl and correct pH for experiments with Bn^{2+}. A control experiment was conducted where an absorption spectrum at each concentration of CB[7] used in the binding isotherm which was used to subtract any absorption of CB[7].

Fluorescence binding isotherms: $MDAP^{2+}$ solutions were made to 1 μM at 50 or 100 mM NaCl. CB[7] solutions were made at 250 μM and the same concentrations of NaCl and $MDAP^{2+}$ so dilution would not need to be accounted for.

Stopped-flow experiments: As discussed in the previous chapter, for stopped-flow experiments the concentrations for CB[7] and guest species were prepared to double the concentration of experimental concentrations because solutions are mixed in a 1:1 ratio, so the species concentrations are diluted in half. For absorption and fluorescence kinetic experiments CB[7] solutions were made at 10, 25, 50, 100, 150 and 200 mM NaCl with CB[7] concentrations of 5-80 μM. For absorption kinetic experiments, the guest molecule solutions were made to a concentration of approximately 40 μM guest and the corresponding concentration of NaCl to match the concentration of NaCl in the CB[7] solutions. For fluorescence kinetic experiments, $MDAP^{2+}$ solutions were made to 2 or 10 μM and the corresponding concentration of NaCl to match the NaCl concentration in the CB[7] solutions.

3.2.4 Equipment

Fluorimeter: Steady-state fluorescence experiments were conducted on a PTI QM-40 spectrofluorimeter. The emission spectra were collected between 400 and 550 nm. The samples were excited at 338 nm with excitation and emission bandwidth of 1 nm. The step size for the collection of the spectra was 0.5 nm and the integration time was set to 0.25 s. The samples were equilibrated to 20 °C for 10 min after the addition of CB[7].

UV/Vis spectroscopy: The absorption spectra were collected on a Varian Cary 100-Bio UV-Vis spectrophotometer or a Varian Cary 1E UV-Vis spectrophotometer. UV-Vis spectra were collected from 200 to 400 nm for solutions containing Bn^{2+} or MV^{2+}, and from 200 to 500 nm for solutions containing $MDAP^{2+}$. The spectra were collected against an air background. Experimental spectra were corrected by taking an absorbance spectrum of the solvent and subtracting the solvent spectrum from the experimental spectra.

Stopped flow: Kinetic experiments were performed on an Applied Photophysics SX-20 stopped-flow device. A Hg-Xe vapor lamp was used as the excitation source for both absorption and fluorescence experiments. The solutions were mixed under pressure at a 1:1

ratio. In the fluorescence experiments, the samples were excited at 340 nm with the slits set to 1 mm on the monochromator used to select the excitation wavelength. The 1.0 mm slit width corresponds to a bandwidth of 4.65 nm for the excitation beam. The fluorescence was collected through a 395 nm cut-off filter, where all light below the wavelength of 395 nm was excluded. The absorption kinetic traces were collected through a 1 cm path length. The absorption wavelength for detection of MV^{2+} was 257 nm and Bn^{2+} was 247 nm. The samples were held at 20 °C for 10 min before kinetic traces were collected. Kinetic traces were corrected by collecting kinetic traces of all components except the fluorophore, and subtracting the trace for the control experiment from the trace corresponding to the sample.

3.2.5 Molar extinction coefficient of Bn^{2+}

The molar extinction coefficient of the dicationic benzidine in water has not been reported in the literature.[143] To determine the correct pH to perform experiments between Bn^{2+} and CB[7], the absorbance of benzidine at different pH's was taken until the absorption maximum was at 247 nm and there were no further spectral changes (figure 3.1).

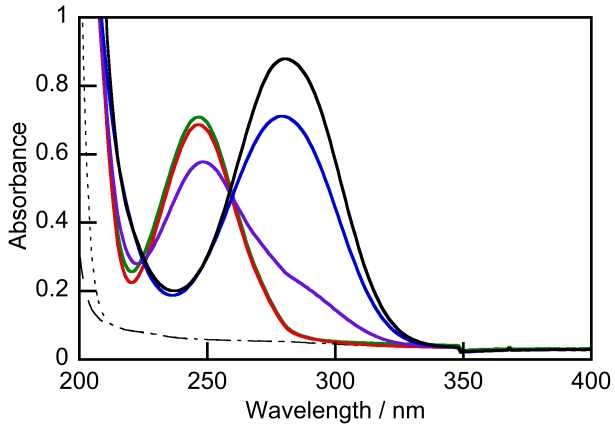

Figure 3.1 Absorbance spectra of benzidine at different pH's (5.89, black; 4.32, blue; 3.03 purple; 2.17, red; 1.31, green). The dotted lines correspond to the absorption of the solvent without benzidine (2.17, large dots; 1.31 small dots).

From figure 3.1 it was determined that a pH to use for experiments between CB[7] and Bn^{2+} is 2.0. To determine the molar extinction coefficient, the absorption at 247 nm at different concentrations of Bn^{2+} at pH 2.0 was measured (figure 3.2). The slope of the fit

line between absorption values and the $Bn^{2=}$ concentration is equal to the molar extinction coefficient by eq. 3.1

$$A = \varepsilon \ell c \quad \text{(Eq. 3.1)}$$

Where A is the absorbance, c is the concentration of benzidine, ℓ is the path length which is 1 cm and ε is the molar extinction coefficient. From these experiments, it was determined, from the average of two experiments, that the molar absorptivity constant for the dicationic form of Bn^{2+} is (18400 ± 300) $M^{-1}cm^{-1}$.

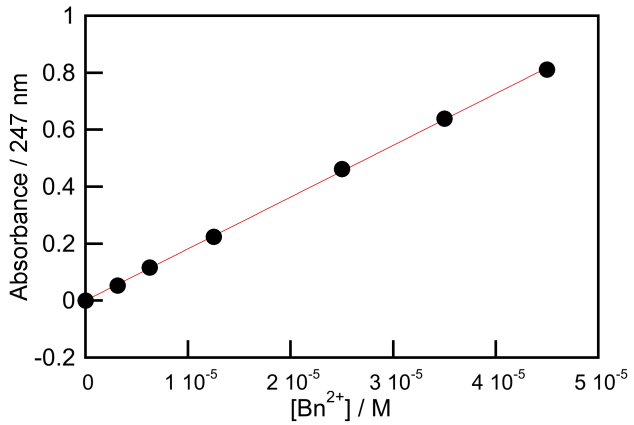

Figure 3.2 Dependence of the absorbance of Bn^{2+} at 247 nm with the concentration of Bn^{2+} at pH 2.0.

3.2.6 Binding isotherm models for the formation of the 1:1 complex between the guest molecules and CB[7] in absorption experiments

The absorption spectra of MV^{2+}, Bn^{2+} and $MDAP^{2+}$ solutions mixed with CB[7] were collected from either 200 to 400 nm (MV^{2+} and Bn^{2+}) or 200 to 500 ($MDAP^{2+}$). The change in absorbance at the absorbance maximum of the guest molecules (Bn^{2+} = 247 nm; MV^{2+} = 257 nm; $MDAP^{2+}$ = 334 nm) was plotted against the concentration of CB[7]. The data were fit to a 1:1 model using numerical analysis on the Scientist 3 software from Micromath:

$$[G@CB[7]]_{eq} = \beta_{11} \times [CB[7]]_{eq} \times [G]_{eq} \quad \text{(Eq. 3.2)}$$

$$[CB[7]]_{eq} = [CB[7]]_T - [G@CB[7]]_{eq} \quad \text{(Eq. 3.3)}$$

$$[G]_{eq} = [G]_T - \left[G@CB[7]\right]_{eq} \quad \text{(Eq. 3.4)}$$

$$A = R \times ([G]_{eq} + C_{11} \times \left[G@CB[7]\right]_{eq}) \quad \text{(Eq. 3.5)}$$

$$R = \frac{A_0}{[G]_T} \quad \text{(Eq. 3.6)}$$

Where the concentration restraints for the dependent variables are:

$$0 < [G]_{eq} < [G]_T \quad \text{(Eq. 3.7)}$$

$$0 < \left[CB[7]\right]_{eq} < \left[CB[7]\right]_T \quad \text{(Eq. 3.8)}$$

$$0 < [G@CB[7]]_{eq} < [G]_T \quad \text{(Eq. 3.9)}$$

The total concentrations of CB[7] and guest molecules present in solution are represented by $[CB[7]]_T$ and $[G]_T$. The equilibrium concentrations of CB[7], guest and the 1:1 CB[7]-guest complex are denoted as $[CB[7]]_{eq}$, $[G]_{eq}$ and $[G@CB[7]]_{eq}$, respectively. The concentration of CB[7] at equilibrium, $[CB[7]]_{eq}$, includes all species of CB[7] not bound to a guest molecule: free CB[7], CB[7] bound to a single Na^+ cation and CB[7] bound to two Na^+ cations. The overall equilibrium constant for the formation of the CB[7]-guest complex at a given concentration of Na^+ cations was denoted as β_{11}. The absorption of the guest molecules in the absence of CB[7] was denoted as A_0. R corresponded to the ratio of the absorption of the guest molecules in the absence of CB[7] (A_0) to the total guest concentration ($[G]_T$), which is equal to the molar extinction coefficient of the guest. C_{11} was the ratio of the molar extinction coefficient of the G@CB[7] complex and guest free in solution.

3.2.7 Binding isotherm models for the formation of the 2:1 complex between the guest molecules and CB[7] in fluorescence experiments

The emission spectra of $MDAP^{2+}$ solutions mixed with CB[7] solutions were integrated from 410 to 510 nm. The integrated values were divided by the integrated value measured for a $MDAP^{2+}$ solution with no CB[7] to convert the integrated emission intensity into a relative integrated intensity value (I). The plot being fit was the dependence of the relative integrated intensity values against the concentration of CB[7]. The data were fit to a 2:1 model using numerical analysis on the Scientist 3 software from Micromath:

$$[G@CB[7]]_{eq} = \beta_{11} \times [CB[7]]_{eq} \times [G]_{eq} \quad \text{(Eq. 3.10)}$$

$$[CB[7] \cdot G \cdot CB[7]]_{eq} = \beta_{12} \times [G@CB[7]]_{eq} \times [CB[7]]_{eq} \quad \text{(Eq. 3.11)}$$

$$[CB[7]]_{eq} = [CB[7]]_T - \left[G@CB[7]\right]_{eq} - 2[CB[7] \cdot G \cdot CB[7]]_{eq} \quad \text{(Eq. 3.12)}$$

$$[G]_{eq} = [G]_T - \left[G@CB[7]\right]_{eq} - [CB[7] \cdot G \cdot CB[7]]_{eq} \quad \text{(Eq. 3.13)}$$

$$I = R \times ([G]_{eq} + C_{11} \times \left[G@CB[7]\right]_{eq} + C_{12}[CB[7] \cdot G \cdot CB[7]]_{eq}) \quad \text{(Eq. 3.14)}$$

$$R = \frac{I_0}{[G]_T} \quad \text{(Eq. 3.15)}$$

Where the concentration restraints for the dependent variables are:

$$0 < [G]_{eq} < [G]_T \quad \text{(Eq. 3.16)}$$

$$0 < \left[CB[7]\right]_{eq} < \left[CB[7]\right]_T \quad \text{(Eq. 3.17)}$$

$$0 < [G@CB[7]]_{eq} < [G]_T \quad \text{(Eq. 3.18)}$$

$$0 < [CB[7] \cdot G \cdot CB[7]]_{eq} < [G]_T \quad \text{(Eq. 3.19)}$$

The total concentrations of CB[7] and guest molecules present in solution are represented by $[CB[7]]_T$ and $[G]_T$. The equilibrium concentrations of CB[7], guest, the 1:1 CB[7]-guest complex and the 2:1 CB[7]-guest complex are denoted as $[CB[7]]_{eq}$, $[G]_{eq}$, $[G@CB[7]]_{eq}$ and $[CB[7]•G•CB[7]]_{eq}$ respectively. The concentration of CB[7] at equilibrium, $[CB[7]]_{eq}$, includes all species of CB[7] not bound to $MDAP^{2+}$: free CB[7], CB[7] bound to a single Na^+ cation and CB[7] bound to two Na^+ cations. The overall equilibrium constants for the formation of the CB[7]-guest complexes at a given concentration of Na^+ cations were denoted as β_{11} and β_{12}. The integrated intensity of $MDAP^{2+}$ in the absence of CB[7] was denoted as I_0. R corresponded to the ratio of fluorescence intensity of $MDAP^{2+}$ in the absence of CB[7] (I_0) to the total guest concentration ($[G]_T$). C_{11} and C_{12} were the ratios of the emission quantum yields of the 1:1 and 2:1 complexes between CB[7] and $MDAP^{2+}$, and $MDAP^{2+}$ free in solution.

3.2.8 Binding isotherm models for the formation of the 2:1 complex between the guest molecules and CB[7] in absorbance experiments

The model remains the same as the one described in section 3.2.7 with 2 modifications because these experiments are done using absorbance measurements. R is now equal to the molar extinction coefficient which is the ratio of the initial absorption of the guest molecule in the absence of CB[7] (A_0) and the total guest concentration ($[G]_T$). C_{11} and C_{12} are the ratios of molar extinction coefficients of the 1:1 and 1:2 complexes between $MDAP^{2+}$ and CB[7], and $MDAP^{2+}$ free in solution.

3.2.9 Analysis of fluorescence stopped-flow data between $MDAP^{2+}$ and CB[7]:

In stopped-flow experiments, 11 traces were collected, the first 2 were removed and the remaining 9 were averaged. The traces were fit to a sum of exponentials function (Eq. 3.20).

$$\Delta I = \alpha_0 + \alpha_1 e^{-k_{obs1}t} + \alpha_2 e^{-k_{obs2}t} + \alpha_3 e^{-k_{obs3}t} \quad \text{(Eq. 3.20)}$$

The change in fluorescence intensity is denoted as ΔI. The change in fluorescence intensity is equal to the sum of the exponentials multiplied by the amplitude for each term (α_x, where x = 0, 1, 2 or 3). Each exponential term corresponds to a single observed rate constant (k_{obs}). There was one amplitude which was not multiplied by an exponential term, α_0, which corresponds to any change in amplitude where the observed rate constant was faster than the time resolution of the instrument used.

3.2.10 Analysis of absorption stopped-flow data for the binding between Bn^{2+} and CB[7]

The kinetic data for absorption stopped-flow experiments were fit to a model using Pro-Kineticist II software. The absorption data needed to be fit to a model because the reactions are not under a pseudo-first order condition as is the case for the reactions that are studied using fluorescence kinetic experiments. In the stopped-flow experiments, 11 traces were collected, the first 2 traces were removed and the remaining 9 were averaged and fit to a model. When building the model, reactions for which the kinetics are faster than the ms time scale are fixed as equilibrium constants and are represented by ⇄ in the model. Reactions that are fit for the association and dissociation rate constants are represented by <> in the model.

$$H + Na \rightleftarrows HNa \quad \text{(Eq. 3.21)}$$

$$HNa + Na \rightleftarrows NaHNa \quad \text{(Eq. 3.22)}$$

$$H + G <> HG \quad \text{(Eq. 3.33)}$$

$$HG <> C \quad \text{(Eq. 3.34)}$$

$$HG + H <> HGH \quad \text{(Eq. 3.35)}$$

$$HG + G <> GHG \quad \text{(Eq. 3.36)}$$

$$GHG <> C + G \quad \text{(Eq. 3.37)}$$

$$HGH <> C + H \quad \text{(Eq. 3.38)}$$

In this model, *H* represents the host molecule (CB[7]), *G* represents the guest molecule and *Na* represents the sodium cations. The formation of an inclusion complex is denoted as C,

the formation of exclusion complexes is denoted by *HG*, *GHG*, and *HGH* to show the opportunity to form a 1:1 exclusion complex, the 2:1, and 1:2 exclusion complexes.

3.3 Results

In the results section of this chapter the objective is to determine the equilibrium constants between the guest molecules and CB[7] and then compare the time scales of the kinetics between the guest molecules and CB[7].

3.3.1 Binding isotherms and kinetics between MV^{2+} and CB[7]

The binding isotherm between MV^{2+} and CB[7] (figure 3.3) in the presence of Na^+ cations was performed to determine the equilibrium constant (K_{11}) between MV^{2+} and CB[7]. Using eq. 3.39, as was done in chapter 2, the equilibrium constants can be recovered from the overall equilibrium constant (β_{11}) at a given concentration of Na^+ cations. The fit to a 2:1 CB[7]:guest exclusion complex model (figure C2) rendered a fit with almost identical residuals as the fit to the 1:1 model presented in figure 3.3.

$$\beta_{11} = \frac{K_{11}}{1+K_1[Na^+]+K_1K_2[Na^+]^2} \qquad \text{(Eq. 3.39)}$$

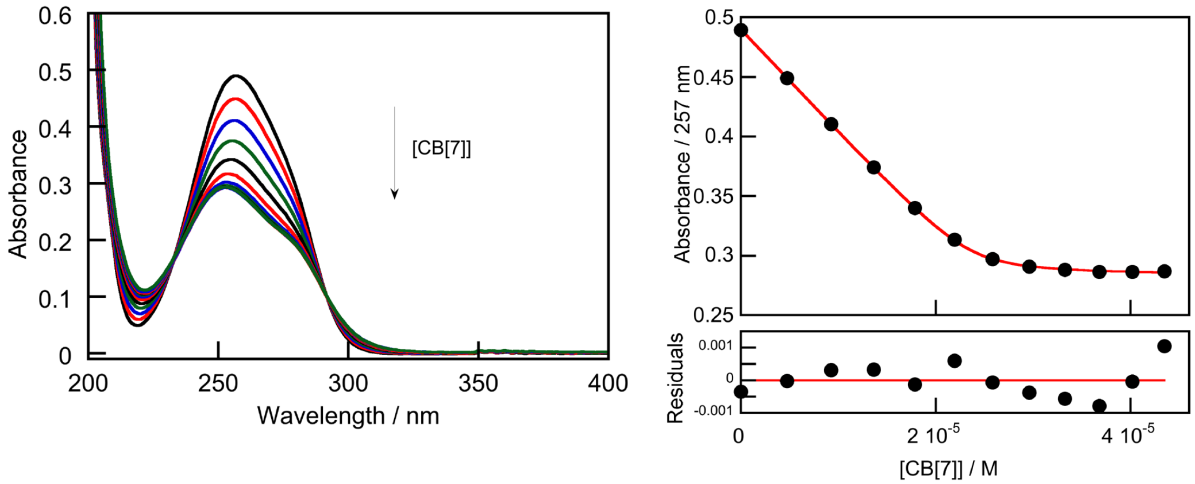

Figure 3.3 Left: Absorption spectra for 23.6 μM MV^{2+} with CB[7] concentrations ranging from 0-43.5 μM at 50 mM Na^+ cations. **Right:** Binding isotherm between MV^{2+} and CB[7] (top panel) using the absorption at 257 nm. The red line represents the numerical fit of the data. The bottom panel shows the residuals between the fit and the experimental data.

The equilibrium constant (K_{11}) recovered from eq. 3.39 was found to be $(4.7 \pm 0.3) \times 10^7$ M^{-1} when the binding isotherm was fit to a 1:1 CB[7] to MV^{2+} model. Most literature report equilibrium constants for MV^{2+} binding with CB[7] that were determined in the presence of tris buffer,[92, 106, 133, 144-145] which is not easily comparable to equilibrium constants in the presence of Na^+ cations. However when applying eq. 3.39 to a literature reported β_{11} value between MV^{2+} and CB[7] in the presence of 0.2 M Na^+ cations, the equilibrium constant recovered was 1.4×10^7 M^{-1}.[92]

The kinetics between MV^{2+} and CB[7] or CB[8] have never been reported using a stopped-flow device. Using rheological experiments, a CB[8] cross-linked hydrogel was used to estimate the dissociation rate constant between MV^{2+} and CB[8] which was 1200 s^{-1}.[20] In a reaction under pseudo-first order conditions, a dissociation rate constant of 1200 s^{-1} would produce a reaction with an observed rate constant that is too high to be detected on the stopped-flow device where the detection limit is an observed rate constant close to 1000 s^{-1}. Therefore, if 1200 s^{-1} was the dissociation rate constant between MV^{2+} and CB[7], it would be reasonable that the kinetics would not be seen on the ms time scale (figure 3.4). The kinetics of MV^{2+} and CB[7] were tested at decreased temperatures and various concentrations of Na^+ cations. Figure 3.4 shows the kinetic experiment between MV^{2+} and

CB[7] at 100 mM Na^+ cations at a decreased temperature (10 °C). The kinetics were shown to be faster than the dead time of the device suggesting that the reported dissociation rate constant making the kinetics too fast for a stopped-flow device from the discussion above may be accurate. In chapter 2, the dissociation rate constant of a guest@CB[7] complex was shown to be lower in the presence of Ca^{2+} cations through the formation of a Ca^{2+} cation capped inclusion complex. The addition of Ca^{2+} cations rather than Na^+ cations did not decrease the dissociation rate constant of MV^{2+} from the MV^{2+}@CB[7] complex for the kinetics to be observed by stopped flow. This result is related to the fact that the formation of a capped inclusion complex would bring two positively charged species in very close proximity to one another resulting in an unfavourable interaction.

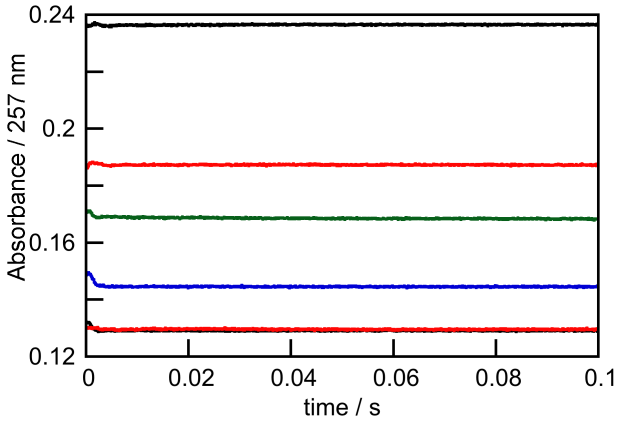

Figure 3.4 Kinetics following the absorption of 11 µM MV^{2+} mixed with CB[7] at 100 mM Na^+ cations and 10 °C (CB[7] = 0 µM = top black, 5 µM = top red, 10 µM = green, 15 µM = blue, 25 µM = bottom black and 40 µM = bottom red). The absorption was taken at 257 nm.

From the recovered equilibrium constant that was retrieved from the binding isotherms, it is clear that the dissociation rate constant between MV^{2+} and CB[8] cannot be applied between MV^{2+} and CB[7]. Equation 3.40 shows the relationship between the equilibrium constant and the association and dissociation rate constants.

$$K_{11} = \frac{k_{11}^{+}}{k_{11}^{-}} \qquad \text{(Eq. 3.40)}$$

The equilibrium constant is equal to the ratio of the association rate constant and the dissociation rate constant. If the dissociation rate constant between CB[7] and MV^{2+} is close to the reported dissociation rate constant of 1200 s^{-1} and the equilibrium constant is $(4.7 \pm 0.3) \times 10^7$ M^{-1}, then using eq. 3.40 the association rate constant is calculated at approximately 7×10^{10} $M^{-1}s^{-1}$. This value is higher than the diffusion-controlled limit for a reaction, which is 7×10^9 $M^{-1}s^{-1}$ at room temperature.[146] Because the diffusion controlled limit is the upper limit for any reaction, a dissociation rate constant of 1200 s^{-1} is an order of magnitude higher than what the dissociation rate constant can be (120 s^{-1}). In absorption experiments the guest molecule concentrations must be higher than the concentrations used in fluorescence experiments due to differences in detection limits. Due to the elevated concentration of MV^{2+} in absorption experiments, the observed rate constant will always be faster than the dead time of the stopped-flow device.

3.3.2 Binding isotherms and kinetics between $MDAP^{2+}$ and CB[7]

The first system with a structural variant to compare to the MV^{2+}@CB[7] system was the $MDAP^{2+}$@CB[7] system. The cationic charges on $MDAP^{2+}$ are similarly located to the cationic charges on MV^{2+}, however, $MDAP^{2+}$ is a more rigid molecule due to its tetracyclic ring system and is wider than MV^{2+}.

$MDAP^{2+}$ is unique in this series of guest molecules because it is fluorescent, whereas the other molecules can only be studied using absorption spectroscopy. The absorption and fluorescence binding isotherms between $MDAP^{2+}$ and CB[7] (figure 3.5 and 3.6 respectively) were both fit to a 2:1 CB[7]:$MDAP^{2+}$ sequential binding model.

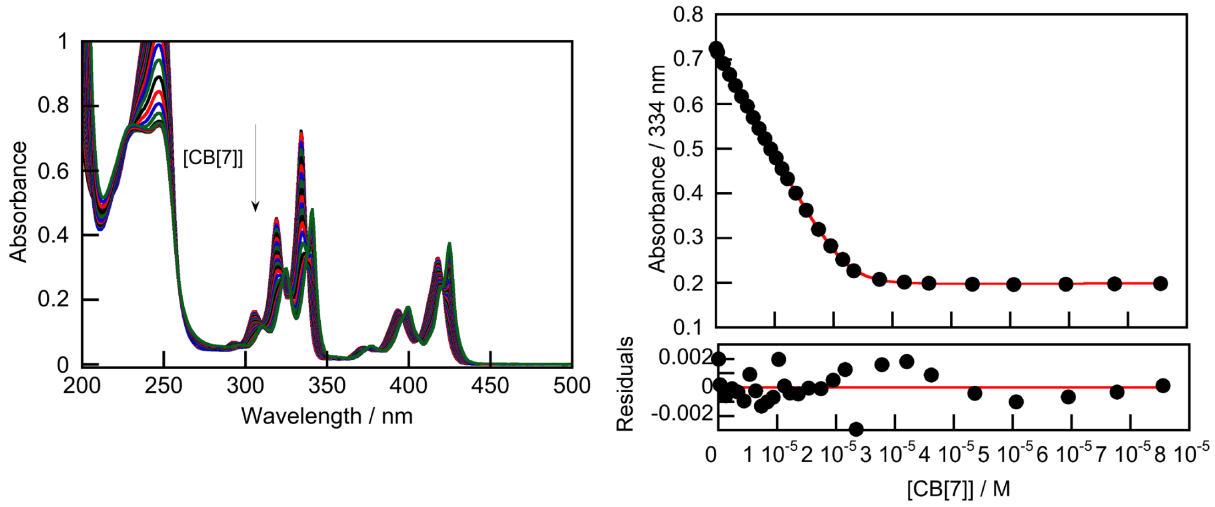

Figure 3.5 Left: Absorption spectra for 22 μM $MDAP^{2+}$ with CB[7] concentrations ranging from 0-76 μM at 100 mM Na^+ cations. **Right:** Binding isotherm between $MDAP^{2+}$ and CB[7] (top panel) using the absorption at 334 nm fit to a 2:1 CB[7]:guest model. The red line represents the numerical fit of the data. The bottom panel shows the residuals of the fit.

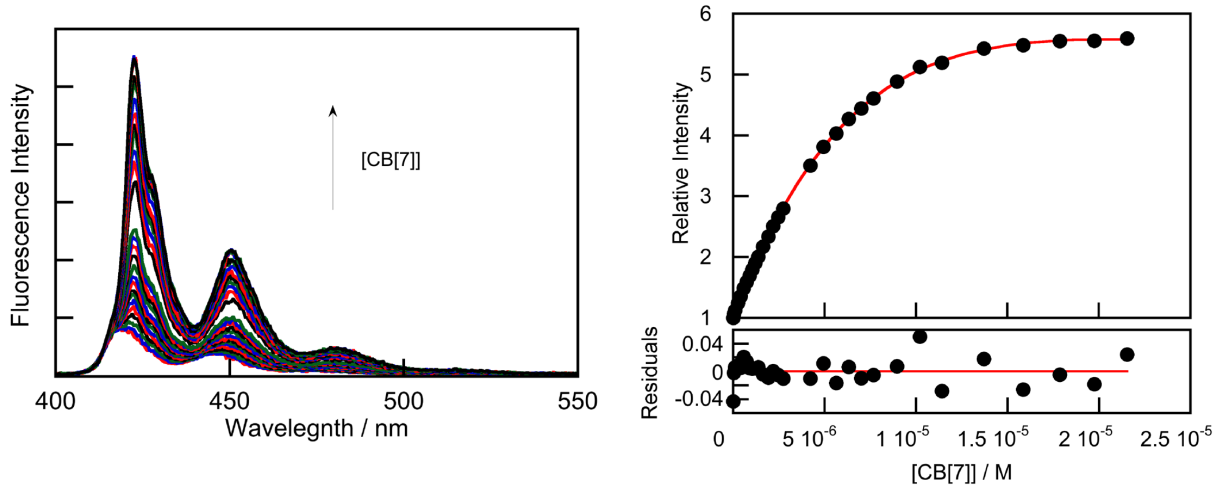

Figure 3.6 Left: Fluorescence spectra for 1 μM $MDAP^{2+}$ with CB[7] concentrations ranging from 0-23 μM at 100 mM Na^+ cations. **Right:** Binding isotherm between $MDAP^{2+}$ and CB[7] (top panel) using the absorption at 334 nm fit to a 2:1 CB[7]:guest model. The red line represents the numerical fit of the data. The bottom panel shows the residuals of the fit.

The recovered equilibrium constants from the fit of the data to a 2:1 CB[7]:guest model were $(1.04 \pm 0.12) \times 10^7\ M^{-1}$ and $(1.12 \pm 0.04) \times 10^5\ M^{-1}$ taken from the absorption binding isotherm in figure 3.5. Scheme 3.1 shows the proposed binding mechanism between

$MDAP^{2+}$ and CB[7]. Scheme 3.1 shows three different complexes between CB[7] and $MDAP^{2+}$: an exclusion complex, an inclusion complex and a 2:1 CB[7]:$MDAP^{2+}$ exclusion complex. The equilibrium constants reported for the fit of the data to the 2:1 sequential model are the equilibrium constants for the inclusion complex and the 2:1 CB[7]:$MDAP^{2+}$ exclusion complex. Due to the structure of $MDAP^{2+}$, or either of the other guest structures, it is not possible for an inclusion complex to be formed without the initial formation of an exclusion complex. However, the formation of the exclusion complex is expected to be transient; therefore, the 1:1 exclusion complex is expected to be seen in the kinetics, but is not a species that contributes to fitting the data in the binding isotherms.

The absorption binding isotherm shown in figure 3.5 was conducted at a $MDAP^{2+}$ concentration of approximately 20 μM, which is the same concentration of guest molecule as the concentration of the MV^{2+} binding isotherm in figure 3.3. The concentration of CB[7] ranges from 0-3.5 fold the concentration of $MDAP^{2+}$, whereas in the binding isotherms between MV^{2+} and CB[7], the CB[7] concentrations were between 0-2 fold the concentration of guest. The absorption binding isotherm between $MDAP^{2+}$ and CB[7] can be fit to a 1:1 CB[7]:$MDAP^{2+}$ inclusion complex model, figure C3, and yield an equilibrium constant of $(1.63 \pm 0.09) \times 10^8$ M^{-1}. However, from the analysis of the residuals of the fits in figure 3.5 and C3, it is clear that the fit to a 2:1 CB[7]:$MDAP^{2+}$ sequential model is a better fit. The fluorescence binding isotherm was collected at 1 μM $MDAP^{2+}$ and CB[7] concentrations ranging from 0-25 μM. The fluorescence binding isotherm data cannot be fit to a 1:1 CB[7]:$MDAP^{2+}$ model. Therefore, it appears that the formation of the 2:1 CB[7]:guest complex is dependent on the ratio of the concentrations between CB[7] and $MDAP^{2+}$. The larger the excess of CB[7], the further the equilibrium is driven towards the formation of the 2:1 CB[7]:$MDAP^{2+}$ exclusion complex.

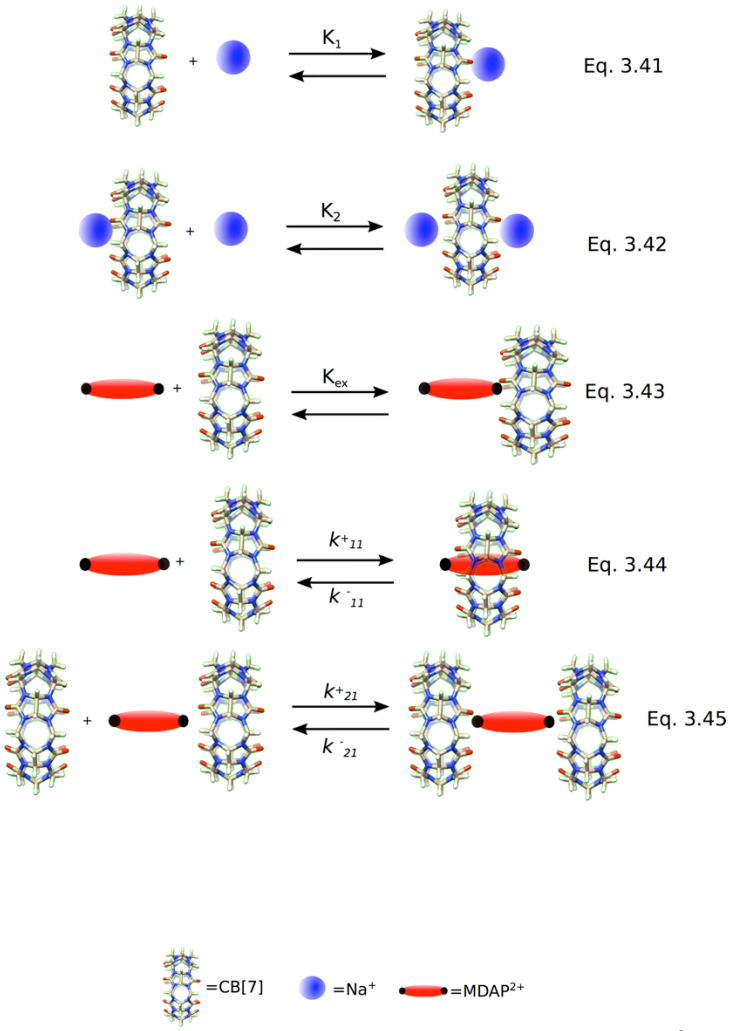

Scheme 3.1 Proposed mechanism for the binding between $MDAP^{2+}$ and CB[7] in the presence of Na^{+} cations.

Because the ratio of the concentration between CB[7] and $MDAP^{2+}$ appears to have an effect on the formation of a 2:1 CB[7]:$MDAP^{2+}$ exclusion complex, an absorption binding isotherm was conducted at 3 µM $MDAP^{2+}$ (figure 3.7). The concentration of CB[7] was between 0-15 µM. While the concentration ratio was not as high in the absorption binding isotherm in figure 3.7 as it was in the fluorescence binding isotherm in figure 3.6, it is higher than the ratio of concentrations between CB[7] and $MDAP^{2+}$ in figure 3.5. The corrected spectra were not able to be fit to a 1:1 CB[7]:$MDAP^{2+}$ complex, but could be fit to the 2:1 CB[7]:guest model. The uncorrected spectra, shown in the inset of figure 3.7, shows scattering in the absorbance between 450 and 500 nm, and between 260 and 300

nm. The scattering of light in an absorption spectra is indicative of the formation of species with similar size to the wavelength of light.[147]

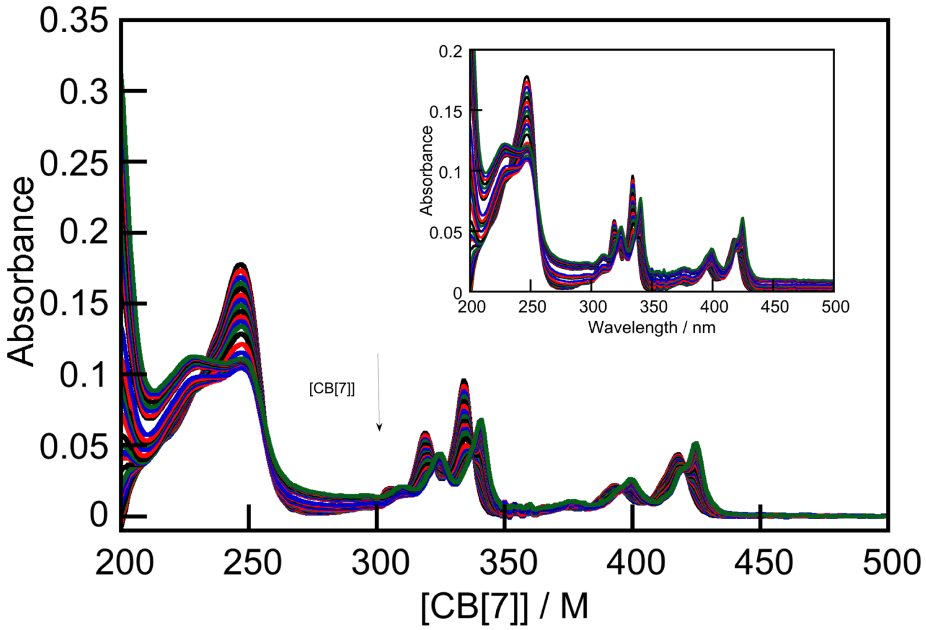

Figure 3.7 Absorption spectra for 3 μM $MDAP^{2+}$ with CB[7] concentrations ranging from 0-15 μM at 100 mM Na^+ cations. The inset shows the uncorrected absorption spectra for the spectra shown in the main figure.

The absorption spectra that are used in binding isotherm studies are corrected for the baseline, and the absorption between 450 and 500 nm is equal to zero. The scattering in the absorption spectra is due to the formation of larger complexes than the 2:1 CB[7]:$MDAP^{2+}$ complex. The scattering is likely due to the oligomerization between $MDAP^{2+}$ and CB[7] into solution (scheme 3.2 in discussion). The higher order complex proposed as a product of the oligomerization between $MDAP^{2+}$ and CB[7] cannot be detected by fluorescence since scattering would only affect the emission intensity without affecting the spectra.

The kinetics between $MDAP^{2+}$ and CB[7] can be measured under pseudo-first order conditions ([CB[7]] >>> [$MDAP^{2+}$]) because of the sensitivity of fluorescent measurements. The kinetics of $MDAP^{2+}$ and CB[7] occur in seconds to minutes, even when no Na^+ cations were added (figure C4). The overall kinetics for mixtures between $MDAP^{2+}$ and CB[7] slow down when the concentration increases above 15 μM of CB[7], when compared to the kinetics below 10 μM CB[7]. Further, as the concentration of CB[7] gets

to a large excess, the final fluorescence intensity starts decreasing (figure 3.8). In figure 3.8, the initial fluorescence intensity appears to be decreasing, however, this is an artifact of the time window that the kinetics are analyzed on, the first few ms are difficult to resolve in a 120 s time window shown in the inset of figure 3.8. As the fluorescence intensity decreases, the overall kinetics continue to get slower.

The work from chapter 2 and previous work in the literature with CB[7] have shown that the rate of kinetics decrease with increasing metal cation concentration.[49] At lower concentrations of Na^+ cations the decrease in final fluorescence intensity happens at a lower CB[7] concentration. The rate of the overall kinetics decreased as the concentration of Na^+ cations increased, which is consistent with the previous findings in the literature.[49] The overall kinetics showed a decrease in rate as the CB[7] concentration increased (figure 3.8), which was further evidence for the formation of the higher-order complexes. The formation of the higher-order complexes also showed a decrease in the rate of formation as the concentration of Na^+ cations increased, which implies that the formation of the higher-order complexes is dependent on the concentration of CB[7] molecules not bound to Na^+ cations.

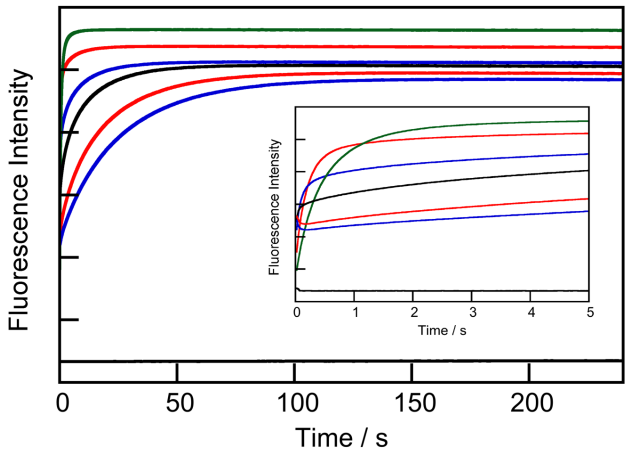

Figure 3.8 Kinetic traces for the mixing of 1 μM $MDAP^{2+}$ with various CB[7] concentrations (2.5 μM, green; 5 μM, red; 10 μM, top blue 15 μM, black; 25 μM, bottom red; 40 μM, bottom blue) in the presence of 100 mM Na^+. The bottom black trace corresponds to the control experiment in the absence of CB[7] ([Na^+ = 100 mM). **Inset:** The first 5 seconds of the kinetic traces shown in figure 3.8 to show the offset in the kinetics traces.

Because kinetic experiments between $MDAP^{2+}$ and CB[7] can be conducted under pseudo-first order conditions, the kinetic traces can be analyzed by fitting to a sum of exponentials function. The kinetic trace at 5 μM CB[7] fit to a sum of four exponentials function when the kinetics are collected over 5 s. When the kinetics traces are collected over 60 s, the kinetic trace fits to the sum of three exponentials function (figure 3.9). The reason the kinetics on a 60 second time scale fit to the sum of three exponentials function rather than four exponentials is because the fast component of the kinetics, proposed as an exclusion complex, reaches equilibrium faster than what can be detected on the 60 s time scale.

The kinetics traces of $MDAP^{2+}$ mixed with CB[7] concentrations from 15-40 μM were not able to be fit to a sum of exponentials function. The slow kinetics show a large deviation from the fit in the residuals when the concentration of CB[7] is significantly larger than the concentration of $MDAP^{2+}$. The kinetics slowing down in the presence of elevated CB[7] concentrations, and the inability to fit the kinetics to a sum of exponentials function, or a model, is further evidence of the formation higher order complexes between $MDAP^{2+}$ and CB[7].

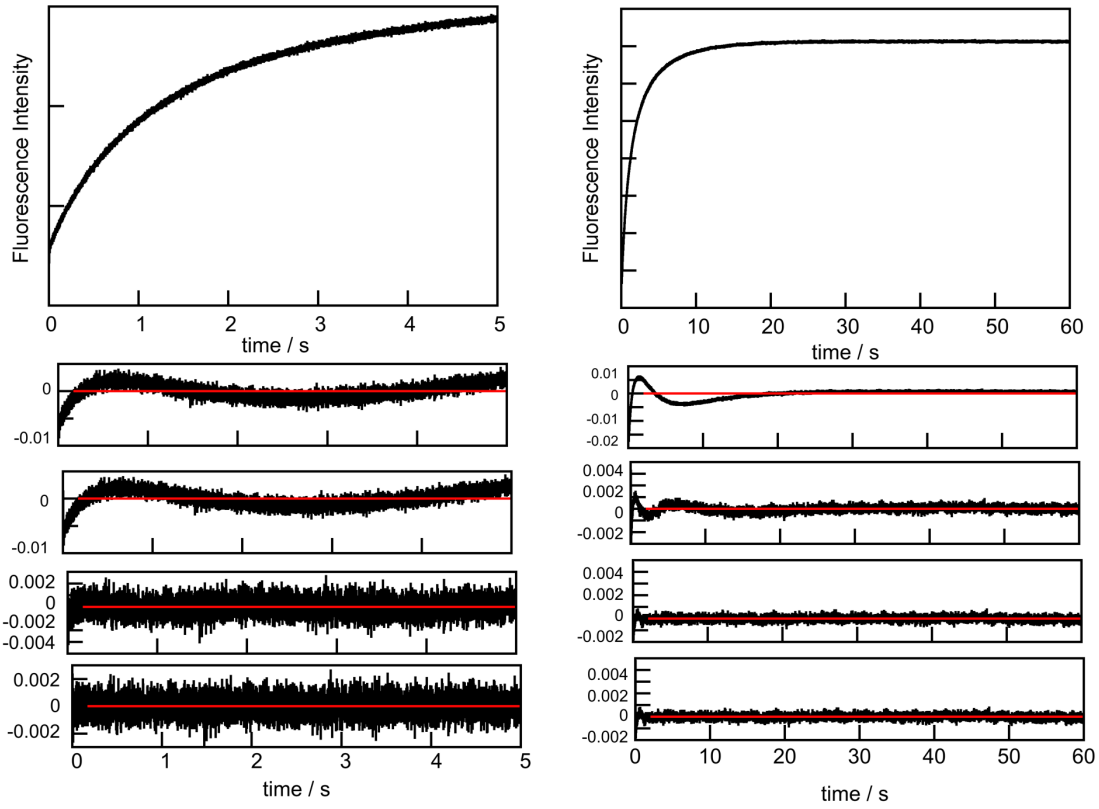

Figure 3.9 Left: Kinetic trace for the mixing of 1 μM $MDAP^{2+}$ with 5 μM CB[7] (top panel). The bottom panel shows the residuals of the fit to a sum of exponentials function (top, sum of one; second, sum of two; third, sum of three; fourth, sum of four) over a 5 s time scale. **Right:** Kinetic trace for the mixing of 1 μM $MDAP^{2+}$ with 5 μM CB[7] (top panel). The bottom panel shows the residuals of the fit to a sum of exponentials function (top, sum of one; second, sum of two; third, sum of three; fourth, sum of four) over a 60 s time scale.

3.3.3 Binding isotherms and kinetics between Bn^{2+} and CB[7]

The third guest in the series to study is Bn^{2+}, which has a similar structure and rigidity to MV^{2+}, but the charged nitrogens are one position removed from the aromatic rings to make them primary ammoniums. Binding isotherms between Bn^{2+} and CB[7] at different concentrations of Na^{+} cations were conducted to determine the equilibrium constant. When collecting binding isotherms between Bn^{2+} and CB[7], control absorption spectra must be collected between the solvent solution and every CB[7] concentration used in the binding isotherm. These control absorption spectra are used to correct for any scattering. Figure

3.10 shows the corrected absorption spectra between Bn^{2+} and CB[7] with the fits to a 1:1 model and the same 2:1 CB[7]:Bn^{2+}model as the model between $MDAP^{2+}$ and CB[7].

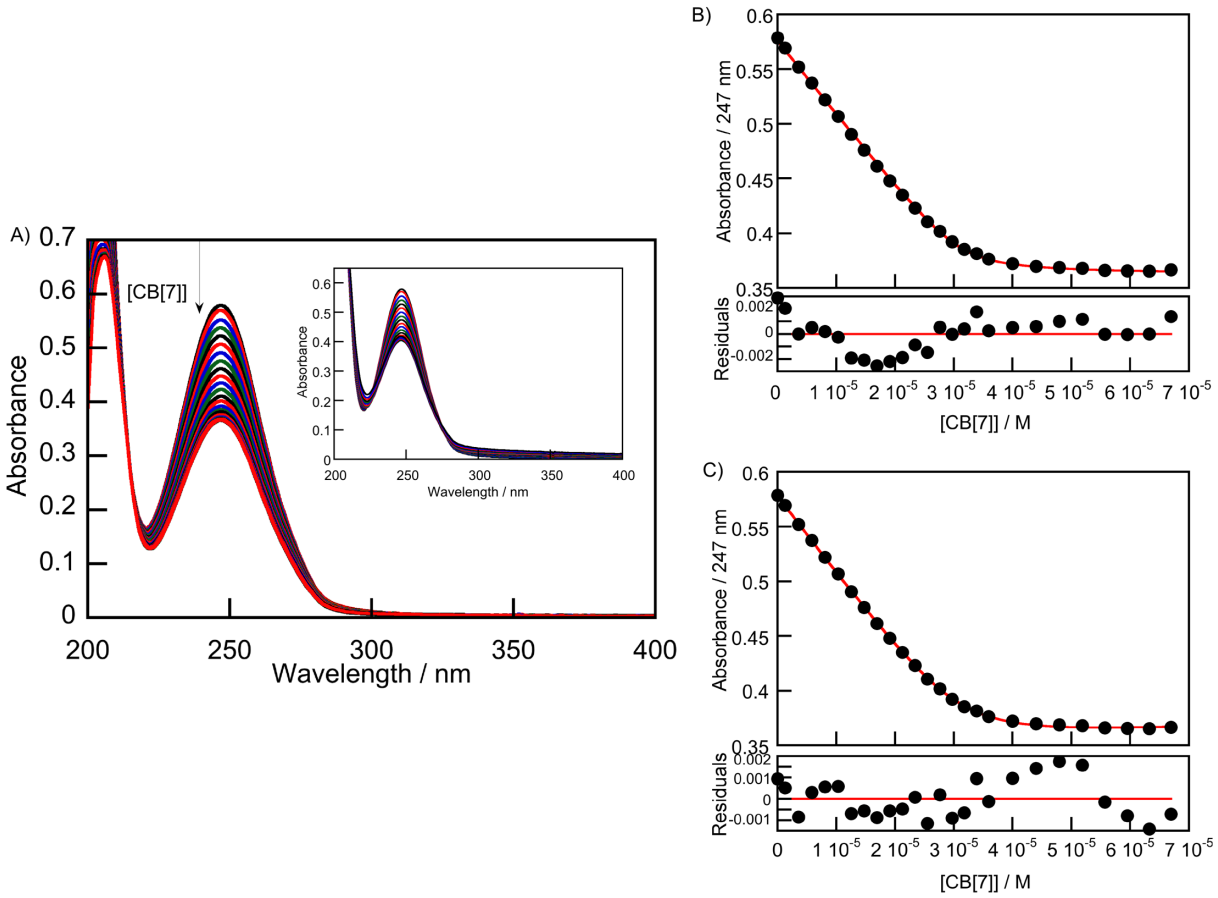

Figure 3.10 A: Absorption spectra for 24 μM Bn^{2+} with CB[7] concentrations ranging from 0-70 μM at 100 mM Na^{+} cations. The inset shows the uncorrected absorption spectra **B:** Binding isotherm between Bn^{2+} and CB[7] (top panel) using the absorption at 247 nm. The red line represents the numerical fit of the data. The bottom panel shows the residuals of the fit for a 1:1 CB[7]:guest model. **C:** Binding isotherm between Bn^{2+} and CB[7] (top panel) using the absorption at 247 nm. The red line represents the numerical fit of the data. The bottom panel shows the residuals of the fit for a 2:1 CB[7]:guest model.

Using eq. 3.39 with the fit to a 1:1 model the extracted equilibrium constant was $(3.2 \pm 0.5) \times 10^{7}$ M^{-1} which is of the same order of magnitude as the 1:1 equilibrium constant between MV^{2+} and CB[7]. However, when comparing the residuals of the fit between the 1:1 fit and the 2:1 CB[7]:Bn^{2+} exclusion complex model, for the binding isotherm between Bn^{2+} and CB[7] in figure 3.10, the 2:1 fit is a better fit. When analyzing the residuals, the important

aspects are the amplitude of the deviation from the fit line and where the deviation occurs. From panels B and C in figure 3.10, the amplitude of deviation is smaller in the 2:1 CB[7]:Bn^{2+} model than the 1:1 model. Further, the deviation from the fit in the 2:1 CB[7]:Bn^{2+} model is when the absorption has stopped decreasing, whereas the deviation in the 1:1 model is while the absorption is decreasing which is more significant. When the absorption spectra above 45 μM are not used, the data seemingly fits to a 1:1 model; however, as was the case in the $MDAP^{2+}$ binding isotherms, when the CB[7] concentration is in 3 fold excess to the guest concentration it becomes clear that the fit is better to the 2:1 CB[7]:guest model.

The inset of figure 3.10 shows the overlay absorption spectra before the baseline correction for the binding isotherm. In the baseline correction, all of the absorbance values from 350 to 400 nm are equal to 0. In the absorption spectra than have not been corrected, the inset shows some scattering with increasing concentration of CB[7]. The increase in baseline scattering is similar to what was seen in the $MDAP^{2+}$ binding isotherms. The scattering is indicative of structures that are as large as the wavelength of light.[147] The scattering seen in the binding isotherms between Bn^{2+} and CB[7] is similar to what was seen in the previous section between $MDAP^{2+}$ and CB[7]. The binding between Bn^{2+} and CB[7] appears to result in the same species in solution that was proposed between $MDAP^{2+}$ and CB[7].

A similar argument can be made for the fitting of binding isotherm data between Bn^{2+} and CB[7] that was made in the previous section. When the concentration of CB[7] remains less than 2.5 fold than the concentration of Bn^{2+}, the binding isotherm appears to fit to a 1:1 model. When the concentration of CB[7] remains less than 2.5 fold the concentration of Bn^{2+}, which favours a 1:1 CB[7]:Bn^{2+} complex, the equilibrium constant between CB[7] and Bn^{2+} is similar to the equilibrium constant between MV^{2+} and CB[7]: 3.5×10^7 M^{-1}. Though the equilibrium constant between CB[7] and Bn^{2+} is similar to the equilibrium constant between MV^{2+} and CB[7], the kinetics between Bn^{2+} and CB[7] were shown to be on the ms timescale across all concentrations of Na^+ cations.

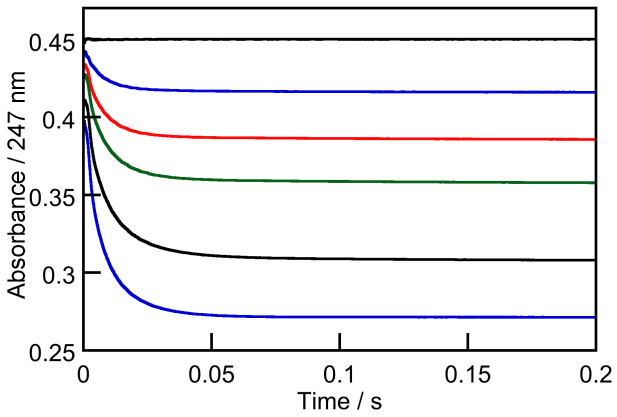

Figure 3.11 Kinetic traces for the mixing of 24 μM Bn^{2+} with various CB[7] concentrations (5 μM, top blue; 10 μM, red; 15 μM, green; 25 μM, black; 40 μM, bottom blue) in the presence of 100 mM Na^+. The top black trace corresponds to the control experiment in the absence of CB[7] ([Na^+ = 100 mM)**.**

The kinetics of the system being on the ms time scale allows the kinetic traces to be fit. While at all concentrations of Na^+ cations the kinetics are on the ms time scale, at lower concentrations of Na^+ (10 and 25 mM) there is an offset in the kinetics that is indicative of the formation of an exclusion complex with kinetics close to the time resolution of the stopped-flow device used as discussed in chapter 2. However, the offset is difficult to judge in the absorption kinetic experiments because the lamp shows a slight drift in the baseline over time, which makes the subtraction of the control kinetic traces with no Bn^{2+} present difficult.

Because Bn^{2+} does not fluoresce, the concentration of Bn^{2+} used was approximately 20 μM, and the CB[7] concentrations for kinetic experiments were kept the same as what was used for the other two guest molecules (5-40 μM). Because of the concentrations used, the kinetic experiments between Bn^{2+} and CB[7] are not under pseudo-first order conditions and cannot be fit to a sum of exponentials function. Instead the kinetics were fit to a model. The model used to fit the kinetics between Bn^{2+} and CB[7] is shown in section **3.2.9**; however, the kinetics could not be fit to the complicated model or any variation of it.

There are two possible explanations for the kinetics not fitting to any variation of the model. The first explanation is the absorption signal can be noisy at 247 nm using a Xe-Hg lamp, if the program is attempting to fit the noise of the kinetic trace to the kinetic model, the trace will not fit. The second explanation is the same circumstance seen in the $MDAP^{2+}$ kinetics and binding isotherms, where there is the potential of some oligomerization of

CB[7] and the Bn^{2+} guest which cannot be fit in a sum of exponentials function or to a kinetic model.

3.4 Discussion

The work presented in this chapter investigates how structural differences in guest molecules effect the kinetic time scales between CB[7] and guest molecules. In various fields such as self-sorting systems,[38, 130] pharmacology,[46] functional materials[108, 116, 133, 148-150] and drug delivery assemblies[45, 118, 121-129, 151] the kinetics between host and guest molecules, or between molecules in the material, have a huge effect on bioavalability,[45-46] release profiles[45, 118, 121-122, 124-125, 128-129] and kinetic versus thermodynamic self-sorting characteristics.[38, 130, 152] In the realm of pharmacology, the slower the association and dissociation rate constants between the drug and the drug carrier the less opportunity for the guest molecule has to be competitively bound by off-target species that may clear the drug from the body before the drug can perform it's task.[46] For drug delivery assemblies, controlled release from polymeric assemblies allows for targeted treatment and fewer drug doses.[122-123, 125-126, 128] In host-guest self-sorting systems, the distribution of kinetic and thermodynamic products with respect to time in a social self-sorting system depends on the time scale of the host-guest interactions.[38, 130] Therefore, studies of molecules with similar equilibrium constants but different kinetic time scales are important to determine which structural factors play larger roles in the time scale of host-guest kinetics in order to design more controllable systems.

All three guest molecules have equilibrium constants within an order of magnitude of one another when the concentration of CB[7] used favour a 1:1 CB[7]:guest complex, but from the kinetics it is very clear that the time scales of the dynamics of complex formation are different between CB[7] and each of the guest molecules. Kinetic information in the literature for these three guest molecules is scarce. The kinetics between MV^{2+} and CB[7] have not been reported on the ms time scale, however, through rheological experiments in a supramolecular hydrogel the dissociation rate constant of MV^{2+} from CB[8] was reported to be 1200 s^{-1}.[20] As discussed in section **3.3.1**, from the equilibrium constant between MV^{2+} and CB[7], the maximum value the dissociation rate constant can be is 120 s^{-1} if the

association rate constant is diffusion controlled. Due to the concentration of MV^{2+} required for an absorption signal (at least 1×10^{-5} M^{-1} after mixing on the stopped flow), it is likely that the diffusion-controlled association rate constant will make the kinetics always too fast to be seen on the stopped-flow device. For Bn^{2+}, the kinetics with CB[7] have never been reported, and the only literature report between Bn^{2+} and CB[7] is with the neutral species of Bn^{2+}using electrochemistry, where $Bn^{2+}$is a member of a series of compounds that is not significantly discussed in the paper.[138] The work in this chapter, however showed that the kinetics were on the ms time scale with CB[7]. Finally, the kinetics between CB[7] and $MDAP^{2+}$ were shown to be the slowest of this series of guest molecules. The first report of the inclusion complex between CB[7] and $MDAP^{2+}$ suggested that the kinetics were slow because the authors reported a broadening of the ^1H NMR peaks showing that the kinetics would be on the NMR time scale.[104] A recent publication showed the kinetics of 5 μM CB[7] mixed with 5 μM $MDAP^{2+}$ were on the same time scale as shown in the results section. Using a competitive displacement reaction, when the concentrations favour a 1:1 $MDAP^{2+}$@CB[7] inclusion complex, these authors determined that the dissociation rate constant was approximately 0.018 s^{-1}.[139] From eq. 3.40, the association rate constant of the 1:1 complex can be approximated at 2.9×10^6 $M^{-1}s^{-1}$, which is three orders of magnitude lower than the diffusion-controlled limit.

The kinetic experiments in this chapter confirmed that the kinetics between MV^{2+} and CB[7] are faster than the ms timescale and the kinetics between $MDAP^{2+}$ and CB[7] are much slower, on the minute time scale. From the kinetic experiments with Bn^{2+}, it can be deduced that changing the position of the cationic charges from the aromatic rings of MV^{2+} slowed down the kinetics onto the ms time scale. It is, however, clear that the width and rigidity of $MDAP^{2+}$ had a far greater effect on the kinetic time scale than the position of the cationic charges. The published results between $MDAP^{2+}$ and CB[7] suggested the slow kinetics was most likely due to the distortion of CB[7] to accommodate the width of $MDAP^{2+}$.[104] The distortion of CB[7] to accommodate the size of $MDAP^{2+}$ is a contributing factor to explain the slow kinetics with CB[7], however it is likely not the entire story. A large driving force for CB[7]-guest complexation is the expulsion of 'high-energy' water within the cavity of CB[7].[153] The water molecules within the hydrophobic cavity of CB[7] are hydrogen bond deficient; therefore, when a guest molecule binds to CB[7] and expels

that water from the cavity there is an enthalpic gain by the water molecules forming more hydrogen bonds in bulk solution. The reported dissociation rate constant of 0.018 s^{-1} suggests that the 1:1 $MDAP^{2+}$@CB[7] complex may have expelled a majority of the high-energy water from the cavity of CB[7] making the complex more stable than the CB[7] complex with the other two guests. The low dissociation rate constant justifies the kinetics between $MDAP^{2+}$ and CB[7] being much slower than the kinetics between the other guests and CB[7], but $MDAP^{2+}$ having the higher equilibrium constant with CB[7] (eq. 3.40).

With the guest molecules having similar structure, there is a desire to uncover a mechanism that can be universal for these aromatic dications. From a kinetics perspective, no useful mechanistic information can be drawn from the stopped-flow kinetic traces between MV^{2+} and CB[7] as all of the kinetics are faster than the dead time of the device. For the binding isotherm between MV^{2+} and CB[7], when the concentration of CB[7] was kept between 0 and 2 fold of the concentration of MV^{2+}, the binding isotherm fits to a 1:1 CB[7]:guest model (figure 3.3) with almost no improvement in the residuals of the fit when the data was fit to a 2:1 CB[7]:guest model (figure C1). The binding isotherms between Bn^{2+} and CB[7], along with the absorption binding isotherms between $MDAP^{2+}$ and CB[7], at elevated concentrations of $MDAP^{2+}$, can be fit to a 1:1 CB[7]:guest model when the concentration of CB[7] remains less than 2.5 fold of the concentration of guest molecule, as the concentration of CB[7] was in the MV^{2+} binding isotherms. However, as the concentrations exceeds three-fold the concentration of guest molecule, the binding isotherms need to be fit to a 2:1 CB[7]:guest exclusion complex model for both Bn^{2+} and $MDAP^{2+}$.

The fluorescence binding isotherm at 1 μM $MDAP^{2+}$ cannot be fit to a 1:1 model, and the absorption binding isotherm at 3 μM $MDAP^{2+}$ cannot be fit to a 1:1 model either. Further, the absorption binding isotherm at 3 μM $MDAP^{2+}$ shows what appears to be scattering in the absorption spectra when the CB[7] concentrations exceeds three-fold the guest concentration. The need to fit the fluorescence binding isotherm and the corrected absorption binding isotherm to a 2:1 CB[7]:$MDAP^{2+}$ exclusion complex model, in conjunction with the scattering seen in the uncorrected absorption spectra suggests the presence of higher order complexes being formed.

There is precedence in the literature for the formation of a 2:1 complex between CB[7] and dicationic guest molecules such as MV^{2+}, Bn^{2+} and $MDAP^{2+}$.[112, 137, 154] The crystal structure between Bn^{2+} and CB[6] shows the oligomerization of exclusion complexes.[112] The guest molecule can act as a bridge between the portals of CB[n]s.[112] Further, for studies with modified forms of MV^{2+}, where the methyl group is replaced with aromatic groups or aliphatic chains, the dominant species in solution is two CB[7]s bound to the chemical group that had replaced the methyl group on MV^{2+}, not the 1:1 CB[7]:MV^{2+} complex where CB[7] is bound to the aromatic rings of MV^{2+}.[107, 154] The 2:1 CB[7]:guest complexes are favourable when the methyl group of MV^{2+} is replaced by a larger group, like a benzyl group.[133, 154] The methyl group is too small to fill the cavity of CB[7], so a large excess of CB[7] is needed for the formation of 2:1 CB[7]:guest complex, or the oligomerization product. The 2:1 CB[7]:guest or oligomerization product between MV^{2+} and CB[7] was not seen in the absorption binding isotherm because the concentration of CB[7] was too low to force the system towards the higher order complexes.

With respect to the kinetics of $MDAP^{2+}$ and Bn^{2+} with CB[7] there is further evidence of higher order complexes being formed. From a qualitative stand point, the kinetics between Bn^{2+} and CB[7] do not appear to be kinetics that need to be fit to a complex model, like the one shown is section **3.2.9**, with four or more relaxation processes. The kinetics between Bn^{2+} and CB[7] must be fit to a model because the concentrations of CB[7] and Bn^{2+} are close to one another, so the reaction is under bimolecular conditions, not pseudo-first order conditions. The kinetics between Bn^{2+} and CB[7] do not fit to a simple model which includes the formation of 1:1 CB[7]:guest, 2:1 CB[7]:guest or 1:2 CB[7]:guest complexes, meaning that there may be larger structures formed in solution that cannot be accounted for in the model. The formation of elongated assemblies is supported by the crystal structure between CB[6] and Bn^{2+}. While crystal structures are not always indicative of the species present in solution, it is possible to form these elongated structures due to the location of the cationic charges on the guest molecules (scheme 3.2).[112] The idea of elongated assemblies is further supported by the kinetics between $MDAP^{2+}$ and CB[7]. The kinetics between $MDAP^{2+}$ and CB[7] can be conducted under pseudo-first order conditions because $MDAP^{2+}$ is fluorescent. The ability to conduct the experiments under pseudo-first order conditions allows the kinetic traces to be fit to a sum of exponentials function rather

than building a complex model. From the number of relaxation processes extracted from the fit to a sum of exponentials function, a model can be predicted. However, the only kinetic traces that can be fit to a sum of exponentials function are when the concentration of CB[7] is between 2.5 and 7.5 µM and the $MDAP^{2+}$ concentration is between 1-2.5 µM. As the concentration of CB[7] increases, the overall kinetics become slower (figure 3.8) and the overall kinetics for the higher concentrations of CB[7] are slower at higher concentrations of Na^{+} cations (figure C4).

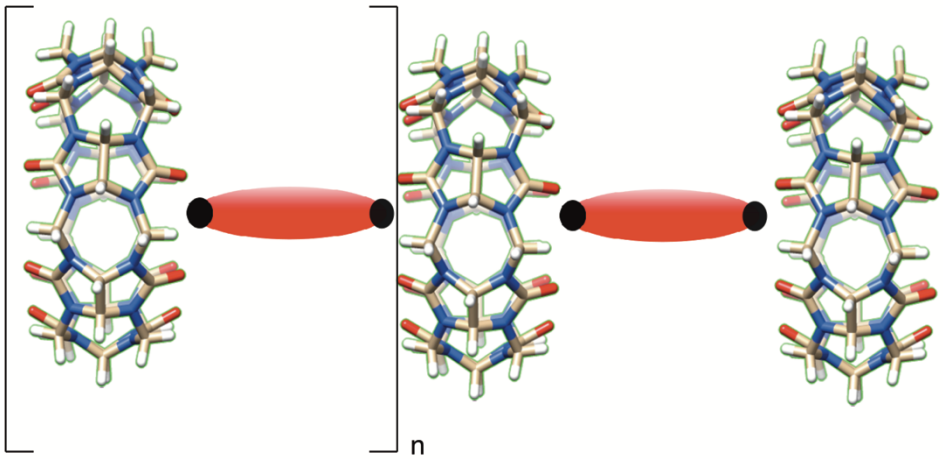

Scheme 3.2 Proposed structure of oligomerization between CB[7] and Bn^{2+}, $MDAP^{2+}$ or MV^{2+}.

The majority of the literature reporting the binding of $MDAP^{2+}$ or MV^{2+} with CB[n]s is focused on the complexes with CB[8]. CB[8] is large enough to fit two aromatic guests in its hydrophobic cavity, and when $MDAP^{2+}$ or MV^{2+} is introduced with an electron rich guest, like a hydroxy-naphthalene derivative a charge transfer complex forms inside the cavity of CB[8].[20, 40, 118, 131, 134-135, 150, 153, 155] The published absorption and fluorescence binding isotherms between $MDAP^{2+}$ and CB[7] or CB[8] are fit to a 1:1 model, though it appears the data should be fit to a 2:1 CB[8]:guest model. In the published binding isotherms between $MDAP^{2+}$ and a CB[n] there are large deviations from the fit line, similar to what was seen when attempting to fit the fluorescence binding isotherm in section **3.3.2** to a 1:1 model. The quality of the fit suggests that there were additional species present in solution.

There are slight differences in the reported absorption binding isotherm between $MDAP^{2+}$ and CB[8] when compared to the absorption binding isotherm between $MDAP^{2+}$ and CB[7]. The absorption spectra for mixtures of CB[7] and $MDAP^{2+}$ show red shifts in the absorption maxima, whereas the absorption spectra for mixtures between CB[8] and $MDAP^{2+}$ show a decrease in absorption, but no shift in maxima.[40, 104] The absorption maxima of $MDAP^{2+}$ at 334 nm and 418 nm with no CB[7] added, from figure 3.5, showed red shifts when CB[7] was added. The shift in absorption maxima may suggest that the species in solution when CB[7] is added to $MDAP^{2+}$ may be different than the species present when CB[8] is added.

Regardless if the mechanism is the same across all guest molecules, the purpose of this project was to determine how the structure of guest molecules effects the kinetic time scales for guest complex formation with CB[7]. From this series of guest molecules, it can be determined that an increase in rigidity and width to the guest molecule ($MDAP^{2+}$) have a greater effect on the time scale of CB[7]-guest complex formation than the location of charge on the guest molecule. There was an increase in the reaction time scale when the charges were one position removed from the aromatic rings (Bn^{2+}) when compared to the kinetics between MV^{2+} and CB[7]. However, the kinetics showed a much larger slowdown when more rigidity, width and surface area was added to the molecule.

The results from this chapter draws some parallels to the conclusions in chapter 2. The dynamics of these CB[7]:guest solutions are more complex than the formation of a simple 1:1 complex, and the product distribution is dependent on the concentration of species present is solution, as was the result between NpH^{+} and CB[7] in the presence of metal cations. The insights gathered from the results in this chapter continue to build the narrative that host-guest chemistry is much more complex than it has been traditionally treated. Further, when studying these dicationic guest molecules with host molecules, such as the CB[n] family, it is important to account for the presence of the higher order structures, though the higher order structures seem to disappear in the case of the charge transfer complexes with CB[8].[133, 150] Understanding the influence the structure of guest molecules has large implications in fields like drug delivery and pharmacology.[45-46, 121, 124, 126, 128] In drug delivery, having slow kinetics between a drug molecule and its carrier is important to avoid competitive binding to off-target species in the body.[46] Because of this,

understanding how the structure characteristics of guest molecules, with similar equilibrium constants to a host molecule, can affect the time scale of kinetics between the guest and host is important.

Chapter 4: Rational design of a kinetically trapped self-sorting system

Kevin A. Vos, Prakhar Gupta, Jessy Oake and Cornelia Bohne

KV and CB came up with the conceptual frame work of the project. KV performed the preliminary binding isotherms and kinetic studies between CB[7] and BNA^+. KV also performed the stability studies of BNA^+ with different bandwidths of light. KV did the preliminary kinetic experiment between CB[6] and BNA^+. JO performed the final binding isotherms and kinetic studies between BNA^+ and CB[6], and between BNA^+ and β-CD. PG performed the preliminary kinetic study between β-CD and BNA^+. PG also performed the final binding isotherms and kinetics studies between CB[7] and BNA^+.

4.1 Introduction

4.1.1 Background

In previous chapters, an emerging field of chemistry called systems chemistry was described as the study of complex mixtures of molecules that give rise to new properties that are not inherently predictable when studying the components of the system in isolation.[56, 58, 60-61, 63, 65] Systems chemistry has been applied to synthetic libraries,[65] drug discovery,[61] prebiotic chemistry,[60, 63] self-sorting[31, 39, 58, 62, 130, 156-162] and self-assembly.[31, 163-164] Prebiotic chemistry is a field that is attempting to assist biologists with understanding the chemistry of the origins of life.[60, 63] Because cells are pre-organized, and the chemistry is compartmentalized, understanding the principles of self-assembly and self-sorting are essential.[60]

CB[n]-guest chemistry in complex mixtures falls into the category of social self-sorting.[37-38, 58, 158] Social self-sorting refers the recognition of non-self with complementary binding motifs in complex mixtures.[130, 159, 161] Within social self-sorting there is a further division into kinetic and thermodynamic self-sorting.[37-38, 159] Reactions in kinetic 'traps' or under kinetic control will eventually evolve to the thermodynamic product if there is no input of energy to avoid the production of the thermodynamic product.[15, 31, 37, 56, 165] However, a self-sorting reaction can be said to be under kinetic control if the system is held in the kinetic state for an extended period of time.[38]

As biological chemistry exists in a kinetic state, using enzymes and compartments for chemical reactions,[38] there is a desire to design kinetically trapped self-sorting systems to

help understand biological systems using simpler synthetic alternatives. Due to the reversibility of the non-covalent interactions in supramolecular host-guest chemistry,[42] host-guest chemistry is well situated to study dynamic self-sorting systems. Further, most biological structures, such as proteins and DNA, are large supramolecular structures or assemblies; therefore, using supramolecular hosts to design self-sorting systems can draw similarities to biological systems.[61]

The use of cucurbit[n]urils (CB[n]s) as synthetic receptors for the development of self-sorting systems is ideal due to the various homologues of CB[n]s (n = 5-8, 10), that each have different selectivities for different functional groups.[87] Beyond the selectivity for different functional groups, the kinetic time scales can be orders of magnitude apart, and the equilibrium constants can range from 10^2 M^{-1} to higher than the biotin-streptavidin complex commonly used in biology.[77, 166-167] Due to the selectivity differences across the family of CB[n]s, and the wide range of kinetic time scale differences, the CB[n] family is a prime candidate to design systems to study kinetically-trapped self-sorting systems.[167]

CB[n]s have been used in thermodynamic self-sorting systems with temporary kinetic control.[37-38] A modified spermine molecule (chart 4.1, **1**) with three available binding sites for CB[n]s was exposed to a mixture of CB[6] and CB[7].[37] The two terminal binding sites of the modified spermine were isopropyl groups attached to an ammonium cation, which was bound by CB[6] under thermodynamic and kinetic control; however, the butyl-diammonium group, in between the terminal isopropyl groups, was under kinetic control by CB[7] and thermodynamic control with CB[6].[37] Initially CB[7] was bound to the butyl moiety, but when the mixture is heated for 2 h, the butyl moiety selectively binds CB[6] (chart 4.1).[37]

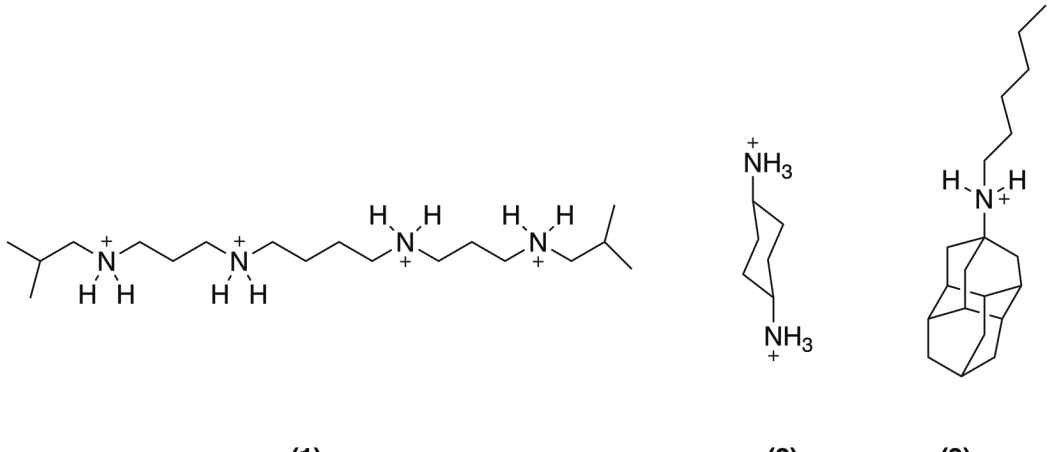

(1) **(2)** **(3)**

Chart 4.1 Structure of guest molecules used in CB[n] self-sorting systems.

The kinetic versus thermodynamic control between CB[6] and CB[7] was further shown with two guest molecules.[38] The first guest molecule was a 1,4-cyclohexyl-diammonium (chart 4.1, **2**) which was the thermodynamic product for CB[6], but the kinetic product for CB[7]. The second guest molecule was a ditopic guest with an adamantyl- group that formed the thermodynamic product of CB[7] as the adamantylammonium group has an equilibrium constant of 10^{14} M^{-1} with CB[7]. The second binding epitope was an alkyl chain (chart 4.1, **3)**, which was the kinetic product for CB[6].[38] When the molecules are all initially mixed, the cyclohexyl-diammonium (chart 4.1, **2**) binds CB[7], while CB[6] binds to the alkyl chain of the ditopic guest (chart 4.1, **3**) because the system in controlled by the association and dissociation rate constants between the guest molecules and CB[n]s. Over time the thermodynamic sink for the entire system dominates when CB[7] binds the adamantyl-group and CB[6] bound the cyclohexyl-diammonium because the system is now dominated by the thermodynamic equilibria.[38]

The two previously described systems are examples of how the CB[n] family can be used in self-sorting systems; however, these self-sorting systems are conducted by mixing the components and checking the product distribution rather than a rationally designed system under kinetic control. The goal of the work in this chapter is to design a self-sorting system, with a ditopic guest, where the thermodynamic sink of the system has slow kinetics (min to h) and the evolution of this equilibrium can be temporarily interrupted at different times

by the introduction of a kinetic trap. The guest molecule chosen was N-benzyl-2-naphthylamine (BNA, chart 4.2).

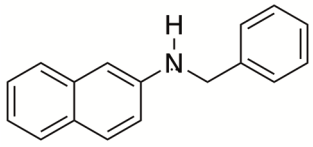

BNA

Chart 4.2 Chemical structure of N-benzyl-2-naphthylamine.

BNA was chosen because both the benzyl motif and the naphthyl motif have been previously shown to bind to CB[6] and CB[7] respectively.[21, 49, 168] The kinetics between CB[6] and benzylammonium were previously shown to be slow.[168] The kinetics between the naphthylammonium were expected to be on the ms time scale, similar to the time scale between CB[7] and NpH^+,[49] and with the naphthyl group on a truncated version of BNA: N-phenyl-naphthylammonium (PNA).[51] The system, containing BNA, CB[6] and CB[7], is designed for the slow evolving kinetics between the benzyl group and CB[6] to be the thermodynamic sink of the system. The introduction of CB[7] to the mixture is designed to create the kinetic trap. Scheme 4.1 shows the proposed self-sorting system. The principal idea is to introduce CB[7] to the evolving CB[6]-BNA equilibrium at different times during the reaction to answer three main questions: (i) for how long is the system kinetically trapped? (ii) How many of the guest molecule can be diverted away from the thermodynamic equilibrium when CB[7] is introduced at different times? (iii) How late is it 'too late' to introduce CB[7] to the evolving equilibrium to divert BNA into a kinetic trap?

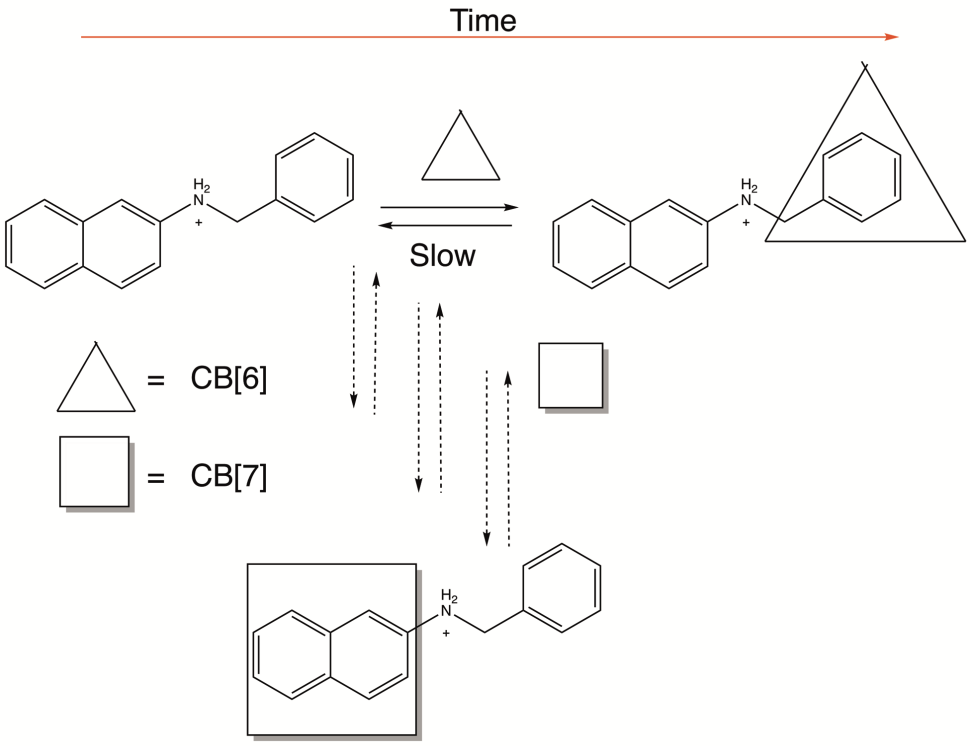

Scheme 4.1 Proposed self-sorting system between BNA^+, CB[6] and CB[7].

In order to ensure that the kinetics were on the proper time scale, Na^+ cations were considered to modulate the concentration of CB[6] and CB[7] available to bind BNA^+, as the addition of Na^+ cations has been shown to slow down the kinetics of CB[n]:guest complexes.[49] However, as seen in chapter 2, the addition of metal cations can add to the complexity of the system and change the binding mechanism between a guest and CB[n]s. Further, published work between PNA and CB[7] showed that as the concentration of Na^+ cations increased, the binding mechanism switched from the formation of a 1:1 complex, to the formation of a 2:1 CB[7]:guest complex. The second CB[7] binds to the phenyl moiety and is capped by a Na^+ cation. Finally, Na^+ cations bind CB[6] with an order of magnitude higher equilibrium constants than Na^+ binds to CB[7],[48-49] which introduces an additional variable to the system. Due to the inherent complexity associated with the addition of metal cations, β-CD was chosen to modulate the concentration of guest molecules that could be bound by CB[6] or CB[7]. Previous work showed that the kinetics between β-CD and a 2-naphthylethanol (NpOH) derivative are faster than the ms time scale, and the equilibrium constant is approximately 10^3 M^{-1}.[81] Therefore, β-CD should

meet the requirements of a concentration modulator: the kinetics are sub-ms and the equilibrium constant is multiple orders of magnitude lower than the equilibrium constant between BNA^+ and CB[6] or CB[7] (scheme 4.2).

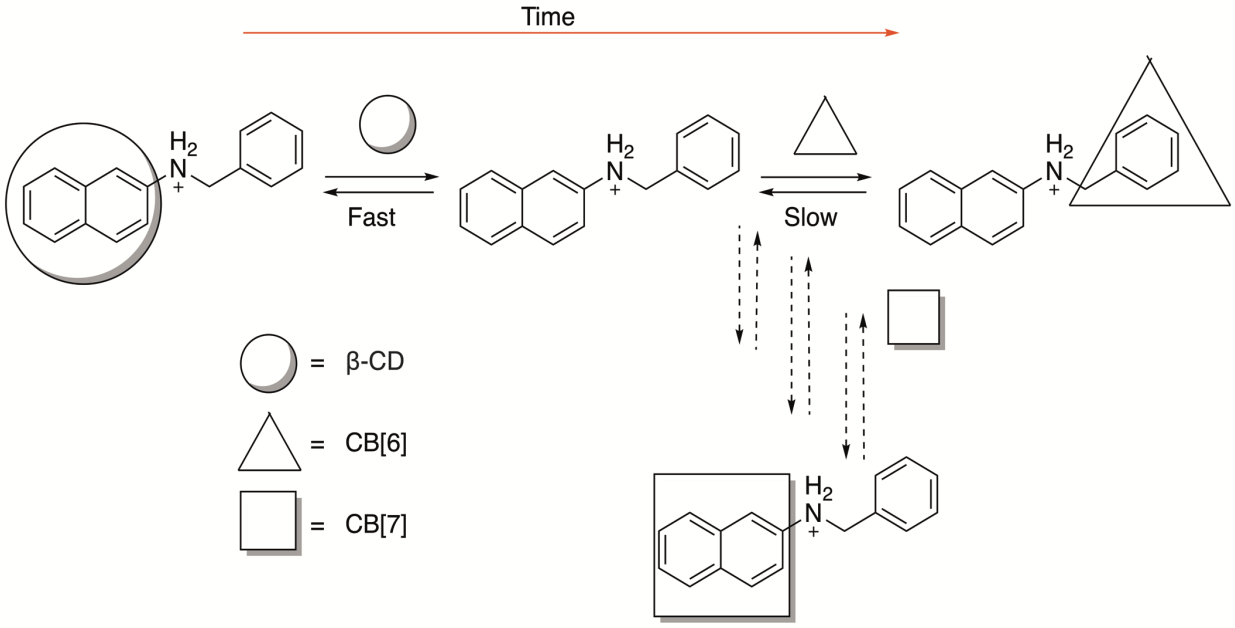

Scheme 4.2 Proposed expanded self-sorting system between BNA^+ and CB[6], CB[7] and β-CD.

4.1.2 Objectives

The objective of the work in this chapter is to determine the feasibility of this self-sorting system by confirming that all the individual interactions between the BNA^+ and the three host molecules have the correct equilibrium constants and the kinetics are on the appropriate time scales. The equilibrium constants between BNA^+ and all three host molecules needed to be determined, and the equilibrium constant with CB[6] must be the highest, followed by the equilibrium constant to CB[7]. The equilibrium constants between BNA^+ and the CB[n]s must be orders of magnitude higher than the equilibrium constant to β-CD. Once the equilibrium constants to the individual host molecules have been determined, the time scales for the binding kinetics was analyzed from a qualitative perspective. The kinetics between BNA^+ and β-CD must be the fastest and be on the sub-

ms time scale. The kinetics between BNA^+ and CB[7] must be on the ms-s time scale, and the kinetics with CB[6] must be the slowest, on the min to h time scale.

4.2 Experimental

4.2.1 Materials

N-benzyl-2-naphthylamine (BNA) was purchased from TCI Chemicals and was used without further purification. Sodium chloride (NaCl) and bis(cyclopentadienyl)cobalt (II) (Cob^+) were purchased from Sigma-Aldrich and were used without any further purification. CB[7] and CB[6] were obtained from a synthesis conducted by a previous graduate student in the group, Dr. Suma Thomas, and CB[6] and CB[7] were synthesized again using the same procedure.[47] β-CD was a gift from Cargill Food and Pharma Specialties and was used without further purification. Hydrochloric acid (HCl, ACS grade, 36.5-38%) was purchased from VWR Analytical and was used as obtained. Spectral grade methanol, for use in the ultraviolet region of the spectrum, was purchased from Fisher Chemical and was used as received. Aqueous solutions were prepared using de-ionized water from a Barnstead NANOpure deionizing system (≥ 17.3 MΩ cm).

4.2.2 Sample Preparation

Stock solutions of NaCl, HCl, BNA, CB[7], CB[6] and β-CD were prepared every 3-4 weeks. BNA stock solutions were made to 1-2 mM in spectral grade methanol. Stock solutions of NaCl were made to 1.0 M by dissolving solid NaCl in de-ionized H_2O. HCl stocks of 1.0 M were prepared from a 4.0 N HCl stock, by diluting in de-ionized water. CB[7] stock solutions were made by dissolving 6-7 mg in 5 mL of de-ionized H_2O. Assuming a 100% purity (completely dry) the concentration of the CB[7] stock solution was between 1.0-1.3 mM. β-CD stock solutions were made to 3-5 mM by dissolving solid β-CD in 10 mM NaCl and 1.0 mM HCl. Assuming a 100% purity, CB[6] stock solutions were made to 0.9 mM by dissolving solid CB[6] in 1.0 mM HCl and 2.0 mM NaCl. The

actual concentration of CB[7] was determined through a previously published purity titration.[95] The actual concentration of CB[6] was determined by two other graduate students in the group: Sree Gayathri Talluri and Ankur Awasthi.

Fluorescence: Solutions of BNA^+ of 1.0 μM were made at 1 mM HCl and 10 mM NaCl for experiments with all three host molecules. CB[7] solutions were made to 400 μM CB[7], 10 mM NaCl and 1.0 mM HCl. CB[6] solutions were made to 400 μM CB[6], 10 mM NaCl and 1-2 mM HCl. The β-CD solution was made to 3 mM β-CD in 1.0 mM HCl and 10 mM NaCl was used in the fluorescence binding isotherm determinations because it was assumed the equilibrium constant with BNA^+ would be much lower than with CB[6] or CB[7].

Stopped flow: BNA^+ solutions at 2 μM were prepared at 1 mM HCl and 10 mM NaCl. CB[7] solutions were made at 1.0 mM HCl, 10 mM NaCl and 10, 20, 30, 50 and 80 μM as the solutions are mixed in a 1:1 ratio under pressure. Solutions of β-CD were made to 1.0 mM HCl, 10 mM NaCl and 50, 100, 150, 250 and 400 μM β-CD.

UV/Vis kinetics: BNA^+ solutions were made to 20 μM BNA^+, 3 mM HCl and 10 mM NaCl. CB[6] solutions were made to 3 mM HCl, 10 mM NaCl and CB[6] concentrations ranging from 40-300 μM. The solutions were mixed in a 1:1 ratio in an absorption cell.

4.2.3 Equipment

Fluorescence: Steady-state fluorescence experiments were conducted on a PTI QM-40 spectrofluorimeter. The emission spectra were collected between 350 and 530 nm. The samples were excited at 274 nm with excitation and emission bandwidth of 0.5 nm. The step size for the collection of the spectra was 0.5 nm and the integration time was set to 0.25 s. The samples were equilibrated to 20 °C for 10 min after the addition of CB[7] or β-CD, and equilibrated for 20 min after each addition of CB[6].

UV/Vis spectroscopy: The absorption spectra were collected on a Varian Cary 100-Bio UV-Vis spectrophotometer or a Varian Cary 1E UV-Vis spectrophotometer. UV-Vis spectra were collected from 200 to 800 nm. The spectra were collected against an air background. Experimental spectra were corrected by taking a trace of solvent and subtracting the solvent spectrum from the experimental spectra. Absorption kinetic

experiments were collected on a Varian Cary 100-Bio UV-Vis spectrophotometer. The samples were prepared as they were for stopped-flow experiments, at double the experimental concentration. Solutions of BNA^+ and CB[6] were mixed at a 1:1 ratio in an absorption cell, and an absorption scan was collected from 200 to 800 nm every minute for 90 min. The experiments were conducted at 20 °C.

Stopped flow: Kinetic experiments were performed on an Applied Photophysics SX-20 stopped-flow system. A Hg-Xe vapor lamp was used as the excitation source for both absorption and fluorescence experiments. The solutions were mixed under pressure at a 1:1 ratio. In the fluorescence experiments, the samples were excited at 274 or 341 nm with the slits set to 0.1 or 1 mm on the monochromator used to select the excitation wavelength. The 0.1 mm and 1.0 mm slit widths correspond to bandwidths of 0.47 nm and 4.65 nm respectively for the excitation beam. The fluorescence was collected through a 395 nm cut-off filter, where all light below the wavelength of 395 nm was excluded. The samples were held at 20 °C for 10 min before kinetic traces were collected. Kinetic traces were corrected by averaging 11 kinetic traces of all components except the fluorophore, and subtracting the trace for the control experiment from the trace corresponding to the sample.

4.2.4 pK_a of BNA determination

When BNA was acquired, there was no published pK_a value for this molecule. The Advanced Chemical Development Labs software calculated a predicted pK_a of 4.2 for the protonation of BNA to form BNA^+. From this calculated pK_a, initial experiments, including experiments discussed in this chapter, were conducted in 1 mM HCl which is a pH of 3.0 or slightly less than 3.0. Evidence from preliminary stopped-flow experiments led to the investigation of the precision of the calculated pK_a. The desire is to work at a pH where the guest is completely protonated when free in solution and when bound to CB[7], or at a pH when the guest is completely deprotonated in solution but completely protonated in CB[n]s. CB[n]s are known to stabilize the cationic charge of an ammonium cation, which increases the pK_a of the bound guest molecule due to the ion-dipole interactions between the carbonyl lined portals of CB[n]s and the cationic ammonium.[44, 51, 72, 169-170]

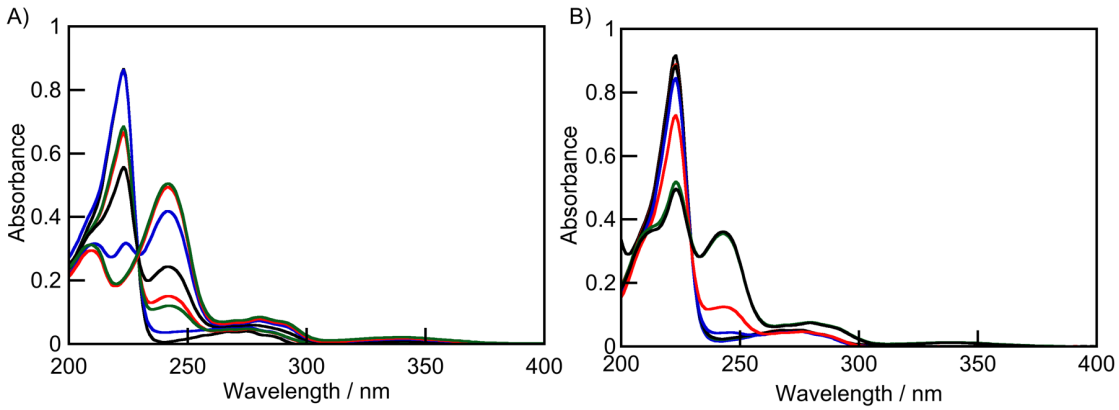

Figure 4.1 A: Absorption spectra of 10 µM BNA at pH values ranging from 5.9 (top green, a) to 1.7 (bottom black, h) using the decrease in absorption at 242 nm to determine the pK_a of BNA. **B:** Absorption spectra of 10 µM BNA mixed with 25 µM CB[7] at pH's ranging from 5.9 (top black, a) to 1.7 (bottom black, h) to determine the pK_a of BNA when bound to CB[7] using the absorption at 242 nm.

The absorbance at 242 nm, which was identified as the absorption band of the unprotonated species, was taken at different measured pH values in the absence and presence of 25 µM CB[7]. From the absorption at 242 plotted against pH, it was found that the pK_a of BNA is 3.6-3.7 in water, and the pK_a in the presence of CB[7] is >5.5 (figure 4.2).

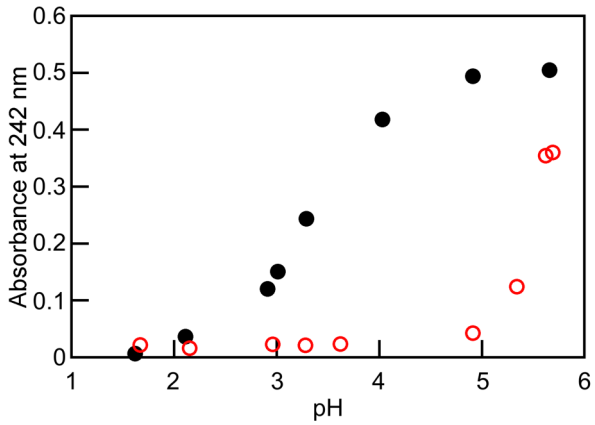

Figure 4.2 Titration curve of 10 µM BNA in the presence of 25 µM CB[7] (red circles) and absence of CB[7] (black dots) generated from the absorption at 242 nm from figure 4.1.

The majority of experiments described in this chapter were conducted at a pH of 3.0, which does not affect the thermodynamic equilibrium constants between BNA^+ and CB[6] or CB[7], because once bound all species are protonated; however, the different protonation

states can play a role in analyzing the kinetics. Because of the different protonation states the kinetics are reported as a qualitative tool to show that the kinetics are on the correct time scale, rather than reporting a quantitative analysis. The kinetic experiments reported were sufficient to determine the appropriateness of the desired time scales.

4.2.5 Stability of BNA^+ irradiated by 274 nm light

Preliminary stopped-flow experiments showed a decrease in fluorescence intensity with time for BNA^+ when mixed with water, when the sample was excited at 274 nm (figure 4.3, panel A). When the BNA^+ was excited at 341 nm, there was no change in fluorescence intensity with respect to time (figure 4.3, panel A). Stopped-flow experiments are commonly conducted in our group with the excitation slits set to a width of 1.0 mm, which corresponds to an excitation bandwidth of 4.65 nm. The decrease in fluorescence intensity with respect to time when the sample was excited at 274 nm was proposed as the decomposition of BNA^+ due to the light intensity. Stopped-flow traces of BNA^+ were then collected with the excitation slits set to 0.1 mm, which corresponds to an excitation bandwidth of 0.47 nm (figure 4.3, panel B). When the excitation bandwidth was decreased, the fluorescence intensity was shown to be stable when the sample was continuously irradiated at 274 nm.

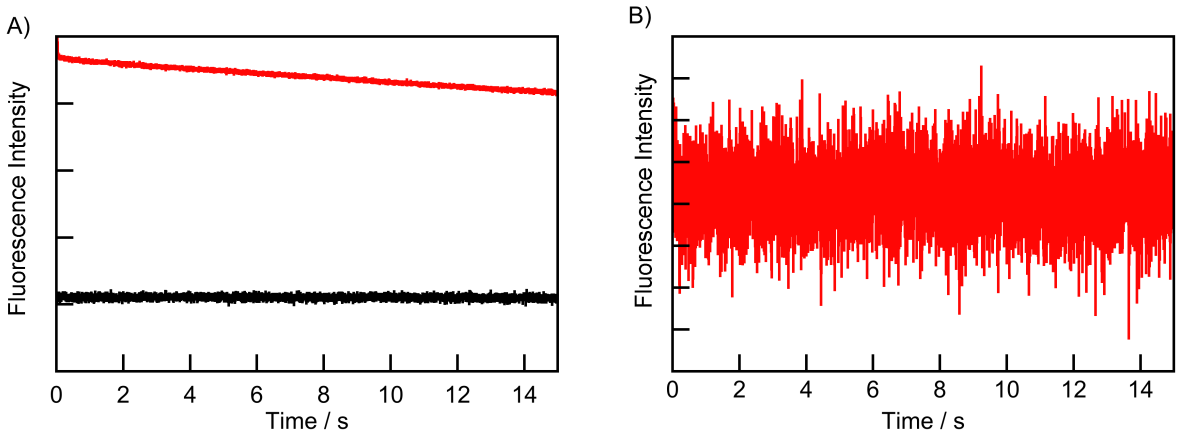

Figure 4.3 A: Kinetic traces of 1 μM BNA^+ mixed with 1.0 mM HCl excited at 274 nm (red) and 341 nm (black) with an excitation bandwidth of 4.65 nm. **B:** Kinetic trace of 1 μM BNA^+ mixed with 1.0 mM HCl excited at 274 nm with an excitation bandwidth of 0.47 nm.

To confirm the decrease in fluorescence intensity found in the stopped-flow experiments, BNA^+ was continuously irradiated at 274 nm and an emission spectrum was collected every 5 min for 20 min at different excitation bandwidths (figure 4.4).

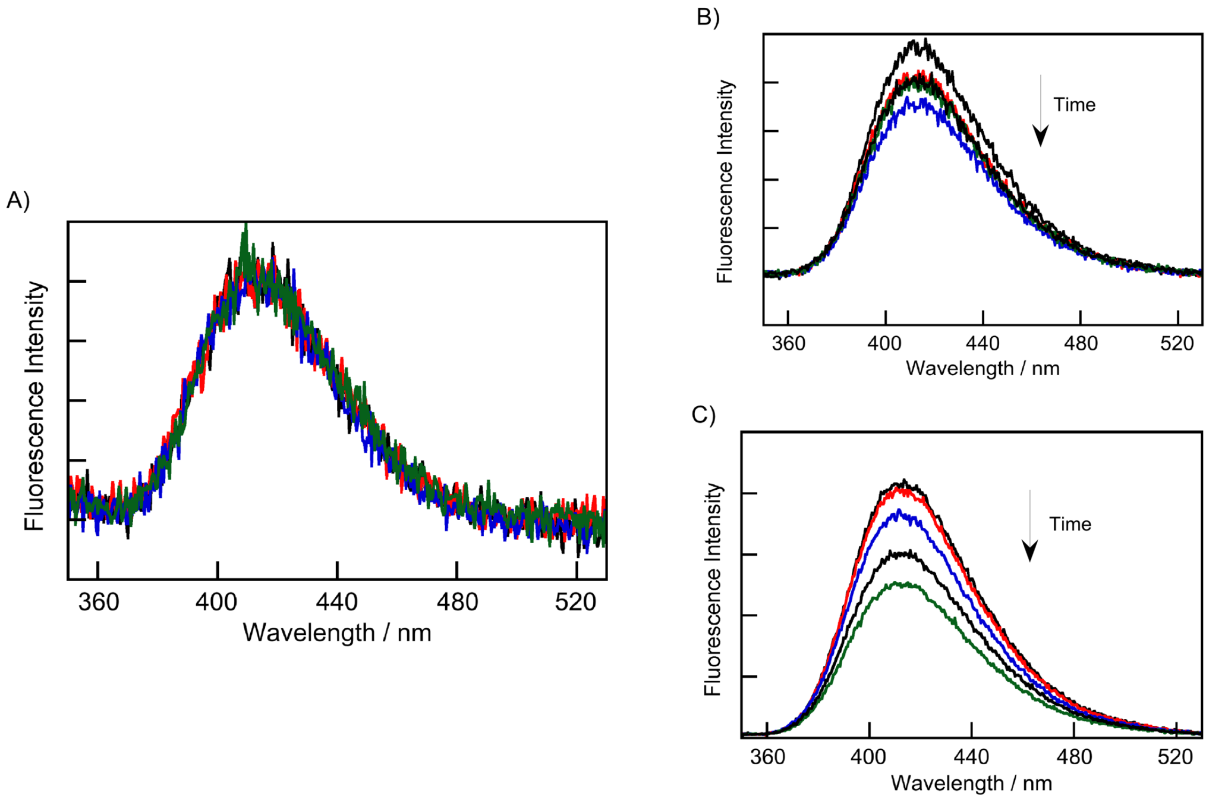

Figure 4.4 Emission spectra of 1 μM BNA^+ in 1.0 mM HCl taken every 5 min at different excitation bandwidths (**A:** 0.50 nm; **B:** 1.00 nm; **C:** 4.65 nm).

From figure 4.4, when the excitation bandwidth was set to 4.65 nm, which is the equivalent excitation bandwidth used for the preliminary experiments on the stopped-flow shown in figure 4.3, there was a decrease in fluorescence intensity when the sample is continuously irradiated (figure 4.4, panel C). Panel B shows the continuous radiation of BNA^+ with the excitation bandwidth set to 1.00 nm. The emission spectra in panel B shows the fluorescence intensity still decreasing with continuous irradiation. However, panel A shows the emission scans taken every 5 min after continuous irradiation at 274 nm with an excitation bandwidth of 0.5 nm, which shows no change in the fluorescence intensity and is consistent with what was found in stopped-flow experiments. The experiments reported in this chapter were conducted with an excitation bandwidth of 0.5 nm.

4.2.6 Binding isotherm model for the formation of the 1:1 complex between BNA^+ and CB[6], CB[7] and β-CD

The emission spectra of BNA^+ solutions mixed with CB[6], CB[7] or β-CD (host molecules) solutions were integrated from 365 to 530 nm. The integrated values were divided by the integrated value measured for a BNA^+ solution with no host molecules added to convert the integrated emission intensity into a relative integrated intensity value (I). The plot being fit was the dependence of the relative integrated intensity values against the concentration of host molecules. The data were fit to a 1:1 model using numerical analysis on the Scientist 3 software from Micromath:

$$[G@H]_{eq} = \beta_{11} \times [H]_{eq} \times [G]_{eq} \quad \text{(Eq. 4.1)}$$

$$[H]_{eq} = [H]_T - [G@H]_{eq} \quad \text{(Eq. 4.2)}$$

$$[G]_{eq} = [G]_T - [G@H]_{eq} \quad \text{(Eq. 4.3)}$$

$$I = R \times ([G]_{eq} + C_{11} \times [G@H]_{eq}) \quad \text{(Eq. 4.4)}$$

$$R = \frac{I_0}{[G]_T} \quad \text{(Eq. 4.5)}$$

Where the concentration constraints for the dependent variables are:

$$0 < [G]_{eq} < [G]_T \quad \text{(Eq. 4.6)}$$

$$0 < [H]_{eq} < [H]_T \quad \text{(Eq. 4.7)}$$

$$0 < [G@H]_{eq} < [G]_T \quad \text{(Eq. 4.8)}$$

The total concentrations of host and guest molecules present in solution are represented by $[H]_T$ and $[G]_T$. The equilibrium concentrations of host, guest and the 1:1 host-guest

complex are denoted as $[H]_{eq}$, $[G]_{eq}$ and $[G@H]_{eq}$, respectively. The concentration of host at equilibrium, $[H]_{eq}$, includes all host molecules not bound to BNA^+. The overall equilibrium constant for the formation of the host-guest complex at a given concentration of Na^+ cations was denoted as β_{11}. The integrated intensity of BNA^+ in the absence of host was denoted as I_0. R corresponded to the ratio of fluorescence intensity of BNA^+ in the absence of host (I_0) to the total guest concentration ($[G]_T$). C_{11} was the ratio of the emission quantum yields of the BNA^+@Host and BNA^+ free in solution.

4.2.7 Analysis of the kinetics between BNA^+ and CB[6], CB[7] and β-CD

Due to the issues of different protonation states of BNA^+ faced in the analysis of this work, the kinetics are being analyzed in a qualitative fashion, not a quantitative fashion. Therefore, there will be no fitting of kinetic traces to a sum of exponentials function or to a model as performed for the kinetic described in previous chapters. The kinetic results will be analyzed for the desired time scale of reactions, rather than mechanistically.

4.3 Results

4.3.1 Binding isotherms and kinetics between BNA^+ and β-CD

As a replacement for metal cations, β-CD was selected to modulate the free guest concentration that can be bound by CB[6] or CB[7]. For β-CD to be a successful integration into the self-sorting system, the equilibrium constant with BNA^+ must be approximately 10^3 M^{-1} and the kinetics must be faster than the ms time scale.

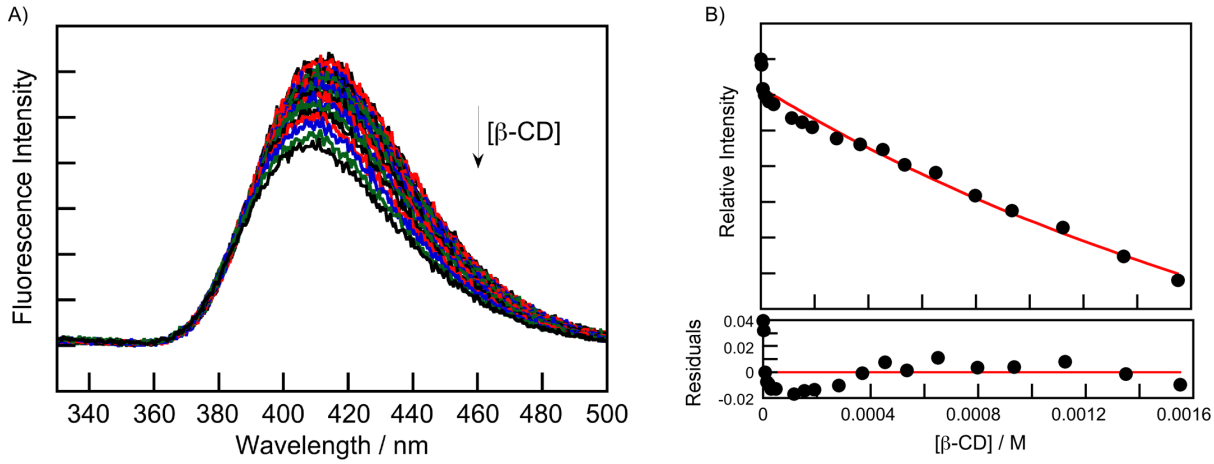

Figure 4.5 A: Fluorescence spectra for 1 μM BNA^+ with β-CD concentrations ranging from 0-1.6 mM at 10 mM Na^+ cations. **B:** Binding isotherm between BNA^+ and β-CD (top panel) using the relative fluorescence intensity fit to a 1:1 β-CD:guest model. The red line represents the numerical fit of the data. The bottom panel shows the residuals of the fit.

The equilibrium constant recovered from the binding isotherm in figure 4.5 is of the correct order of magnitude for β-CD in this self-sorting system. For the analysis of the fit of the binding isotherm, no exact value of the equilibrium constant can be determined because saturation is not reached. Further, because BNA^+ was not added to the solution with β-CD, the dilution of guest became too large to be corrected for by a dilution factor, as the dilution was 30%. The data was fit with the decreasing concentration of guest because of the magnitude of the dilution.

The residuals of the fit of the 1:1 model shows some deviation from the fit line. The deviation from the fit line may suggest that there are more species than the 1:1 complex between β-CD and BNA^+. The alternative species may be two β-CD molecules binding to a single BNA^+, or it is the β-CD binding to the two-different species of BNA in solution: protonated and deprotonated. CB[n]s cause a shift in the pK_a of a guest molecule, which means even if there is some unprotonated BNA in solution, it will be protonated once bound to CB[6] or CB[7].[44, 72, 169] β-CD binds neutral guest species stronger than β-CD binds the charged guest molecules; previous work has shown the equilibrium constant between β-CD and a guest decreases when a charge is introduced to a guest molecule.[25] Therefore, the deviation from the fit may be β-CD binding to the unprotonated species first, and the charged species second.

The equilibrium constant of β-CD to the naphthyl group of BNA is close to where it would predictably be: in the high 10^2 M^{-1}. The binding isotherm between β-CD and BNA^+ could not fit to 1:1 model. The inability to fit to a 1:1 model is not problematic because the purpose is to introduce competition for the binding of BNA^+ with the CB[n]s, with an equilibrium constant of 10^2-10^3 M^{-1}. Whatever complexes are formed between β-CD and BNA^+ will be out competed with the introduction of CB[6] or CB[7].

Once the equilibrium constant between β-CD and BNA^+ was confirmed to be in the range of 10^2-10^3 M^{-1}, the kinetic time scale needed to be determined.

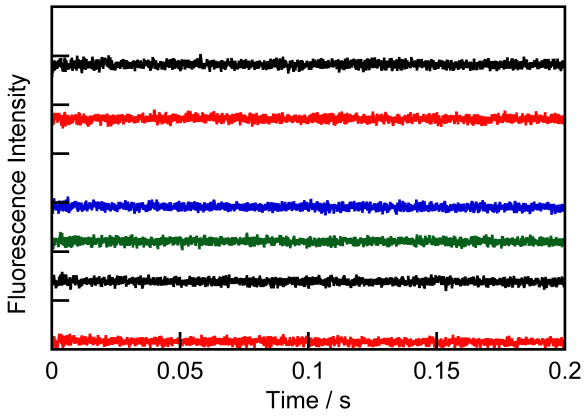

Figure 4.6 Kinetic traces for the mixing of 1 μM BNA^+ with various CB[7] concentrations (50 μM, top red; 100 μM, blue; 150 μM, green; 200 μM, bottom black; 250 μM, bottom red) in the presence of 10 mM Na^+. The top black trace corresponds to the control experiment in the absence of β-CD ([Na^+ = 10 mM)**.**

Figure 4.6 shows that all the kinetics are faster than the ms time scale. For kinetics to be faster than the ms time scale, only amplitude changes in fluorescence intensity should be seen, with no growth or decay. The kinetics being faster than the ms time scale, and the binding isotherm yielding an equilibrium constant between 10^2-10^3 M^{-1} meant that β-CD met all the requirements necessary to be the concentration modulator in the self-sorting system.

4.3.2 Binding isotherm and kinetics between BNA^+ and CB[7]

The complex between CB[7] and BNA^+ is meant to be the kinetic trap of the self-sorting system. Therefore, the requirements between CB[7] and BNA^+ were the equilibrium

constant of BNA^+ needs to be higher than for the binding with β-CD and but lower than for the binding with CB[6], and the kinetics for complex formation needed to be slower than for binding with β-CD, but faster than for the binding with CB[6].

Figure 4.7 shows the binding isotherm and fit of the binding isotherm to a 1:1 model. From equation 4.9 the recovered equilibrium constant from the binding isotherms conducted in the presence of 10 mM NaCl was $(1.6 \pm 0.1) \times 10^7$ M^{-1}.

$$\beta_{11} = \frac{K_{11}}{1+K_1[Na^+]+K_1K_2[Na^+]^2} \qquad \text{(Eq. 4.9)}$$

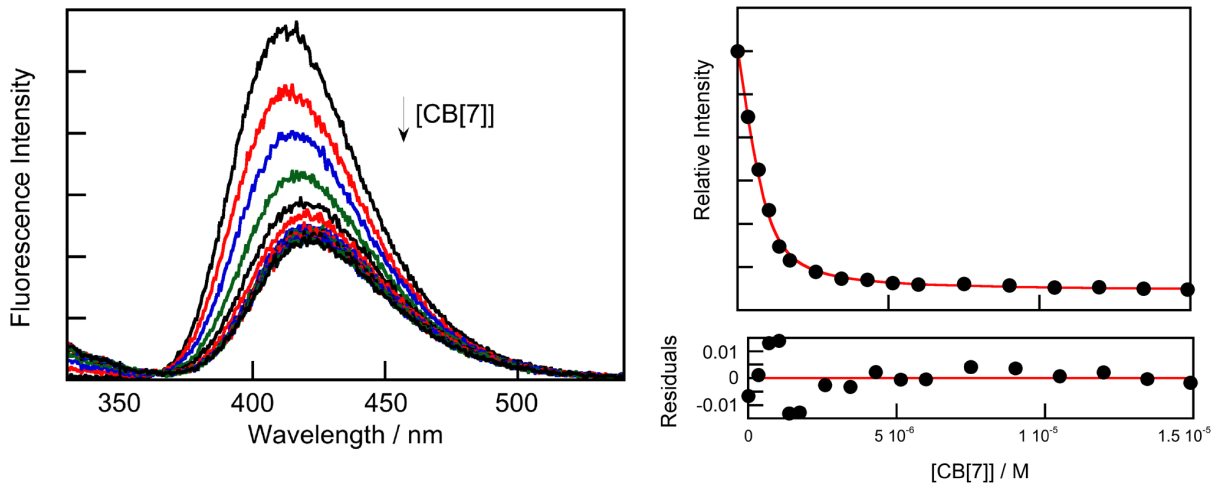

Figure 4.7 A: Fluorescence spectra for 1 μM BNA^+ with CB[7] concentrations ranging from 0-15 μM at 10 mM Na^+ cations. **B:** Binding isotherm between BNA^+ and CB[7] (top panel) using the change in the relative fluorescence intensity for the fit to a 1:1 CB[7]:guest model. The red line represents the numerical fit of the data. The bottom panel shows the residuals between the data and the fit.

Because the equilibrium constant was higher than the equilibrium constant between β-CD and BNA^+ and the binding isotherm fit well to a 1:1 model, the kinetics could be analyzed. The equilibrium constant of CB[7] to the naphthyl moiety of BNA^+ is similar to the equilibrium constant between NpH^+ and CB[7] which is 1.06×10^7 M^{-1} (discussed in chapter 2).

The desired time scale for the kinetics between BNA^+ and CB[7] is on the ms to second time scale. Kinetics on the second time scale would be much slower than the kinetics

between β-CD and BNA^+, and allows the kinetics of CB[6] to be much longer on the min-h time scale.

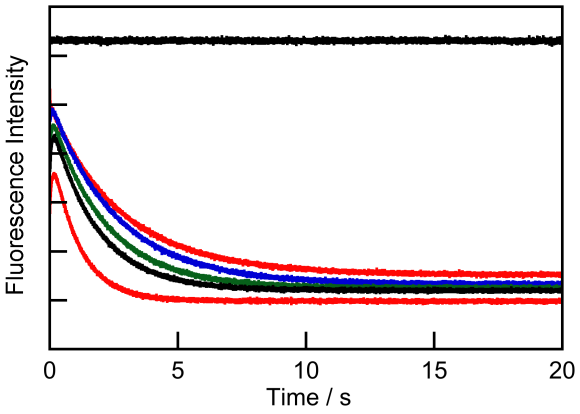

Figure 4.8 Kinetic traces for the mixing of 1 μM BNA^+ with various CB[7] concentrations (5 μM, top red; 10 μM, blue; 15 μM, green; 25 μM, bottom black; 40 μM, bottom red) in the presence of 10 mM Na^+. The top black trace corresponds to the control experiment in the absence of CB[7] ([Na^+ = 10 mM).

The kinetics are on the desired s time scale. Within the first second of the kinetics there is an offset in the kinetics which is consistent with what was found between CB[7] and PNA (figure D1).[51] The offset is attributed to the transient binding of CB[7] to the phenyl moiety, before binding to the naphthyl moiety.[51] The fast component with BNA will likely be attributed to the transient binding of the benzyl moiety competitively with the naphthyl moiety. The slower component of the kinetics is proposed as the thermodynamic sink of CB[7] binding to the naphthyl motif of BNA^+. The overall kinetics with BNA^+ are slower than the kinetics with PNA. This difference is likely due to the kinetics with a benzyl moiety being slower than the kinetics with the phenyl moiety of PNA.

Because the kinetics are on the seconds time scale, the kinetics between CB[7] and BNA^+ meet the kinetic requirements for the self-sorting system. Further, the equilibrium constant recovered from the binding isotherm in figure 4.7 show an equilibrium constant that is larger than β-CD, which meets a requirement, however, it will depend on the equilibrium constant between CB[6] and BNA^+ to determine if all the requirements of CB[7] are met for the self-sorting system.

4.3.3 Binding isotherm and kinetics between BNA^+ and CB[6]

The final aspect to establish for the self-sorting system is the equilibrium constant and kinetic time scale between CB[6] and BNA^+. The thermodynamic requirement between CB[6] and BNA^+ is that the equilibrium constant must be the highest of the three host molecules to act as the thermodynamic sink of the system. The kinetic requirements between CB[6] and BNA^+ are that the kinetics must be the slowest of the three host molecules, and preferably be on the min-h time scale.

The kinetics between BNA^+ and CB[6] was determined by mixing a CB[6] solution and BNA^+ solution in a 1:1 mixture and collecting an absorption scan every minute for 90 minutes, as the kinetics were expected to be on the min-h time scale.

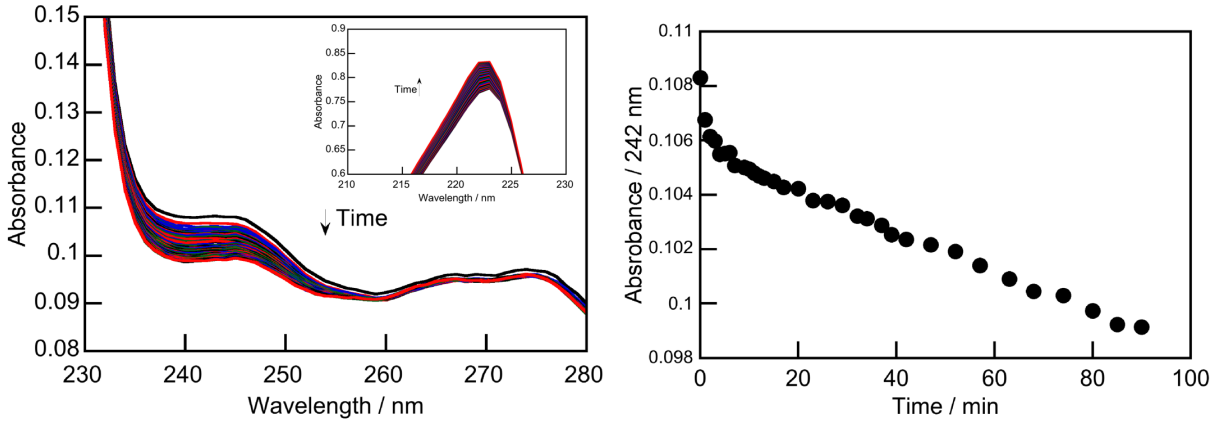

Figure 4.9 A: Absorption spectra taken over time of 10 µM BNA^+ mixed with 40 µM CB[6]. Absorption scans were taken from 200-800 nm every min for 90 min, and the absorption at 242 nm was tracked. The inset shows the absorption from 210-230 nm. **B:** The change in absorption between BNA^+ and CB[6] at 242 nm with respect to time.

The absorption kinetics at 242 nm was tracked for 90 min. From figure 4.9, equilibrium was not reached after 90 min. The kinetics are therefore on the desired time scale for the self-sorting system. To ensure that the prolonged change in absorbance was not due to the degradation of BNA^+, figure D2 shows the overlay of BNA^+ mixed with solvent containing no CB[6] with absorption scans taken every minute for 20 min.

The absorption band of 242 nm is the absorption band of the unprotonated BNA species. The change in absorption is the change of protonation state of BNA^+ as it binds to CB[6]. Because both species are present in solution, the kinetics seen in figure 4.9 are the binding

of CB[6] and the unprotonated BNA, because at the pH the experiment was conducted a large fraction of the guest molecules are already protonated. Therefore, a quantitative analysis of the kinetics is not warranted, however figure 4.9 does prove that the kinetics were on the correct time scale to fit the requirements needed for CB[6] in this self-sorting system because the kinetics did not reach equilibrium in 90 min.

Once the kinetics were confirmed to be on the correct time scale, the equilibrium constant needed to be determined. Figure 4.10 shows the binding isotherm and fit of the binding isotherm to a 1:1 model between CB[6] and BNA^+. The equilibrium constant is reported to an order of magnitude as it was for β-CD because saturation was not met.

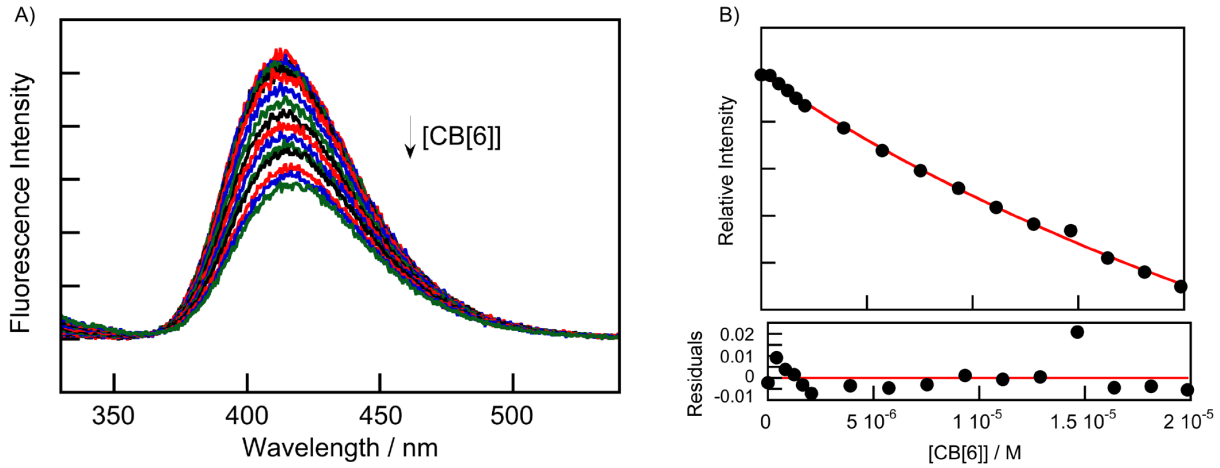

Figure 4.10 A: Fluorescence spectra for 1 μM BNA^+ with CB[6] concentrations ranging from 0-2 μM at 10 mM Na^+ cations. **B:** Binding isotherm between BNA^+ and CB[6] (top panel) using the changes in the relative fluorescence intensity fit to a 1:1 CB[6]:guest binding model. The red line represents the numerical fit of the data. The bottom panel shows the residuals between the data and the fit.

The issue with 4.10, is that when the binding isotherm was conducted the solution was allowed to equilibrate for 20 min after each addition of CB[6]. From the kinetics acquired in figure 4.9, the system may not be at equilibrium when the emission scans were acquired in the binding isotherm shown in figure 4.10. Therefore, the equilibrium constant discussed below may be lower than what its actual value would be if the system had equilibrated.

The overall equilibrium constant in 10 mM Na^+ cations was found to be approximately 2×10^4 M^{-1}. Using eq. 4.9, the equilibrium constant between CB[6] and BNA^+ is approximately 1.6×10^6 M^{-1} from the fit to a 1:1 binding model. A problem with the

binding isotherm between CB[6] is that the equilibrium constants with Na^+ are an order of magnitude higher than the equilibrium constants between Na^+ cations and CB[7].[49] The equilibrium constants between CB[6] and Na^+ cations are reported at 1450 M^{-1} and 362 M^{-1} for the first and second equilibrium constants respectively.[113] The recovered equilibrium constant was an order of magnitude below the equilibrium constant between CB[7] and BNA^+. Further, the difference in equilibrium constants between Na^+ and CB[6] versus CB[7] presents a challenge for the development of the self-sorting system.

4.4 Discussion

Traditional supramolecular self-sorting systems analyze the product distribution of complex mixtures with respect to time.[34, 37-39, 130, 157, 159, 161, 165, 171-172] The analysis of self-sorting systems is still in the scope of 'trial and error' where complex mixtures are mixed together and the thermodynamic products that result give information about how these species interact with one another.[56, 58, 61, 65] Systems that are under kinetic control are labelled as such because a kinetic product was seen along the path to forming the thermodynamic product. However, rarely are these kinetically controlled host-guest systems designed as such. The unique principle of the self-sorting system that was attempted to be designed in this chapter is the kinetic trap designed to be introduced as the thermodynamic pathway is evolving. The kinetic trap creates a transient species that can be studied out of equilibrium for a short time, before the reaction ultimately reaches its thermodynamic equilibrium.

In the design of the system, the decision to change the modulator for the system from Na^+ cations to β-CD was meant to decrease some of the complexity of the evolving system. The change in concentration modulator was made because Na^+ cations have different equilibrium constants to different CB[n]s, but β-CD modulates the guest concentration, so the competition with the CB[n]s is equal. The requirements for β-CD were that the kinetics had to be faster than the ms time scale and the equilibrium constant between β-CD and BNA^+ had to be multiple orders of magnitude lower than the equilibrium constants to CB[6] or CB[7]. The kinetics were sub ms and the equilibrium constant was in the mid to high 10^2 M^{-1}. The kinetic and thermodynamic results were consistent with what was seen

previously between NpOH and β-CD.[81] The equilibrium constant between BNA^+ and β-CD was slightly lower than the equilibrium constant between β-CD and NpOH because introduction a charge onto BNA^+ will decrease the equilibrium constant to β-CD, whereas it increases the equilibrium constant to CB[n]s.[25]

β-CD was chosen as a concentration modulator due to the complexity introduced by different concentrations and identities of metal cations as described in chapter 2 and in the literature.[51] Some Na^+ cations were added to the solution in order to have better control of the metal cation concentration in solution, rather than using water where the concentration of metals can vary. However, 10 mM Na^+ may be too high of a concentration to conduct these experiments because of the difference in equilibrium constants between Na^+ and the CB[n]s.[48-49] Further, the work with PNA and CB[7] showed that at concentrations above 5 mM Na^+, a 2:1 CB[7]:PNA complex was formed, where the CB[7] bound to the phenyl moiety was capped by a Na^+ cation to stabilize it. While there is no evidence of a 2:1 complex between BNA^+ and CB[7], the concentration of Na^+ cations for future experiments should be lowered into the 2-5 mM range.

The requirements for the binding interactions between CB[7] and BNA^+, as the kinetic trap, were that the kinetics had to be slower than the kinetics of BNA^+ with β-CD, but faster than the kinetics with CB[6]; further, the equilibrium constant for the binding of BNA^+ had to be much higher than that for β-CD, but lower than the equilibrium constant for CB[6]. Figure 4.8 shows that the kinetics were slower than the kinetics with β-CD, and the equilibrium constant was much higher than the equilibrium constant for β-CD. The recovered equilibrium constant between BNA^+ and CB[7] was $(1.6 \pm 0.1) \times 10^7$ M^{-1} is close to the equilibrium constant between CB[7] and NpH^+.[49] This result was expected as in both cases CB[7] is binding to a naphthyl moiety with a cationic charge in close proximity. As mentioned above, work between CB[7] and PNA showed a higher order complex in the presence of 10 mM Na^+ cations, however, BNA^+ showed no evidence of a higher order complex being formed in the thermodynamic studies.

The final component of the self-sorting system to resolve was the proposed thermodynamic sink between CB[6] and BNA^+. The kinetic and thermodynamic requirements for the interactions between CB[6] and BNA^+ were that the kinetics had to be the slowest of the three host molecules and the equilibrium constant had to be the highest of the three host

molecules. Figure 4.10 shows that when CB[6] is mixed with BNA^+, the solution does not reach equilibrium within 90 min. While equilibrium was never reached in this kinetic experiment, this experiment did confirm that the kinetics between BNA^+ and CB[6] were the slowest. Though the kinetics were only analyzed in a qualitative manner, the kinetics were on the desired min-h time scale. However, the equilibrium constant that was recovered from the binding isotherms was found to be approximately 1.6×10^6 M^{-1}, which is an order of magnitude lower than the equilibrium constant between BNA^+ and CB[7]. The recovered equilibrium constant may be slightly lower than the actual equilibrium constant. Due to the time scale of the kinetics, if the system had not reached equilibrium before each emission scan was collected because the solutions were only allowed to equilibrate for 20 min after each addition of CB[6], the recovered equilibrium constant may be lower than its actual value. Because the equilibrium constants are only an order of magnitude apart, conceivably CB[6] could be the thermodynamic sink of the system if the concentration of CB[6] is much greater than the concentration of CB[7] (~10^2 M); however, due to CB[6]s solubility in water, a large excess of CB[6] to CB[7] is difficult to achieve. Therefore, some work will need to be done to optimize the guest structure to ensure that the equilibrium constant to CB[6] is sufficiently high that the guest@CB[6] complex corresponds to the thermodynamic sink, while still having slow kinetics.

There are two modifications that will likely solve the problems faced in designing this self-sorting system. The first problem to address is the stability of BNA^+. The protonated inclusion complex in CB[7] appears to be stable, therefore, one solution to solve the stability issue is to work at pH 4.9 where the guest is deprotonated when free in solution, and protonated when bound to CB[7] (figure 4.2). Another solution to this problem is to change the location of the amine, and add a carbon as a spacer between the naphthyl moiety and the amine (chart 4.3), as is the case in NpH^+. The second modification is to change the benzyl moiety to an alkyl di-ammonium (chart 4.3). Previous self-sorting systems have shown that the alkyl ammoniums are selective for CB[6] over CB[7].[37-38] Making the alkyl group a di-ammonium will, not only, increase the equilibrium constant to CB[6], making it the thermodynamic sink of the system,[168] but adding the extra ammonium group will slow down the kinetics.[21] Previous work in the literature has shown that, not only does adding a cationic charge increase the equilibrium constant between CB[6] and a guest

molecule, but it also slows down the kinetics through the formation of an exclusion complex.[21]

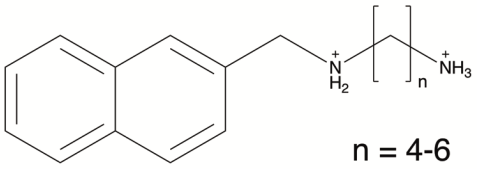

Chart 4.3 Proposed chemical structure for BNA^+ modifications

The work in this chapter explored the feasibility of kinetically trapping an already evolving system toward its thermodynamically equilibrium. The goal of designing systems like this is to move self-sorting systems from a standpoint of mixing complex mixtures together and analyzing the products, to self-sorting systems with rational design: where out of equilibrium properties of systems can be studied. As seen from the results above, there are a lot of complicated parameters that go into the design of these systems. The design of these systems may benefit from studying the different binding epitopes individually before the molecule is assembled in order to reduce some complexity. However, these results are an encouraging start that rationally designed self-sorting systems can be designed in the near future.

Chapter 5: Summary

The main objective of the work in this dissertation was to understand the complexity of CB[7]-guest chemistry, and to use that understanding of complexity to rationally design systems. Understanding the complexity of supramolecular systems has potential applications in drug delivery, catalysis, self-sorting and systems chemistry. Kinetic studies, like the studies presented in this dissertation, are essential to understanding how dynamic systems evolve.

The projects described in this dissertation provides a better understanding of two aspects of CB[7]-guest chemistry. The kinetic study between NpH^+ and CB[7] revealed the significant role the concentration and identity of biologically relevant metal cations can have on the mechanism of host-guest binding. The binding mechanism between NpH^+ and CB[7] was shown to have more than one relaxation process: the formation of an exclusion complex and an inclusion complex between the guest and the host. By elevating the concentration of Ca^{2+} or Na^+ in solution, the exclusion complex was out competed by the metal cations binding to CB[7]. But in the presence of Ca^{2+} cations, there was the formation of an Ca^{2+} cation capped inclusion complex with a decreased dissociation rate constant from the uncapped complex seen in the presence of Na^+ cations.

Insight into the effect of guest structure on the rate of formation between CB[7] and aromatic dications was gathered. It was found that moving cationic charges further apart on the guest molecule increased the time scale of the kinetics between CB[7] and guest from the sub millisecond onto the millisecond time scale; however, adding width to the guest molecule shifted the kinetics onto the minute time scale. These results showed that the fit within the cavity of CB[7] had a greater influence on the kinetic time scale than the distance between the cationic charges.

The understanding of complexity gained in the metal cations and structural features projects was used to attempt to develop a kinetically-trapping self-sorting system. While the self-sorting system was not attempted, and the guest molecule show some stability issues, it was shown that it is feasible to use supramolecular macrocycles to rationally design kinetically-trapping self-sorting systems.

Supramolecular host-guest systems are used increasingly in functional materials, drug delivery, self-sorting, self-assembly, catalysis and systems chemistry. Using kinetic studies

to understand the fundamentals of the complexity of host-guest systems, will unlock the opportunity for rationally designed systems in these field. The studies presented here lay the ground work for understanding how CB[n]-guest complexes react in the presence of biologically relevant cations, how structural features can be modified to increase the efficacy of CB[n] as a drug carrier, and the potential of CB[n]s to be used in kinetically trapping self-sorting systems.

Bibliography

1. Lehn, J.-M., Towards complex matter: supramolecular chemistry and self-organization. *European Review* **2009,** *17* (2), 263-280.
2. Menger, F. M., Supramolecular chemistry and self-assembly. *Proc Natl Acad Sci U S A* **2002,** *99* (8), 4818-4822.
3. Steed, J. W.; Atwood, J. L., *Supramolecular chemistry*. John Wiley & Sons: **2013**.
4. Ariga, K.; Kunitake, T., *Supramolecular chemistry-fundamentals and applications: advanced textbook*. Springer Science & Business Media: 2006.
5. Mattia, E.; Otto, S., Supramolecular systems chemistry. *Nature nanotechnology* **2015,** *10* (2), 111.
6. Schneider, H.-J.; Yatsimirsky, A. K., *Principles and methods in supramolecular chemistry*. Wiley Chichester: 2000; Vol. 5.
7. Lehn, J.-M., Supramolecular chemistry: receptors, catalysts, and carriers. *Science* **1985,** *227* (4689), 849.
8. Lehn, J.-M., Supramolecular chemistry—scope and perspectives molecules, supermolecules, and molecular devices (Nobel lecture). *Angewandte Chemie International Edition in English* **1988,** *27* (1), 89-112.
9. Oshovsky, G. V.; Reinhoudt, D. N.; Verboom, W., Supramolecular chemistry in water. *Angewandte Chemie International Edition* **2007,** *46* (14), 2366-2393.
10. Pratt, L. R.; Chandler, D., Theory of the hydrophobic effect. *The Journal of Chemical Physics* **1977,** *67* (8), 3683-3704.
11. Tanford, C., The hydrophobic effect and the organization of living matter. *Science* **1978,** *200* (4345), 1012-1018.
12. Atwood, J. L., *Comprehensive supramolecular chemistry II*. Elsevier: 2017.
13. Schueler-Furman, O.; Wang, C.; Bradley, P.; Misura, K.; Baker, D., Progress in modeling of protein structures and interactions. *Science* **2005,** *310* (5748), 638-642.
14. Prescher, J. A.; Bertozzi, C. R., Chemistry in living systems. *Nature chemical biology* **2005,** *1* (1), 13-21.
15. Hasenknopf, B.; Lehn, J.-M.; Boumediene, N.; Leize, E.; Van Dorsselaer, A., Kinetic and thermodynamic control in self-assembly: sequential formation of linear and circular helicates. *Angewandte Chemie International Edition* **1998,** *37* (23), 3265-3268.
16. Whitesides, G. M.; Grzybowski, B., Self-assembly at all scales. *Science* **2002,** *295* (5564), 2418.
17. Davis, A. V.; Yeh, R. M.; Raymond, K. N., Supramolecular assembly dynamics. *Proceedings of the National Academy of Sciences* **2002,** *99* (8), 4793.
18. Mai, Y.; Eisenberg, A., Self-assembly of block copolymers. *Chemical Society Reviews* **2012,** *41* (18), 5969-5985.
19. Lehn, J.-M., Supramolecular chemistry. *Science* **1993,** *260* (5115), 1762-1764.
20. Appel, E. A.; Biedermann, F.; Rauwald, U.; Jones, S. T.; Zayed, J. M.; Scherman, O. A., Supramolecular cross-linked networks via host−guest complexation with cucurbit[8]uril. *Journal of the American Chemical Society* **2010,** *132* (40), 14251-14260.
21. Hoffmann, R.; Knoche, W.; Fenn, C.; Buschmann, H.-J., Host–guest complexes of cucurbituril with the 4-methylbenzylammonium lon, alkali-metal cations and NH_4^+. *Journal of the Chemical Society, Faraday Transactions* **1994,** *90* (11), 1507-1511.

22. Ni, X.-L.; Xiao, X.; Cong, H.; Liang, L.-L.; Cheng, K.; Cheng, X.-J.; Ji, N.-N.; Zhu, Q.-J.; Xue, S.-F.; Tao, Z., Cucurbit[n]uril-based coordination chemistry: from simple coordination complexes to novel poly-dimensional coordination polymers. *Chemical Society Reviews* **2013,** *42* (24), 9480-9508.
23. Cram, D. J.; Cram, J. M., Host-guest chemistry. *Science* **1974,** *183* (4127), 803-809.
24. Freeman, W. A.; Mock, W. L.; Shih, N. Y., Cucurbituril. *Journal of the American Chemical Society* **1981,** *103* (24), 7367-7368.
25. Zia, V.; Rajewski, R. A.; Stella, V. J., Effect of cyclodextrin charge on complexation of neutral and charged substrates: comparison of (SBE)7M-β-CD to HP-β-CD. *Pharmaceutical Research* **2001,** *18* (5), 667-673.
26. Appel, E. A.; Loh, X. J.; Jones, S. T.; Biedermann, F.; Dreiss, C. A.; Scherman, O. A., Ultrahigh-water-content supramolecular hydrogels exhibiting multistimuli responsiveness. *Journal of the American Chemical Society* **2012,** *134* (28), 11767-11773.
27. Assaf, K. I.; Nau, W. M., Cucurbiturils: from synthesis to high-affinity binding and catalysis. *Chemical Society Reviews* **2015,** *44* (2), 394-418.
28. Neirynck, P.; Brinkmann, J.; An, Q.; van der Schaft, D. W.; Milroy, L.-G.; Jonkheijm, P.; Brunsveld, L., Supramolecular control of cell adhesion via ferrocene–cucurbit[7]uril host–guest binding on gold surfaces. *Chemical communications* **2013,** *49* (35), 3679-3681.
29. Nguyen, H. D.; Dang, D. T.; Van Dongen, J. L.; Brunsveld, L., Protein dimerization induced by supramolecular interactions with cucurbit[8]uril. *Angewandte Chemie International Edition* **2010,** *49* (5), 895-898.
30. Chen, G.; Jiang, M., Cyclodextrin-based inclusion complexation bridging supramolecular chemistry and macromolecular self-assembly. *Chemical Society Reviews* **2011,** *40* (5), 2254-2266.
31. Holloway, L. R.; Bogie, P. M.; Hooley, R. J., Controlled self-sorting in self-assembled cage complexes. *Dalton Transactions* **2017,** *46* (43), 14719-14723.
32. Yan, L.-L.; Tan, C.-H.; Zhang, G.-L.; Zhou, L.-P.; Bünzli, J.-C.; Sun, Q.-F., Stereocontrolled self-assembly and self-sorting of luminescent europium tetrahedral cages. *Journal of the American Chemical Society* **2015,** *137* (26), 8550-8555.
33. Zheng, Y.-R.; Yang, H.-B.; Northrop, B. H.; Ghosh, K.; Stang, P. J., Size selective self-Sorting in coordination-driven self-assembly of finite ensembles. *Inorganic Chemistry* **2008,** *47* (11), 4706-4711.
34. He, Z.; Jiang, W.; Schalley, C. A., Integrative self-sorting: a versatile strategy for the construction of complex supramolecular architecture. *Chemical Society Reviews* **2015,** *44* (3), 779-789.
35. Jiang, W.; Schalley, C. A., Integrative self-sorting is a programming language for high level self-assembly. *Proceedings of the National Academy of Sciences* **2009,** *106* (26), 10425.
36. Lal Saha, M.; Schmittel, M., Degree of molecular self-sorting in multicomponent systems. *Organic & Biomolecular Chemistry* **2012,** *10* (24), 4651-4684.
37. Masson, E.; Lu, X.; Ling, X.; Patchell, D. L., Kinetic vs thermodynamic self-Sorting of cucurbit[6]uril, cucurbit[7]uril, and a spermine derivative. *Organic Letters* **2009,** *11* (17), 3798-3801.

38. Mukhopadhyay, P.; Zavalij, P. Y.; Isaacs, L., High fidelity kinetic self-sorting in multi-component systems based on guests with multiple binding epitopes. *Journal of the American Chemical Society* **2006,** *128* (43), 14093-14102.
39. Wu, A.; Isaacs, L., Self-sorting: the exception or the rule? *Journal of the American Chemical Society* **2003,** *125* (16), 4831-4835.
40. Sindelar, V.; Cejas, M. A.; Raymo, F. M.; Chen, W.; Parker, S. E.; Kaifer, A. E., Supramolecular assembly of 2,7-dimethyldiazapyrenium and cucurbit[8]uril: a new fluorescent host for detection of catechol and dopamine. *Chemistry – A European Journal* **2005,** *11* (23), 7054-7059.
41. Bernasconi, C., *Relaxation kinetics*. Elsevier: **2012**.
42. Bohne, C., Supramolecular dynamics. *Chemical Society Reviews* **2014,** *43* (12), 4037-4050.
43. Bohne, C., Supramolecular dynamics studied using photophysics. *Langmuir* **2006,** *22* (22), 9100-9111.
44. Thomas, S. S.; Bohne, C., Determination of the kinetics underlying the pK_a shift for the 2-aminoanthracenium cation binding with cucurbit[7]uril. *Faraday Discussions* **2015,** *185* (0), 381-398.
45. Dash, S.; Murthy, P. N.; Nath, L.; Chowdhury, P., Kinetic modeling on drug release from controlled drug delivery systems. *Acta Poloniae Pharmaceutica* **2010,** *67* (3), 217-23.
46. Rosenbaum, S. E., *Basic pharmacokinetics and pharmacodynamics : an integrated textbook and computer simulations*. John Wiley & Sons, Incorporated: Somerset, United States, **2016**.
47. Thomas, S. S. Mechanistic diversity in the guest binding with cucurbit[7]uril or octa acid complexes. *Dissertation*, *University of Victoria*, **2016**.
48. Márquez, C.; Hudgins, R. R.; Nau, W. M., Mechanism of host−guest complexation by cucurbituril. *Journal of the American Chemical Society* **2004,** *126* (18), 5806-5816.
49. Tang, H.; Fuentealba, D.; Ko, Y. H.; Selvapalam, N.; Kim, K.; Bohne, C., Guest binding dynamics with cucurbit[7]uril in the presence of cations. *Journal of the American Chemical Society* **2011,** *133* (50), 20623-20633.
50. Tarmyshov, K. B.; Müller-Plathe, F., Ion binding to cucurbit[6]uril: structure and dynamics. *The Journal of Physical Chemistry B* **2006,** *110* (29), 14463-14468.
51. Thomas, S. S.; Tang, H.; Bohne, C., Noninnocent role of Na^+ ions in the Binding of the N-phenyl-2-naphthylammonium cation as a ditopic guest with cucurbit[7]uril. *Journal of the American Chemical Society* **2019,** *141* (24), 9645-9654.
52. Grote, R. F.; Hynes, J. T., Energy diffusion-controlled reactions in solution. *The Journal of Chemical Physics* **1982,** *77* (7), 3736-3743.
53. Shoup, D.; Lipari, G.; SzABO, A., Diffusion-controlled bimolecular reaction rates. The effect of rotational diffusion and orientation constraints. *Biophysical Journal* **1981,** *36* (3), 697-714.
54. Swinehart, J. A., Relaxation kinetics: An experiment for physical chemistry. *Journal of Chemical Education* **1967,** *44* (9), 524.
55. Ramamurthy, V.; Inoue, Y., *Supramolecular photochemistry : controlling photochemical processes*. John Wiley & Sons, Incorporated: New York, UNITED STATES, 2011.

56. Ludlow, R. F.; Otto, S., Systems chemistry. *Chemical Society Reviews* **2008,** *37* (1), 101-108.
57. Miljanić, O. Š., Small-molecule systems chemistry. *Chem* **2017,** *2* (4), 502-524.
58. Peyralans, J. J. P.; Otto, S., Recent highlights in systems chemistry. *Current Opinion in Chemical Biology* **2009,** *13* (5), 705-713.
59. Strazewski, P., The beginning of systems chemistry. *Life* **2019,** *9* (1), 11.
60. Ruiz-Mirazo, K.; Briones, C.; de la Escosura, A., Prebiotic systems chemistry: new perspectives for the origins of life. *Chemical Reviews* **2014,** *114* (1), 285-366.
61. Brown, J. B.; Okuno, Y., Systems biology and systems chemistry: new directions for drug discovery. *Chemistry & Biology* **2012,** *19* (1), 23-28.
62. Jiang, W.; Schalley, C. A., Integrative self-sorting is a programming language for high level self-assembly. *Proceedings of the National Academy of Sciences* **2009,** *106* (26), 10425-10429.
63. Islam, S.; Powner, M. W., Prebiotic systems chemistry: complexity overcoming clutter. *Chem* **2017,** *2* (4), 470-501.
64. Robertson, C. C.; Mackenzie, H. W.; Kosikova, T.; Philp, D., An environmentally responsive reciprocal replicating network. *Journal of the American Chemical Society* **2018,** *140* (22), 6832-6841.
65. Hunt, R. A. R.; Otto, S., Dynamic combinatorial libraries: new opportunities in systems chemistry. *Chemical Communications* **2011,** *47* (3), 847-858.
66. Li, J.; Nowak, P.; Otto, S., Dynamic combinatorial libraries: from exploring molecular recognition to systems chemistry. *Journal of the American Chemical Society* **2013,** *135* (25), 9222-9239.
67. Corbett, P. T.; Leclaire, J.; Vial, L.; West, K. R.; Wietor, J.-L.; Sanders, J. K. M.; Otto, S., Dynamic combinatorial chemistry. *Chemical Reviews* **2006,** *106* (9), 3652-3711.
68. Thordarson, P., Determining association constants from titration experiments in supramolecular chemistry. *Chemical Society Reviews* **2011,** *40* (3), 1305-1323.
69. Lee, J. W.; Samal, S.; Selvapalam, N.; Kim, H.-J.; Kim, K., Cucurbituril homologues and derivatives: new opportunities in supramolecular chemistry. *Accounts of Chemical Research* **2003,** *36* (8), 621-630.
70. Behrend, R.; Meyer, E.; Rusche, F., I. Ueber Condensationsproducte aus Glycoluril und Formaldehyd. *Justus Liebigs Annalen der Chemie* **1905,** *339* (1), 1-37.
71. Montes-Navajas, P.; Garcia, H., Complexes of basic tricyclic dyes in their acid and basic forms with cucurbit[7]uril: Determination of pKa and association constants in the ground and singlet excited state. *Journal of Photochemistry and Photobiology A: Chemistry* **2009,** *204* (2), 97-101.
72. Saleh, N. i.; Koner, A. L.; Nau, W. M., Activation and stabilization of drugs by supramolecular pK_a shifts: drug-delivery applications tailored for cucurbiturils. *Angewandte Chemie International Edition* **2008,** *47* (29), 5398-5401.
73. Shaikh, M.; Dutta Choudhury, S.; Mohanty, J.; Bhasikuttan, A. C.; Nau, W. M.; Pal, H., Modulation of excited-state proton transfer of 2-(2′-hydroxyphenyl)benzimidazole in a macrocyclic cucurbit[7]uril host cavity: dual emission behavior and pK_a shift. *Chemistry – A European Journal* **2009,** *15* (45), 12362-12370.
74. Kim, J.; Jung, I.-S.; Kim, S.-Y.; Lee, E.; Kang, J.-K.; Sakamoto, S.; Yamaguchi, K.; Kim, K., New cucurbituril homologues: syntheses, isolation, characterization, and x-

ray crystal structures of cucurbit[n]uril (n = 5, 7, and 8). *Journal of the American Chemical Society* **2000,** *122* (3), 540-541.
75. Biedermann, F.; Nau, W. M.; Schneider, H.-J., The hydrophobic effect revisited—studies with supramolecular complexes imply high-energy water as a noncovalent driving force. *Angewandte Chemie International Edition* **2014,** *53* (42), 11158-11171.
76. Jansen, K.; Buschmann, H.-J.; Wego, A.; Döpp, D.; Mayer, C.; Drexler, H.-J.; Holdt, H.-J.; Schollmeyer, E., Cucurbit[5]uril, decamethylcucurbit[5]uril and cucurbit[6]uril. synthesis, solubility and amine complex formation. *Journal of inclusion phenomena and macrocyclic chemistry* **2001,** *39* (3), 357-363.
77. Cao, L.; Šekutor, M.; Zavalij, P. Y.; Mlinarić-Majerski, K.; Glaser, R.; Isaacs, L., Cucurbit[7]uril·guest pair with an attomolar dissociation constant. *Angewandte Chemie International Edition* **2014,** *53* (4), 988-993.
78. Mohanty, J.; Pal, H.; Ray, A. K.; Kumar, S.; Nau, W. M., Supramolecular dye laser with cucurbit[7]uril in water. *A Eruopean Journal of Chemical Physics and Physical Chemistry* **2007,** *8* (1), 54-56.
79. Masson, E.; Ling, X.; Joseph, R.; Kyeremeh-Mensah, L.; Lu, X., Cucurbituril chemistry: a tale of supramolecular success. *RSC Advances* **2012,** *2* (4), 1213-1247.
80. Webber, M. J.; Langer, R., Drug delivery by supramolecular design. *Chemical Society Reviews* **2017,** *46* (21), 6600-6620.
81. Tang, H.; Sutherland, A. S. M.; Osusky, L. M.; Li, Y.; Holzwarth, J. F.; Bohne, C., Chiral recognition for the complexation dynamics of β-cyclodextrin with the enantiomers of 2-naphthyl-1-ethanol. *Photochemical & Photobiological Sciences* **2014,** *13* (2), 358-369.
82. Choudhury, S. D.; Mohanty, J.; Pal, H.; Bhasikuttan, A. C., Cooperative metal ion binding to a cucurbit[7]uril−thioflavin T complex: demonstration of a stimulus-responsive fluorescent supramolecular capsule. *Journal of the American Chemical Society* **2010,** *132* (4), 1395-1401.
83. Cong, H.; Zhu, Q.; Xue, S.; Tao, Z.; Wei, G., Direct coordination of metal ions to cucurbit[n]urils. *Chinese Science Bulletin* **2010,** *55* (32), 3633-3640.
84. Shinde, M. N.; Dutta Choudhury, S.; Barooah, N.; Pal, H.; Bhasikuttan, A. C.; Mohanty, J., Metal-ion-mediated assemblies of thiazole orange with cucurbit[7]uril: a photophysical study. *The Journal of Physical Chemistry B* **2015,** *119* (9), 3815-3823.
85. Whang, D.; Heo, J.; Park, J. H.; Kim, K., A molecular bowl with metal ion as bottom: reversible inclusion of organic molecules in cesium ion complexed cucurbituril. *Angewandte Chemie International Edition* **1998,** *37* (1-2), 78-80.
86. Zhang, S.; Grimm, L.; Miskolczy, Z.; Biczók, L.; Biedermann, F.; Nau, W. M., Binding affinities of cucurbit[n]urils with cations. *Chemical Communications* **2019,** *55* (94), 14131-14134.
87. Barrow, S. J.; Kasera, S.; Rowland, M. J.; del Barrio, J.; Scherman, O. A., Cucurbituril-based molecular recognition. *Chemical Reviews* **2015,** *115* (22), 12320-12406.
88. Pichierri, F., DFT study of caesium ion complexation by cucurbit[n]urils (n = 5–7). *Dalton Transactions* **2013,** *42* (17), 6083-6091.
89. Samsonenko, Denis G.; Lipkowski, J.; Gerasko, Olga A.; Virovets, Alexander V.; Sokolov, Maxim N.; Fedin, Vladimir P.; Platas, Javier G.; Hernandez-Molina, R.;

Mederos, A., Cucurbituril as a new macrocyclic ligand for complexation of lanthanide cations in aqueous solutions. *European Journal of Inorganic Chemistry* **2002,** *2002* (9), 2380-2388.
90. Teyssandier, J.; De Feyter, S.; Mali, K. S., Host–guest chemistry in two-dimensional supramolecular networks. *Chemical Communications* **2016,** *52* (77), 11465-11487.
91. Connors, K. A., *Binding constants: the measurement of molecular complex stability*. Wiley-Interscience: **1987**.
92. Ong, W.; Kaifer, A. E., Salt effects on the apparent stability of the cucurbit[7]uril−methyl viologen inclusion complex. *The Journal of Organic Chemistry* **2004,** *69* (4), 1383-1385.
93. Shaikh, M.; Mohanty, J.; Bhasikuttan, A. C.; Uzunova, V. D.; Nau, W. M.; Pal, H., Salt-induced guest relocation from a macrocyclic cavity into a biomolecular pocket: interplay between cucurbit[7]uril and albumin. *Chemical Communications* **2008,** (31), 3681-3683.
94. Wyman, I. W.; Macartney, D. H., Cucurbit[7]uril host–guest complexes with small polar organic guests in aqueous solution. *Organic & Biomolecular Chemistry* **2008,** *6* (10), 1796-1801.
95. Yi, S.; Kaifer, A. E., Determination of the purity of cucurbit[n]uril (n = 7, 8) host samples. *The Journal of Organic Chemistry* **2011,** *76* (24), 10275-10278.
96. Mattia, E.; Otto, S., Supramolecular systems chemistry. *Nature Nanotechnology* **2015,** *10*, 111.
97. Palma, A.; Artelsmair, M.; Wu, G.; Lu, X.; Barrow, S. J.; Uddin, N.; Rosta, E.; Masson, E.; Scherman, O. A., Cucurbit[7]uril as a Supramolecular Artificial Enzyme for Diels–Alder Reactions. *Angewandte Chemie International Edition* **2017,** *56* (49), 15688-15692.
98. Wang, R.; Yuan, L.; Macartney, D. H., Cucurbit[7]uril Mediates the Stereoselective [4+4] Photodimerization of 2-Aminopyridine Hydrochloride in Aqueous Solution. *The Journal of Organic Chemistry* **2006,** *71* (3), 1237-1239.
99. Zhao, G.; Wang, Z.; Wang, R.; Li, J.; Zou, D.; Wu, Y., Cucurbit[7]uril promoting $PdCl_2$-catalyzed cross-coupling reaction of benzyl halides and arylboronic acids in aqueous media. *Tetrahedron Letters* **2014,** *55* (38), 5319-5322.
100. Dsouza, R. N.; Hennig, A.; Nau, W. M., Supramolecular Tandem Enzyme Assays. *Chemistry – A European Journal* **2012,** *18* (12), 3444-3459.
101. Wang, B.; Han, J.; Bender, M.; Hahn, S.; Seehafer, K.; Bunz, U. H. F., Poly(para-phenyleneethynylene)-Sensor Arrays Discriminate 22 Different Teas. *ACS Sensors* **2018,** *3* (2), 504-511.
102. Rekharsky, M. V.; Yamamura, H.; Ko, Y. H.; Selvapalam, N.; Kim, K.; Inoue, Y., Sequence recognition and self-sorting of a dipeptide by cucurbit[6]uril and cucurbit[7]uril. *Chemical Communications* **2008,** (19), 2236-2238.
103. Yang, F.; Dearden, D. V., Guanidinium-capped cucurbit[7]uril molecular cages in the gas phase. *Supramolecular Chemistry* **2011,** *23* (1-2), 53-58.
104. Sindelar, V.; Cejas, M. A.; Raymo, F. M.; Kaifer, A. E., Tight inclusion complexation of 2,7-dimethyldiazapyrenium in cucurbit[7]uril. *New Journal of Chemistry* **2005,** *29* (2), 280-282.

105. Zhang, S.; Grimm, L.; Miskolczy, Z.; Biczók, L.; Biedermann, F.; Nau, W. M., Binding affinities of cucurbit[n]urils with cations. *Chemical Communications* **2019,** *55*, 14131-14134.
106. Kim, H.-J.; Jeon, W. S.; Ko, Y. H.; Kim, K., Inclusion of methylviologen in cucurbit[7]uril. *Proceedings of the National Academy of Sciences* **2002,** *99* (8), 5007-5011.
107. Moon, K.; Kaifer, A. E., Modes of binding interaction between viologen guests and the cucurbit[7]uril host. *Organic Letters* **2004,** *6* (2), 185-188.
108. Striepe, L.; Baumgartner, T., Viologens and their application as functional materials. *Chemistry – A European Journal* **2017,** *23* (67), 16924-16940.
109. Day, A.; Arnold, A. P.; Blanch, R. J.; Snushall, B., Controlling factors in the synthesis of cucurbituril and Its homologues. *The Journal of Organic Chemistry* **2001,** *66* (24), 8094-8100.
110. Jiang, G.; Li, G., Preparation and biological activity of novel cucurbit[8]uril–fullerene complex. *Journal of Photochemistry and Photobiology B: Biology* **2006,** *85* (3), 223-227.
111. Sueldo Occello, V. N.; de Rossi, R. H.; Veglia, A. V., Complexation (cucurbit[6]uril-pyrene): thermodynamic and spectroscopic properties. *Journal of Luminescence* **2015,** *158*, 435-440.
112. Yan, Y.; Xue, S.-F.; Cong, H.; Zhang, J.-X.; Zhang, Y.-Q.; Zhu, Q.-J.; Tao, Z., Exclusion complexes of the HCl salts of benzidine and bis(4-aminophenyl) methane with two methyl-substituted cucurbiturils. *New Journal of Chemistry* **2009,** *33* (10), 2136-2143.
113. Marquez, C.; Nau, W. M., Two mechanisms of slow host–guest complexation between cucurbit[6]uril and cyclohexylmethylamine: pH-responsive supramolecular kinetics. *Angewandte Chemie International Edition* **2001,** *40* (17), 3155-3160.
114. Jeon, Y.-M.; Kim, J.; Whang, D.; Kim, K., Molecular container assembly capable of controlling binding and release of its guest molecules: reversible encapsulation of organic molecules in sodium ion complexed cucurbituril. *Journal of the American Chemical Society* **1996,** *118* (40), 9790-9791.
115. Marcus, Y., Ionic radii in aqueous solutions. *Chemical Reviews* **1988,** *88* (8), 1475-1498.
116. Qi, Z.; Schalley, C. A., Exploring macrocycles in functional supramolecular gels: from stimuli responsiveness to systems chemistry. *Accounts of Chemical Research* **2014,** *47* (7), 2222-2233.
117. Zhang, W.; Gan, S.; Vezzoli, A.; Davidson, R. J.; Milan, D. C.; Luzyanin, K. V.; Higgins, S. J.; Nichols, R. J.; Beeby, A.; Low, P. J.; Li, B.; Niu, L., Single-molecule conductance of viologen–cucurbit[8]uril host–guest complexes. *ACS Nano* **2016,** *10* (5), 5212-5220.
118. Appel, E. A.; Forster, R. A.; Rowland, M. J.; Scherman, O. A., The control of cargo release from physically crosslinked hydrogels by crosslink dynamics. *Biomaterials* **2014,** *35* (37), 9897-9903.
119. Conlisk, A. T., *Essentials of micro- and nanofluidics: with applications to the biological and chemical sciences*. Cambridge University Press: 2013.
120. Giuseppone, N., Toward self-constructing materials: a systems chemistry approach. *Accounts of Chemical Research* **2012,** *45* (12), 2178-2188.

121. Lee, J. S.; Feijen, J., Polymersomes for drug delivery: design, formation and characterization. *Journal of Controlled Release* **2012,** *161* (2), 473-483.
122. Bajpai, A. K.; Shukla, S. K.; Bhanu, S.; Kankane, S., Responsive polymers in controlled drug delivery. *Progress in Polymer Science* **2008,** *33* (11), 1088-1118.
123. Goole, J.; Amighi, K., 3D printing in pharmaceutics: a new tool for designing customized drug delivery systems. *International Journal of Pharmaceutics* **2016,** *499* (1), 376-394.
124. Gupta, P.; Vermani, K.; Garg, S., Hydrogels: from controlled release to pH-responsive drug delivery. *Drug Discovery Today* **2002,** *7* (10), 569-579.
125. Hoffman, A. S., The origins and evolution of "controlled" drug delivery systems. *Journal of Controlled Release* **2008,** *132* (3), 153-163.
126. Langer, R., Drug delivery and targeting. *Nature London* **1998**, 5-10.
127. Langer, R.; Tirrell, D. A., Designing materials for biology and medicine. *Nature* **2004,** *428* (6982), 487-492.
128. Li, J.; Mooney, D. J., Designing hydrogels for controlled drug delivery. *Nature Reviews Materials* **2016,** *1* (12), 16071.
129. Peppas, N. A.; Narasimhan, B., Mathematical models in drug delivery: how modeling has shaped the way we design new drug delivery systems. *Journal of Controlled Release* **2014,** *190*, 75-81.
130. Mukhopadhyay, P.; Wu, A.; Isaacs, L., Social self-sorting in aqueous solution. *The Journal of Organic Chemistry* **2004,** *69* (19), 6157-6164.
131. Kim, H.-J.; Heo, J.; Jeon, W. S.; Lee, E.; Kim, J.; Sakamoto, S.; Yamaguchi, K.; Kim, K., Selective inclusion of a hetero-guest pair in a molecular host: formation of stable charge-transfer complexes in cucurbit[8]uril. *Angewandte Chemie International Edition* **2001,** *40* (8), 1526-1529.
132. Andersson, S.; Zou, D.; Zhang, R.; Sun, S.; Åkermark, B.; Sun, L., Selective positioning of CB[8] on two linked viologens and electrochemically driven movement of the host molecule. *European Journal of Organic Chemistry* **2009,** *8*, 1163-1172.
133. Peerannawar, S. R.; Gobre, V. V.; Gejji, S. P., Binding of viologen derivatives to cucurbit[8]uril. *Computational and Theoretical Chemistry* **2012,** *983*, 16-24.
134. Moon, K.; Grindstaff, J.; Sobransingh, D.; Kaifer, A. E., Cucurbit[8]uril-mediated redox-controlled self-assembly of viologen-containing dendrimers. *Angewandte Chemie International Edition* **2004,** *43* (41), 5496-5499.
135. Biedermann, F.; Scherman, O. A., Cucurbit[8]uril mediated donor–acceptor ternary complexes: a model system for studying charge-transfer interactions. *The Journal of Physical Chemistry B* **2012,** *116* (9), 2842-2849.
136. Rauwald, U.; Scherman, O. A., Supramolecular block copolymers with cucurbit[8]uril in water. *Angewandte Chemie International Edition* **2008,** *47* (21), 3950-3953.
137. Kalmár, J.; Ellis, S. B.; Ashby, M. T.; Halterman, R. L., Kinetics of Formation of the host–guest complex of a viologen with cucurbit[7]uril. *Organic Letters* **2012,** *14* (13), 3248-3251.
138. Wei, F.; Liu, S.-M.; Xu, L.; Cheng, G.-Z.; Wu, C.-T.; Feng, Y.-Q., The formation of cucurbit[n]uril (n = 6, 7) complexes with amino compounds in aqueous formic acid studied by capillary electrophoresis. *Electrophoresis* **2005,** *26* (11), 2214-2224.

139. Biczók, L.; Miskolczy, Z.; Megyesi, M.; Prabodh, A.; Biedermann, F., Kinetics and mechanism of cation-induced guest release from cucurbit[7]uril. *Chemistry – A European Journal* **2020**, (in press), doi:10.1002/chem.2019050633.
140. R. Ashton, P.; E. Boyd, S.; Brindle, A.; J. Langford, S.; Menzer, S.; Pe′rez-García, L.; A. Preece, J.; M. Raymo, i.; Spencer, N.; Fraser Stoddart, J.; J. P. White, A.; J. Williams, D., Diazapyrenium-containing catenanes and rotaxanes. *New Journal of Chemistry* **1999,** *23* (6), 587-602.
141. Hünig, S.; Groβ, J.; Lier, E. F.; Quast, H., Über zweistufige redoxsysteme, XII1) synthese und polarographie von quartärsalzen der phenanthroline, des 2,7-diazapyrens sowie der diazoniapentaphene. *Justus Liebigs Annalen der Chemie* **1973,** *1973* (2), 339-358.
142. Balzani, V.; Credi, A.; Langford, S. J.; Prodi, A.; Stoddart, J. F.; Venturi, M., Spectroscopic and electrochemical properties of catenanes containing the 2,7-diazapyrenium unit. *Supramolecular Chemistry* **2001,** *13* (2), 303-311.
143. Taniguchi, M.; Lindsey, J. S., Database of absorption and fluorescence spectra of >300 common compounds for use in photochemCAD. *Photochemistry and Photobiology* **2018,** *94* (2), 290-327.
144. Jeon, W. S.; Kim, H.-J.; Lee, C.; Kim, K., Control of the stoichiometry in host–guest complexation by redox chemistry of guests: Inclusion of methylviologen in cucurbit[8]uril. *Chemical Communications* **2002,** (17), 1828-1829.
145. Khan, M. S. A.; Heger, D.; Necas, M.; Sindelar, V., Remarkable salt effect on stability of supramolecular complex between modified cucurbit[6]uril and methylviologen in aqueous media. *The Journal of Physical Chemistry B* **2009,** *113* (32), 11054-11057.
146. Behar, D.; Neta, P.; Schultheisz, C., Reaction kinetics in ionic liquids as studied by pulse radiolysis: redox reactions in the solvents methyltributylammonium bis(trifluoromethylsulfonyl)imide and N-butylpyridinium tetrafluoroborate. *The Journal of Physical Chemistry A* **2002,** *106* (13), 3139-3147.
147. Latimer, P., Light scattering and absorption as methods of studying cell population parameters. *Annual review of biophysics and bioengineering* **1982,** *11* (1), 129-150.
148. Beaujuge, P. M.; Fréchet, J. M. J., Molecular design and ordering effects in π-functional materials for transistor and solar cell applications. *Journal of the American Chemical Society* **2011,** *133* (50), 20009-20029.
149. Green, O.; Grubjesic, S.; Lee, S.; Firestone, M. A., The design of polymeric ionic iquids for the preparation of functional materials. *Polymer Reviews* **2009,** *49* (4), 339-360.
150. Uhlenheuer, D. A.; Young, J. F.; Nguyen, H. D.; Scheepstra, M.; Brunsveld, L., Cucurbit[8]uril induced heterodimerization of methylviologen and naphthalene functionalized proteins. *Chemical Communications* **2011,** *47* (24), 6798-6800.
151. Nishiyama, N.; Kataoka, K., Nanostructured devices based on block copolymer assemblies for drug delivery: designing structures for enhanced drug function. In *Polymer Therapeutics II*, Satchi-Fainaro, R.; Duncan, R., Eds. Springer Berlin Heidelberg: Berlin, Heidelberg, 2006; pp 67-101.

152. Jiang, W.; Wang, Q.; Linder, I.; Klautzsch, F.; Schalley, C. A., Self-sorting of water-soluble cucurbituril pseudorotaxanes. *Chemistry – A European Journal* **2011,** *17* (8), 2344-2348.
153. Biedermann, F.; Vendruscolo, M.; Scherman, O. A.; De Simone, A.; Nau, W. M., Cucurbit[8]uril and blue-box: high-energy water release overwhelms electrostatic interactions. *Journal of the American Chemical Society* **2013,** *135* (39), 14879-14888.
154. Senler, S.; Li, W.; Tootoonchi, M. H.; Yi, S.; Kaifer, A. E., The cucurbituril 'portal' effect. *Supramolecular Chemistry* **2014,** *26* (9), 677-683.
155. Ko, Y. H.; Kim, E.; Hwang, I.; Kim, K., Supramolecular assemblies built with host-stabilized charge-transfer interactions. *Chemical Communications* **2007,** (13), 1305-1315.
156. Aronsson, C.; Dånmark, S.; Zhou, F.; Öberg, P.; Enander, K.; Su, H.; Aili, D., Self-sorting heterodimeric coiled coil peptides with defined and tuneable self-assembly properties. *Scientific Reports* **2015,** *5* (1), 14063.
157. Burd, C.; Weck, M., Self-sorting in polymers. *Macromolecules* **2005,** *38* (17), 7225-7230.
158. Celtek, G.; Artar, M.; Scherman, O. A.; Tuncel, D., Sequence-specific self-sorting of the binding sites of a ditopic guest by cucurbituril homologues and subsequent formation of a hetero[4]pseudorotaxane. *Chemistry – A European Journal* **2009,** *15* (40), 10360-10363.
159. Mayoral, M. J.; Rest, C.; Schellheimer, J.; Stepanenko, V.; Fernández, G., Narcissistic versus social self-sorting of oligophenyleneethynylene derivatives: from isodesmic self-assembly to cooperative co-assembly. *Chemistry – A European Journal* **2012,** *18* (49), 15607-15611.
160. Schaufelberger, F.; Ramström, O., Kinetic self-sorting of dynamic covalent catalysts with systemic feedback regulation. *Journal of the American Chemical Society* **2016,** *138* (25), 7836-7839.
161. Tomimasu, N.; Kanaya, A.; Takashima, Y.; Yamaguchi, H.; Harada, A., Social self-sorting: alternating supramolecular oligomer consisting of isomers. *Journal of the American Chemical Society* **2009,** *131* (34), 12339-12343.
162. Wang, F.; Han, C.; He, C.; Zhou, Q.; Zhang, J.; Wang, C.; Li, N.; Huang, F., Self-sorting organization of two heteroditopic monomers to supramolecular alternating copolymers. *Journal of the American Chemical Society* **2008,** *130* (34), 11254-11255.
163. Hori, A.; Yamashita, K.-i.; Fujita, M., Kinetic self-assembly: selective cross-catenation of two sterically differentiated PdII-coordination rings. *Angewandte Chemie International Edition* **2004,** *43* (38), 5016-5019.
164. Wang, Y.-S.; Feng, T.; Wang, Y.-Y.; Hahn, F. E.; Han, Y.-F., Homo- and heteroligand poly-NHC metal assemblies: synthesis by narcissistic and social self-sorting. *Angewandte Chemie* **2018,** *130* (48), 15993-15997.
165. Osowska, K.; Miljanić, O. Š., Kinetic and thermodynamic self-sorting in synthetic systems. *Synlett* **2011,** *2011* (12), 1643-1648.
166. Shetty, D.; Khedkar, J. K.; Park, K. M.; Kim, K., Can we beat the biotin–avidin pair?: cucurbit[7]uril-based ultrahigh affinity host–guest complexes and their applications. *Chemical Society Reviews* **2015,** *44* (23), 8747-8761.

167. Liu, S.; Ruspic, C.; Mukhopadhyay, P.; Chakrabarti, S.; Zavalij, P. Y.; Isaacs, L., The cucurbit[n]uril family: prime components for self-sorting systems. *Journal of the American Chemical Society* **2005,** *127* (45), 15959-15967.
168. Mock, W. L.; Shih, N. Y., Dynamics of molecular recognition involving cucurbituril. *Journal of the American Chemical Society* **1989,** *111* (7), 2697-2699.
169. Barooah, N.; Mohanty, J.; Pal, H.; Bhasikuttan, A. C., Cucurbituril-induced supramolecular pK_a shift in fluorescent dyes and its prospective applications. *Proceedings of the National Academy of Sciences, India Section A: Physical Sciences* **2014,** *84* (1), 1-17.
170. Mock, W. L.; Pierpont, J., A cucurbituril-based molecular switch. *Journal of the Chemical Society, Chemical Communications* **1990,** (21), 1509-1511.
171. Neal, E. A.; Goldup, S. M., A kinetic self-sorting approach to heterocircuit [3]rotaxanes. *Angewandte Chemie International Edition* **2016,** *55* (40), 12488-12493.
172. Safont-Sempere, M. M.; Fernández, G.; Würthner, F., Self-sorting phenomena in complex supramolecular systems. *Chemical Reviews* **2011,** *111* (9), 5784-5814.

Appendix

Chapter 2:

B-1: To confirm the previously published mechanism experimental data used in the inset of figure 2.3 was fit to a single exponential function to within the concentration parameters of previously published between NpH^+ and CB[7] in the presence of Na^+ cations ([Na^+] = 100 mM, [NpH^+] = 0.5 µM, [CB[7]] = 6-27 µM).[49]

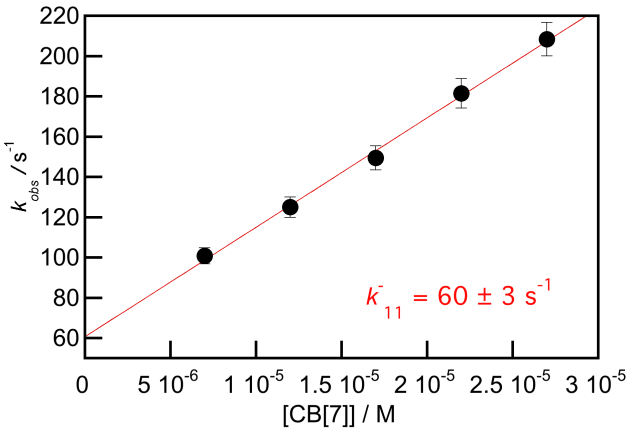

Figure B1. Dependence of the observed rate constant with the concentration of CB[7] for the formation of the NpH^+@CB[7] complex ([NpH^+] = 0.5 µM; [Na^+] = 100 mM). The observed rate constants were determined by fitting the kinetic traces of the inset in figure 2.3 to a single exponential function.

B-2: Kinetic traces at different concentrations of Na^+ cations (**A:** 10 mM, **B:** 50 mM and **C:** 100 mM) at 1.0 µM NpH^+ and 15.0 µM CB[7] fit to the sum of two exponentials function to confirm whether or not the offset in the kinetic trace was a real offset or not. If the fit of the kinetic trace extrapolates to the baseline, then the offset is not a true offset instead there is a kinetic process with an observed rate constant is close to the dead time of the stopped-flow instrument.

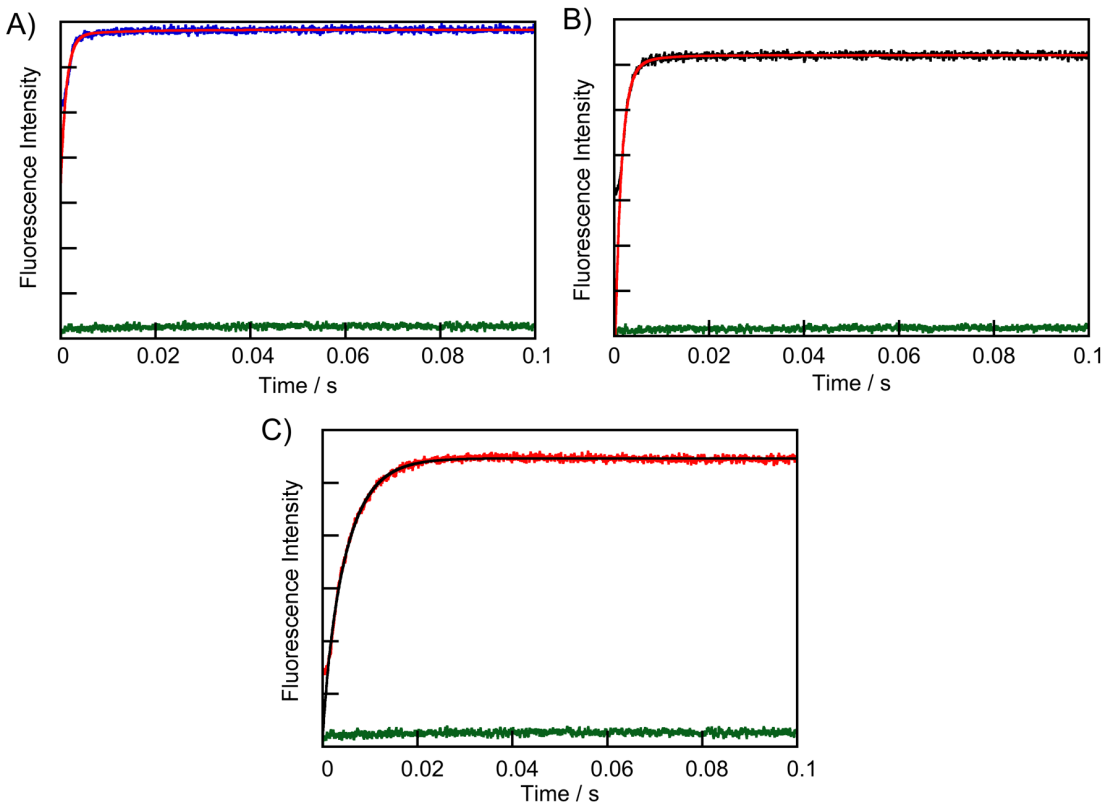

Figure B2. Fits of the kinetic traces for the mixing of 1.0 μM NpH^+ with 15 μM CB[7] (figure 2.4) to a sum of two exponentials function at different Na^+ cation concentrations (**A:** 10 mM, **B:** 50 mM and **C:** 100 mM).

B-3: The fits and residuals to a 1:1 CB[7]:methyl viologen binding model in the presence of different Ca^{2+} cation concentrations (**A:** 2 mM, **B:** 5 mM and **C:** 10 mM) using the model shown in section 2.2.5.

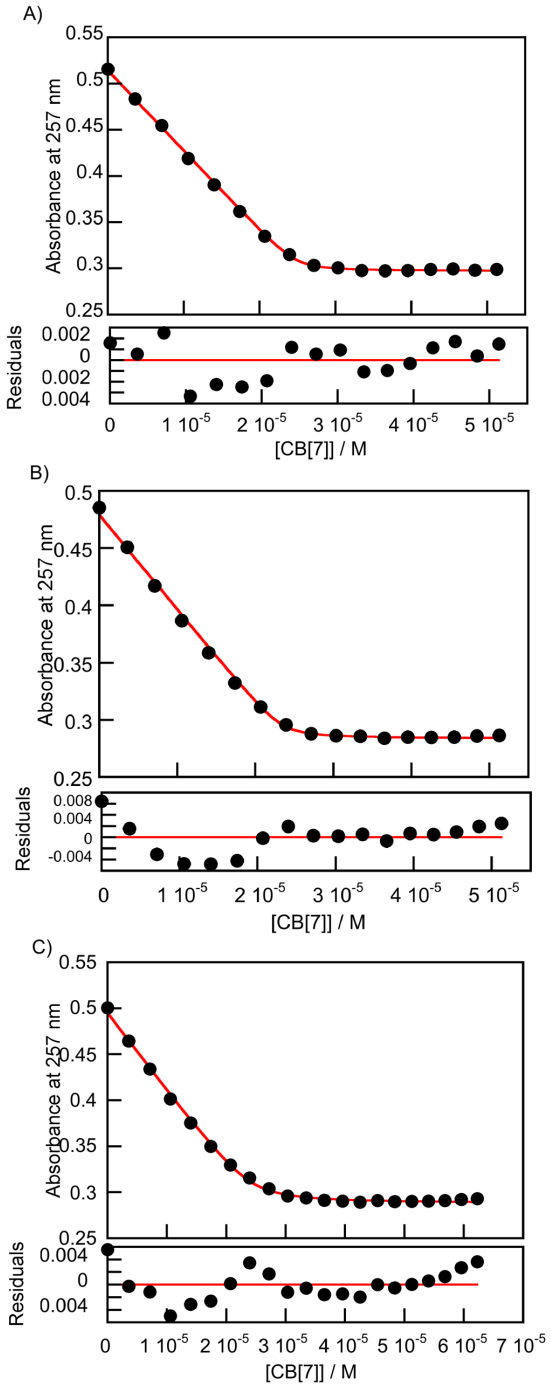

Figure B3. Fits of the binding isotherms for the formation of the complex between methyl viologen (20 µM) and CB[7] at various Ca^{2+} concentrations: **A**: 2 mM, **B**: 5 mM and **C**:10 mM.

B-4: Fit of a kinetic trace between NpH^{+} (1.0 µM) and CB[7] (15 µM) to the sum of three exponentials function to confirm the offset was not a true offset.

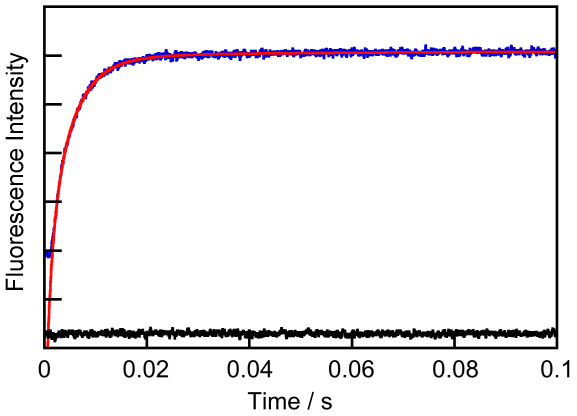

Figure B4. Fit of the kinetic trace for the mixing between 1.0 μM NpH^+ and 15 μM CB[7] in 10 mM Ca^{2+} cations fit to a sum of three exponentials function.

B-5-7: The fits and residuals of kinetic traces to a single exponential function at 1.0 μM NpH^+ and the CB[7] concentrations of the lowest and highest concentrations of the k_{obs} plot. These are the kinetic traces from the observed rate constants reported in table 2.1.

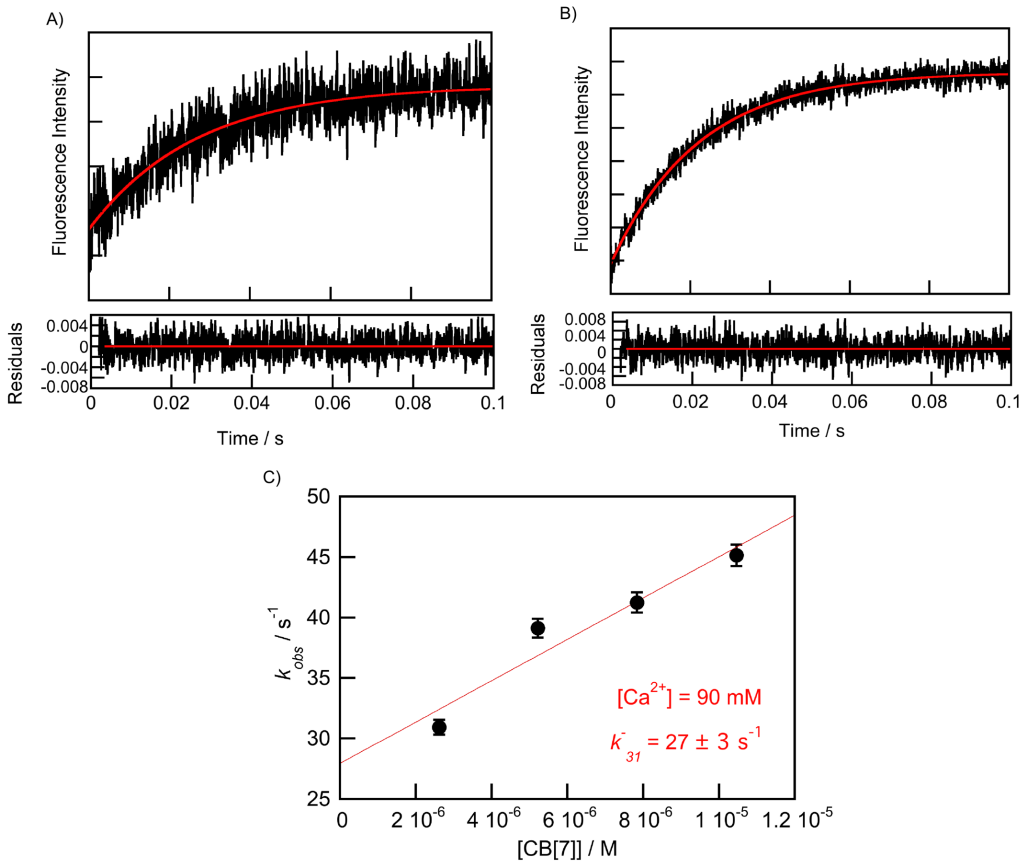

Figure B5. Top: Kinetic traces for the mixing of CB[7] (**A:** 2.62 µM CB[7], **B:** 10.6 µM CB[7]) with 1.0 µM NpH^+ where both solutions contain 90 mM Ca^{2+} (black trace) and the fit to a single exponential function (red). **Bottom:** Residuals between the data and the fit are shown in the lower panel (black) concentrations in the presence of 90 mM Ca^{2+} cations (CB[7] = 2.62 µM (A), 10.36 µM (B). **C:** Dependence of the observed rate constant with the concentration of CB[7] for the formation of the NpH^+@CB[7] complex (NpH^+ = 1.0 µM; [Ca^{2+}] = 90 mM).

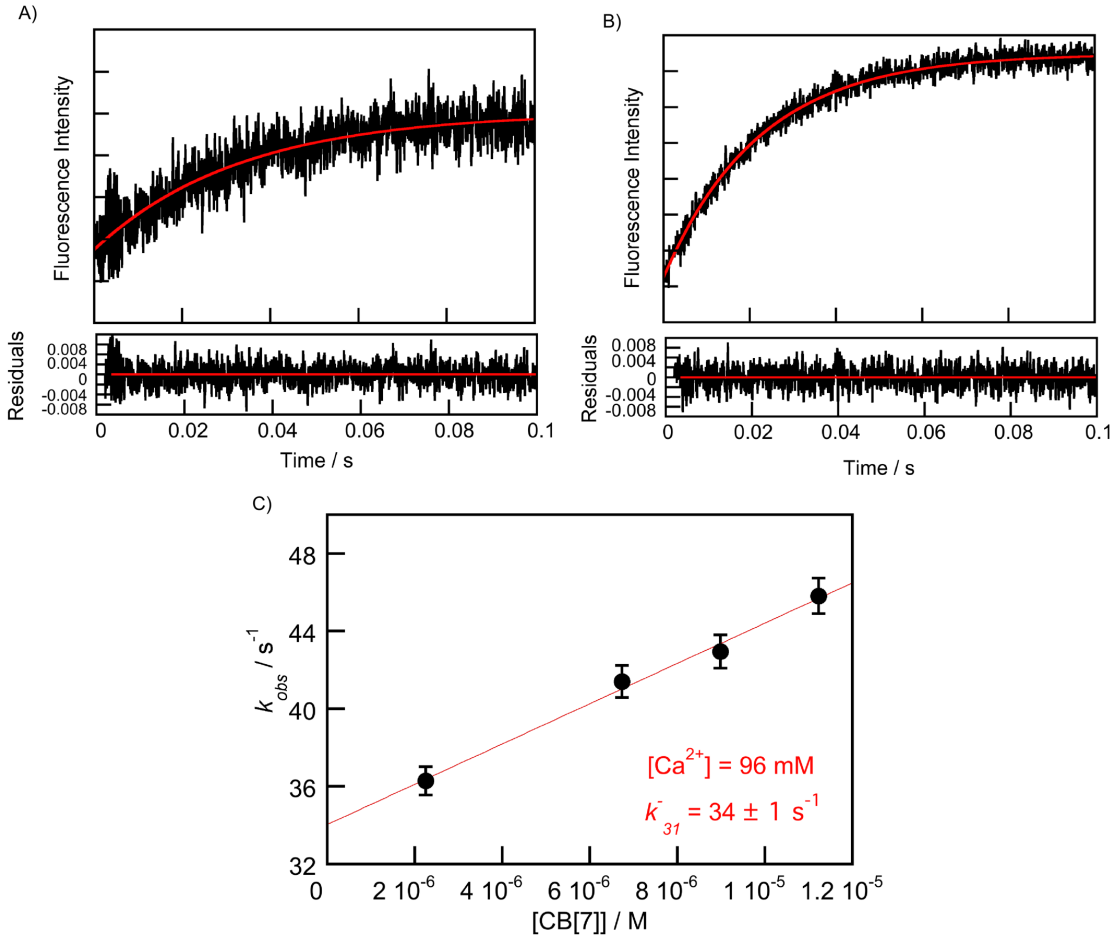

Figure B6. Top: Kinetic traces for the mixing of CB[7] (**A:** 2.62 μM CB[7], **B:** 10.6 μM CB[7]) with 1.0 μM NpH^+ where both solutions contain 96 mM Ca^{2+} (black trace) and the fit to a single exponential function (red). **Bottom:** Residuals between the data and the fit are shown in the lower panel (black) concentrations in the presence of 96 mM Ca^{2+} cations (CB[7] = 2.55 μM (A), 10.52 μM (B). **C:** Dependence of the observed rate constant with the concentration of CB[7] for the formation of the NpH^+@CB[7] complex (NpH^+ = 1.0 μM; [Ca^{2+}] = 96 mM).

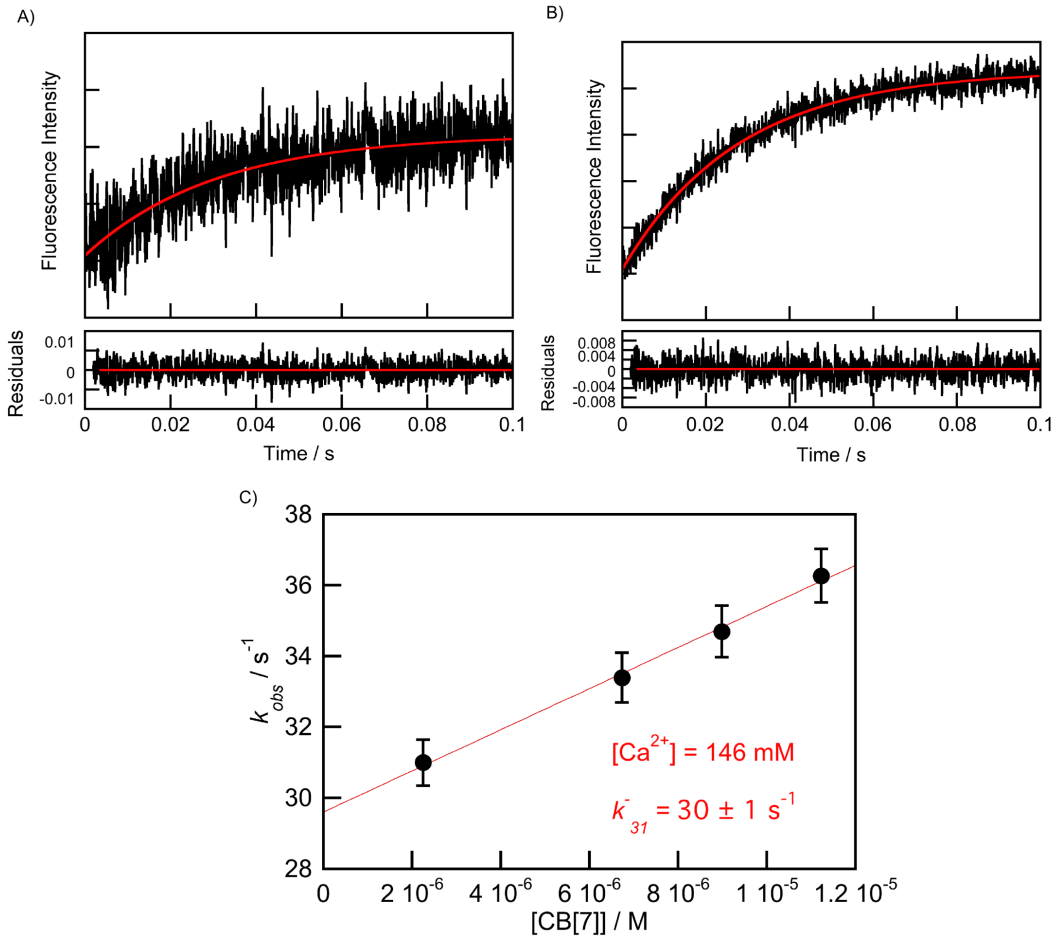

Figure B7. Top: Kinetic traces for the mixing of CB[7] (**A:** 2.25 µM CB[7], **B:** 11.23 µM CB[7]) with 1.0 µM NpH^+ where both solutions contain 146 mM Ca^{2+} (black trace) and the fit to a single exponential function (red). **Bottom:** Residuals between the data and the fit are shown in the lower panel (black) concentrations in the presence of 146 mM Ca^{2+} cations (CB[7] = 2.25 µM (A), 11.23 µM (B). **C:** Dependence of the observed rate constant with the concentration of CB[7] for the formation of the NpH^+@CB[7] complex (NpH^+ = 1.0 µM; [Ca^{2+}] = 146 mM).

Table B-1 The distribution of CB[7] and Na^+ was calculated using previously reported equilibrium constants between CB[7] and Na^+ to understand why the exclusion complex is outcompeted in the system and no longer contributes to the overall kinetics on the ms time scale.

Table B1. Distribution of CB[7] species at different concentrations of Na^+ cations.[b]

$[Na^+]$ / mM	Fraction of $[CB[7]]_{eq}$	Fraction of $[Na^+•CB[7]]_{eq}$	Fraction of $[Na^+•CB[7]•Na^+]_{eq}$
0	1.00	0	0
10	0.389	0.505	0.106
20	0.213	0.554	0.233
30	0.136	0.530	0.334
40	0.095	0.492	0.413
50	0.070	0.454	0.476
60	0.054	0.419	0.528
70	0.043	0.388	0.570
80	0.035	0.360	0.605
90	0.029	0.336	0.635
100	0.024	0.315	0.661

[b] The distribution of products was simulated using previously reported equilibrium constants between CB[7] and Na^+ cations (K_1 = 130 M^{-1} and K_2 = 21 M^{-1}).[49]

Derivation of Eq. 2.21:

The derivation of eq. 2.21 results from the rate law of a triangular binding mechanism (scheme B1).[41] The equations for the 2 relaxation processes are given by equations B1 and B2 in the presence of Na^+ cations.

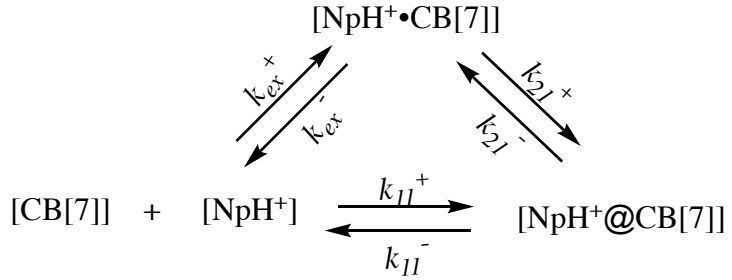

Scheme B1. Triangular binding mechanism between NpH^+ and CB[7].

$$k_{obs1} = k_{ex}^{+}\left([CB[7]]_{eq} + [NpH^+]_{eq}\right) + k_{ex}^{-} \quad \text{(Eq. B1)}$$

Where $k_{obsX} = \frac{1}{\tau_X}$ (X = 1 or 2).

When $\tau_1 << t$, where *t* is the time for data acquisition considering the time resolution of the experiment, which is 1 ms, the first process (k_{obs1}) is considered to be at equilibrium, defined by K_{ex}, which is much faster that the second relaxation process, defined by k_{obs2}. Therefore, the relaxation of the system simplifies to equation B2.[41]

$$k_{obs2} = \frac{(K_{ex}k_{21}^{+}+k_{11}^{+})([CB[7]]_{eq}+[NpH^{+}]_{eq})}{1+K_{ex}([CB[7]]_{eq}+[NpH^{+}]_{eq})} + k_{21}^{-} + k_{11}^{-} \quad \text{(Eq. B2)}$$

The mass balance equations and definitions of equilibrium constants are given by equations B3-B10:

$$[NpH^{+}]_T = [NpH^{+}]_{eq} + [NpH^{+} \bullet CB[7]]_{eq} + [NpH^{+}@CB[7]]_{eq} \quad \text{(Eq. B3)}$$

$$[CB[7]]_T = [CB[7]]_{eq} + [Na^{+} \bullet CB[7]]_{eq} + [Na^{+} \bullet CB[7] \bullet Na^{+}]_{eq} + [NpH^{+} \bullet CB[7]]_{eq} + [NpH^{+}@CB[7]]_{eq} \quad \text{(Eq. B4)}$$

$$\beta_{11} = \frac{[NpH^{+}\bullet CB[7]]_{eq}+[NpH^{+}@CB[7]]_{eq}}{[CB[7]]_{GF}[NpH^{+}]_{eq}} \quad \text{(Eq. B5)}$$

$$[CB[7]]_{GF} = [CB[7]]_{eq} + [Na^{+} \bullet CB[7]]_{eq} + [Na^{+} \bullet CB[7] \bullet Na^{+}]_{eq} \quad \text{(Eq. B6)}$$

$$K_1 = \frac{[Na^{+}\bullet CB[7]]_{eq}}{[CB[7]]_{eq}[Na^{+}]_{eq}} \quad \text{(Eq. B7)}$$

$$K_2 = \frac{[Na^{+}\bullet CB[7]\bullet Na^{+}]_{eq}}{[Na^{+}\bullet CB[7]]_{eq}[Na^{+}]_{eq}} \quad \text{(Eq. B8)}$$

$$K_{ex} = \frac{[NpH^{+}\bullet CB[7]]_{eq}}{[CB[7]]_{eq}[NpH^{+}]_{eq}} \quad \text{(Eq. B9)}$$

$$K_{21} = \frac{[NpH^{+}@CB[7]]_{eq}}{[NpH^{+}\bullet CB[7]]_{eq}} \quad \text{(Eq. B10)}$$

$$K_{11} = \frac{[NpH^{+}@CB[7]]_{eq}}{[CB[7]]_{eq}[NpH^{+}]_{eq}} \quad \text{(Eq. B11)}$$

Since the binding of Na^+ with CB[7] is considered to be in fast equilibrium, the relative concentrations are expressed by:

$$\left[Na^{+} \bullet CB[7]\right] = K_1\left[CB[7]\right][Na^{+}] \quad \text{(Eq. B12)}$$

Any change in concentration is expressed by:

$$[Na^{+} \bullet CB[7]]_{eq} + \Delta[Na^{+} \bullet CB[7]] = K_1(\left[CB[7]\right]_{eq} + \Delta\left[\mathrm{CB[7]}\right])([Na^{+}]_{eq} + \Delta[Na^{+}]) \quad \text{(Eq. B13)}$$

Where:

$$[Na^{+} \bullet CB[7]]_{eq} = K_1[Na^{+}]_{eq}[CB[7]]_{eq} \quad \text{(Eq. B14)}$$

Substituting eq. B14 into eq. B13 gives the expression for the change in concentration of a species:

$$\Delta[Na^{+} \bullet CB[7]] = K_1(\left[CB[7]\right]_{eq}\Delta[Na^{+}] + [Na^{+}]_{eq}\Delta[CB[7]] + \Delta[Na^{+}]\Delta[CB[7]]) \quad \text{(Eq. B15)}$$

Where $\Delta[Na^{+}]\Delta[CB[7]]$ can be assumed to be negligibly small, and eq. B15 becomes B16:

$$\Delta[Na^{+} \bullet CB[7]] = K_1(\left[CB[7]\right]_{eq}\Delta[Na^{+}] + [Na^{+}]_{eq}\Delta[CB[7]]) \quad \text{(Eq. B16)}$$

The equivalent equations for the Na^+•CB[7]•Na^+ species are shown by in equations B17-B21:

$$[Na^+ \bullet CB[7] \bullet Na^+] = K_2\left[Na^+ \bullet CB[7]\right][Na^+] \quad \text{(Eq. B17)}$$

$$[Na^+ \bullet CB[7] \bullet Na^+]_{eq} + \Delta[Na^+ \bullet CB[7] \bullet Na^+] = K_1(\left[Na^+ \bullet CB[7]\right]_{eq} + \Delta\left[Na^+ \bullet \mathrm{CB}[7]\right])([Na^+]_{eq} + \Delta[Na^+]) \quad \text{(Eq. B18)}$$

$$[Na^+ \bullet CB[7] \bullet Na^+]_{eq} = K_2[Na^+ \bullet CB[7]]_{eq}[Na^+]_{eq} \quad \text{(Eq. B19)}$$

$$\Delta[Na^+ \bullet CB[7] \bullet Na^+] = K_2(\left[Na^+ \bullet CB[7]\right]_{eq}\Delta[Na^+] + [Na^+]_{eq}\Delta[Na^+ \bullet CB[7]] + \Delta[Na^+]\Delta[Na^+ \bullet CB[7]]) \quad \text{(Eq. B20)}$$

Where $\Delta[Na^+]\Delta[Na^+ \bullet CB[7]]$ is negligibly small, and eq. B20 becomes B21:

$$\Delta[Na^+ \bullet CB[7] \bullet Na^+] = K_2(\left[Na^+ \bullet CB[7]\right]_{eq}\Delta[Na^+] + [Na^+]_{eq}\Delta[Na^+ \bullet CB[7]]) \quad \text{(Eq. B21)}$$

The mass balance equations for the changes in concentration are given in eq. B22-B24

$$\Delta[Na^+ \bullet CB[7] \bullet Na^+] + \Delta[Na^+ \bullet CB[7]] + \Delta[Na^+] = 0 \quad \text{(Eq. B22)}$$

$$\Delta[Na^+ \bullet CB[7] \bullet Na^+] + \Delta[Na^+ \bullet CB[7]] + \Delta[CB[7]] + \Delta[NpH^+ \bullet CB[7]] + \Delta[NpH^+@CB[7]] = 0 \quad \text{(Eq. B23)}$$

$$\Delta[NpH^+] + \Delta[NpH^+ \bullet CB[7]] + \Delta[NpH^+@CB[7]] = 0 \quad \text{(Eq. B24)}$$

In order to relate the change in CB[7] concentrations ($\Delta[CB[7]]$) to the changes in concentrations of $\Delta[NpH^+ \bullet CB[7]]$ and $\Delta[NpH^+@CB[7]]$, we substituted the change in concentration expressions for $\Delta[Na^+ \bullet CB[7]]$ (eq. B16) and $\Delta[Na^+ \bullet CB[7] \bullet Na^+]$ (eq. B21) into equation B23 to obtain equation B25:

$$\Delta\left[CB[7]\right]\left(1 + K_1[Na^+]_{eq} + K_1K_2[Na^+]_{eq}^2\right) + \Delta[Na^+](K_1[CB[7]]_{eq} + K_2\left[Na^+ \bullet CB[7]\right]_{eq} + K_1K_2[Na^+]_{eq}\left[CB[7]\right]_{eq}\right) + \Delta\left[NpH^+ \bullet CB[7]\right] + \Delta\left[NpH^+@CB[7]\right] = 0 \quad \text{(Eq. B25)}$$

Equating equation B22 to B23 we get equation B26:

$$\Delta[Na^+] = \Delta[CB[7]] + \Delta[NpH^+ \bullet CB[7]] + \Delta[NpH^+@CB[7]] \quad \text{(Eq. B26)}$$

Substituting equation B26 into equation B25 and rearranging gives equation B27:

$$\Delta\left[CB[7]\right] = -R \times \left(\Delta[NpH^+ \bullet CB[7]\right] + \Delta[NpH^+@CB[7]]) \quad \text{(Eq. B27)}$$

Where,

$$R = \frac{1+K_1[CB[7]]_{eq}+K_2[Na^+ \bullet CB[7]]_{eq}+K_1K_2[Na^+]_{eq}[CB[7]]_{eq}}{1+K_1[CB[7]]_{eq}+K_2[Na^+ \bullet CB[7]]_{eq}+K_1[Na^+]_{eq}+K_1K_2[Na^+]_{eq}^2} \quad \text{(Eq. B28)}$$

Equation B28 can be simplified to eq. B29 using the following assumptions:

$K_1[CB[7]]_{eq} << 1$

$K_2[Na^+ \bullet CB[7]]_{eq} << 1$

$K_1K_2[CB[7]]_{eq}[Na^+]_{eq} << 1$

$[Na^+]_{eq} >> [CB[7]]_{eq}$

$$R = \frac{1}{1+K_1[Na^+]_{eq}+K_1K_2[Na^+]_{eq}^2} \quad \text{(Eq. B29)}$$

Using B3 to B4 and substituting in B6, we get:

$$[CB[7]]_T - [NpH^+]_T = \left[CB[7]\right]_{GF} - [NpH^+]_{eq} \quad \text{(Eq. B30)}$$

where,

$$[CB[7]]_T >> [NpH^+]_T$$

$$[CB[7]]_{GF} >> [NpH^+]_{eq}$$

therefore,

$$[CB[7]]_T = [CB[7]]_{GF} \quad \text{(Eq. B31)}$$

Using the rate law to derive of equation B2 there is the need for a substitution[41] of $\Delta[NpH^+ \bullet CB[7]]$ in terms of $\Delta[NpH^+@CB[7]]$ to get all terms to include a $\Delta[NpH^+@CB[7]]$ component. The substitution is shown in equation B32:

$$\Delta[NpH^+ \bullet CB[7]] = \frac{-K_{ex}([CB[7]]_{eq}+[NpH^+]_{eq})}{1+K_{ex}([CB[7]]_{eq}+[NpH^+]_{eq})}\Delta[NpH^+@CB[7]] \quad \text{(Eq. B32)}$$

By applying the assumptions stated between eq. B30 and B31, substituting equations B31 into equation B2 for $[NpH^+]_{eq}$, and equating $K_{ex}k_{21}^+ + k_{11}^+$ to k_+ and $k_{21}^- + k_{11}^-$ to k_-, eq. B2 simplifies to eq. 2.21.

$$k_{obs} = \frac{k_+[CB[7]]_T}{1+K_1[Na^+]+K_1K_2[Na^+]^2+K_{ex}[CB[7]]_T} + k_- \quad \text{(Eq. 2.21)}$$

Chapter 3:

C-1 After the synthesis and recrystallization of MDAP2+, the compound was dried for 30 min on a vacuum line. Figure C1 shows the 1H NMR spectrum acquired after drying $MDAP^{2+}$.

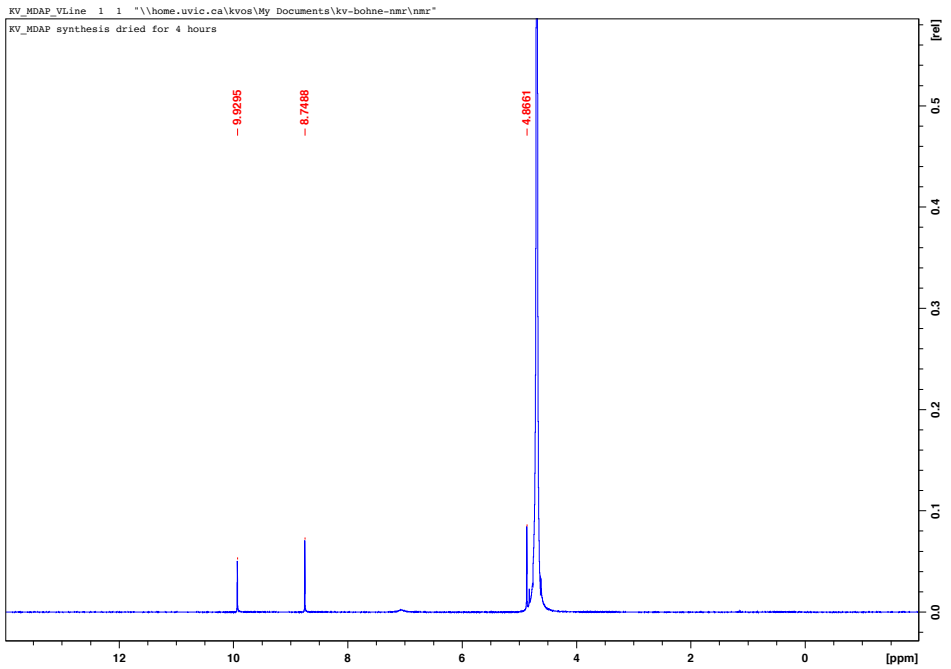

Figure C1 ^{1}H NMR of $MDAP^{2+}$ in D_2O.

C-2 The fit of the binding isotherm between MV^{2+} and CB[7] shown in figure 3.3 to a 2:1 CB[7]: guest sequential model.

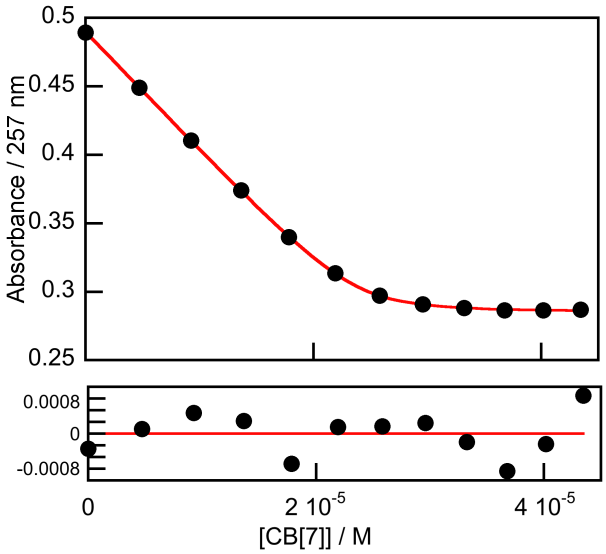

Figure C2 Fit and residuals of the fit to a 2:1 CB[7]:guest:CB[7] generated from the binding isotherm between MV^{2+} and CB[7] in figure 3.3.

C-3 The fit of the binding isotherm between $MDAP^{2+}$ and CB[7] shown in figure 3.5 fit to a 1:1 CB[7]:$MDAP^{2+}$ model.

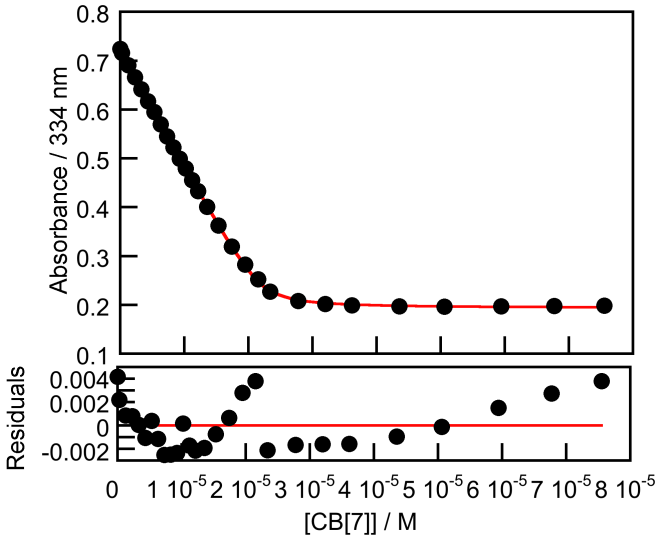

Figure C3 Fit and residuals of the fit to a 1:1 CB[7]:guest generated from the binding isotherm between $MDAP^{2+}$ and CB[7] in figure 3.5.

C-4 Kinetic traces between 40 μM CB[7] and 5 μM $MDAP^{2+}$ at different concentrations of Na^{+} cations to show the time scale differences for the formation of higher order complexes.

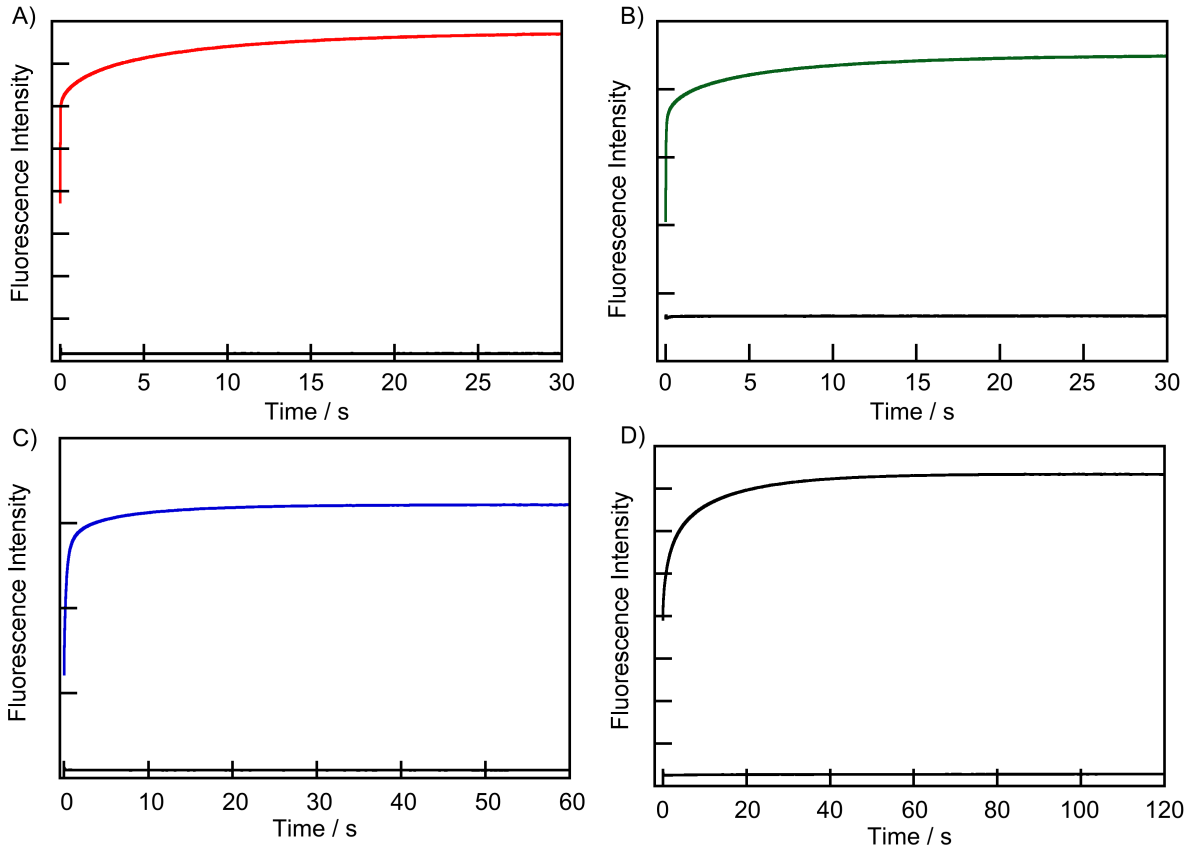

Figure C4 Kinetic traces of 5 μM $MDAP^{2+}$ mixed with 40 μM CB[7] at different concentrations of Na^+ (**A**, $[Na^+]$ = 0 mM; **B**, $[Na^+]$ = 10 mM; **C**, $[Na^+]$ = 50 mM; **D**, $[Na^+]$ = 100 mM).

Chapter 4:

D-1 The first 2 seconds of the kinetic traces between CB[7] and BNA^+ presented in figure 4.8.

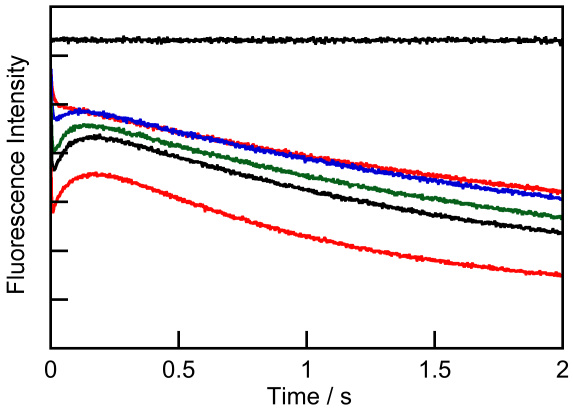

Figure D1. Kinetic traces for the mixing of 1 μM BNA^+ with various CB[7] concentrations (5 μM, top red; 10 μM, blue; 15 μM, green; 25 μM, bottom black; 40 μM, bottom red) in the presence of 10 mM Na^+. The top black trace corresponds to the control experiment in the absence of CB[7] ([Na^+ = 10 mM).

D-2 An overlay of absorption spectra of BNA^+ taken every minute for 15 min. This is a control experiment to show that BNA did not degrade as it did in the fluorescence spectra when the excitation bandwidth was too large.

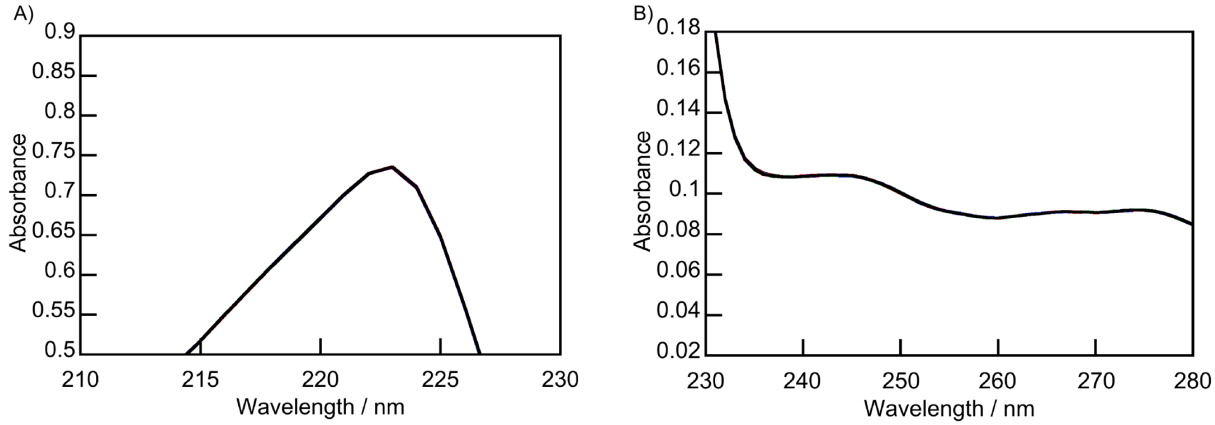

Figure D2. Absorption spectra taken over 15 minutes of 10 μM BNA^+ mixed with solvent at 10 mM Na^+. Absorption scans were taken from 200-800 nm every minute to show the absorption did not change with respect to time. (**A:** 210-230 nm; **B:** 230-280 nm)